EPFL

Unequal cleavage of the *C. elegans* zygote ensures robust embryogenesis

Radek JANKELE

École
polytechnique
fédérale
de Lausanne

2020

Abstract

Asymmetric cell divisions play key roles in generating cellular diversity during embryogenesis, and in tissue homeostasis during postembryonic life. Particular asymmetric cell divisions producing differentially sized daughter cells were described in many systems, yet the importance of cell size asymmetry was demonstrated only in few cases. To further address this question, we used the *C. elegans* zygote that divides asymmetrically into a larger anterior AB cell and a smaller posterior P1 cell as a model of size asymmetric cell division. AB and P1 descendants give rise to vastly different tissues and organs in the worm body. Interestingly, cell size asymmetry of the first division is conserved in the *Caenorhabditis* genus spanning at least 100 million years of evolution. However, whether AB and P1 need to have unequal sizes to support normal *C. elegans* embryogenesis remains an open question.

To generate embryos that will have the same size of AB and P1 without perturbing their anterior-posterior polarity, we used a temperature-sensitive allele of *lin-5*, which governs asymmetric spindle positioning in the wild-type zygote. This LIN-5 protein variant can be reversibly inactivated by upshift to elevated temperature, allowing us to generate embryos with a range of relative AB/P1 sizes, including equalized embryos, and even inverted embryos with a smaller AB than P1. We then followed the development of such embryos at the permissive temperature using 3D timelapse microscopy followed by lineage tracing.

We observed increasing lethality with decreasing size of AB, indicating that unequal cell size is vital for embryonic development of *C. elegans.* Furthermore, we found that inverted embryos with an AB size below 48% of total volume died in all cases, pointing to the existence of a clear size-asymmetry threshold for viability. Interestingly, we discovered that P1, but not AB, descendants exhibited accelerated cell cycles in equalized and inverted embryos. Moreover, we found that both cells originating from the anterior AB lineage and those of posterior P1 lineage end up in abnormal positions, or fail to express differentiation markers of endoderm and pharynx at wild-type levels or in a characteristic pattern. We uncovered markedly increased variability in timing, division orientation, and cell positions in equalized embryos, and even more so in those that eventually died. In conclusion, our results demonstrate that the size asymmetry of the first cleavage is necessary for the robust and stereotypic embryogenesis of *C. elegans*.

Keywords: asymmetric cell division, fate specification, cell volume, unequal size, *C. elegans,* lineage tracing

Résumé

Le processus de division asymétrique des cellules est essentiel à la diversité cellulaire au cours du développement de l'embryon ainsi qu'à l'homéostasie des tissus lors de la vie post-embryonnaire. Dans de nombreux systèmes, des divisions asymétriques particulières conduisent à la formation de cellules filles de tailles différentes. L'importance de la taille de la cellule n'a été démontré que dans peu de cas. Afin d'approfondir nos connaissances, nous utilisons la première division de l'embryon du nématode *C. elegans* comme système modèle. Celle-ci se déroule de manière asymétrique générant ainsi une cellule antérieure AB de taille plus importante que la cellule postérieure P1. Les descendants des cellules AB et P1 sont impliquées dans la formation de tissus et organes différents chez le ver adulte. L'asymétrie de la première division de l'embryon est conservée dans l'ensemble du genre *Caenorhabditis* qui couvre au minimum 100 millions d'années d'évolution. Toutefois, l'importance de la différence de taille entre les cellules AB et P1 n'a jusqu'alors pas été évaluée.

Afin d'obtenir des embryons formés de cellules AB et P1 de taille équivalente sans altérer la polarité antéro-postérieur, nous utilisons un allèle thermosensible du gène *lin-5*. Ce gène code pour une protéine qui dirige le positionnement asymétrique du fuseau mitotique. La version mutante thermosensible de LIN-5 est inactivée de manière réversible par une augmentation de température. Cela permet de modifier de manière transitoire la position du fuseau mitotique et d'ainsi générer des embryons contenant des cellules AB et P1 de tailles relatives variées, y compris de taille équivalente et même inversées avec P1 de taille plus importante que AB. Après un retour à température permissive, nous avons étudié le développement de ces embryons à l'aide de la vidéo-microscopie 3D et du traçage de lignée cellulaire.

Nos résultats indiquent que la différence de taille entre les cellules AB et P1 est essentielle au développement embryonnaire de *C. elegans*. En effet, nous avons observés que plus la taille de AB est réduite plus la létalité embryonnaire est augmentée. De plus, les embryons inversés contenant une cellule AB de taille inférieure à 48% du volume total meurent de manière systématique ce qui suggère l'existence d'un seuil limite d'asymétrie des tailles indispensable à la viabilité embryonnaire. De façon intéressante, nous avons découvert que les descendants de P1, mais pas de AB, présentent des cycles cellulaires accélérés dans les embryons formés de cellules de taille équivalente ou de cellules de tailles inversées. Nous avons aussi montré que pour les deux lignées cellulaires, certaines cellules sont anormalement positionnées ou n'expriment pas de manière fidèle les marqueurs de différentiation de l'endoderme ou du pharynx. Nous avons observé une variabilité significative de la durée et de l'orientation des divisions ainsi que de la position des cellules dans les embryons inversés, une variabilité d'autant plus marquée lorsque le développement est interrompu précocement. Pour conclure, nos résultats démontrent que la différence de la taille des cellules résultant de l'asymétrie de la première division embryonnaire est indispensable au développement normal et stéréotypé de l'embryon de *C. elegans*.

Mots clefs : division cellulaire asymétrique, destin cellulaire, volume cellulaire, différence de taille, *C. elegans*, traçage de lignée cellulaire.

Acknowledgements

I would like to express my gratitude for the opportunity to spend nearly five years of my life in a great collective of smart and kind people. I learned a lot of new skills that exceeded my own expectations and had the chance to do science in a very stimulating environment, which EPFL definitely is.

I thank you for this opportunity, Pierre. You were a great mentor over past years, you taught me to be even more critical and to strive for perfection. I got your support and understanding at hard times; I am genuinely grateful for your attitude. You were able to motivate me at better times and infect me with your endless energy. And if it was not for this motivation, we would never get to the end of this story. I hope that I was able to answer at least some of your burning questions concerning the curious first division of *C. elegans* zygote.

Intermezzo: Dear jury members, thank you for your valuable time spent over my thesis and for your useful input.

I was pleased to share my time with all UPGONIES over the years. Alexandra, Benita, and Marie, many thanks for your support, scientific advice, and friendship. Melina, Veronika, and Nils, thank you for being the brave and only co-PhDs in the lab, and for sharing the hardships and happy hours (quite literally) of PhD life with me.

I also thank to all worm scientist that helped me during my PhD by providing their worm strains and input. First, I thank Rob Jelier for his help with the cell lineaging and for his input about early embryogenesis. Einhard Schierenberg pointed us to the gastrulation and shared his knowledge about embryogenesis. Labs of Bob Goldstein, Geraldine Seydoux, Sander van der Heuvel, Morris Maduro, and John Murray shared their strains with us.

My thanks go to my friends for their support, and the fun and experiences we had together. First of all, thank you, Maria, for being my soulmate in crime since the beginning of our doctoral studies, for hosting me in you winter house, and for being great friend. Equally, Kathleen and Simone, thank you for sharing the ride with me. Girls, you were all faster than me, but I got to the finish line, too. Can you believe it?

I thank my parents for bringing me to this World and for their unconditional support and freedom they gave me from a young age. Thank you for never inhibiting my fascination with biology and all the exciting stuff around us. You were patient with me even when you had no answers for my why questions.

A huge hug and thanks to you, Lucie. I would be lost without you, and eat just fried eggs every day. You are my true partner standing by my side and helping me to overcome all bumps on the road. Thank you for being so stable and organized, and for having so much patience with me. I love you.

Declaration

I hereby declare that this thesis is a presentation of my original research work and that all used sources were duly cited. I furthermore declare that wherever contributions of others are involved, this is indicated, clearly acknowledged and due reference is given to the author and source. I also certify that all content without reference or citation contained in this thesis is original work.

Table of Contents

List of Figures

List of Tables

Abbreviations

ACD   – Asymmetric cell division
AP   – Anterior-Posterior
DV   – Dorso-Ventral
LR   – Left-Right
Ctrl   – Control – typically unequal *lin-5(ev571)* embryo upshifted at the two-cell stage
EQ   – Equalized – an embryo with AB in the range of 48-52.5% of total embryos size
EA   – Equalized alive
ED   – Equalized dead
INV   – Inverted - embryo with AB smaller than 48% of total embryos size
WT   – Wild-type
SPIM   – Selective plane illumination microscopy, or light-sheet

1 Introduction

Asymmetric cell division (ACD) generates two daughter cells with distinct fates. As such, ACD is crucial for development, differentiation, regeneration as well as tissue homeostasis from yeast through to plants and mammals (reviewed in Gönczy, 2008; Rose and Gönczy, 2014; Shao and Dong, 2016). Defects in ACD have been implicated in several diseases, including cancer and microcephaly (reviewed in Bajaj et al., 2015; Mukherjee et al., 2014). Some ACDs produce daughter cells that also differ in their physical sizes, in addition to their fates. We will refer to such divisions as "unequal" for the purpose of this thesis. Textbook examples of unequal ACD include division of budding yeast into a large mother cell and a small bud (Freisinger et al., 2013), cleavage of early sea urchin embryos into micromeres and macromeres (Boveri, 1902; Dan, 1979), divisions of neuroblast stem cells in *Drosophila* (Kang and Reichert, 2014), as well as the unequal division of Q-neuroblasts in *C. elegans*, whereby asymmetric contractions of the cortical actomyosin network result in size expansion of one daughter cell and consequent change of its fate (Ou et al., 2010).

Two general mechanisms can generate ACD: 1) Two sister cells are born identical but differentiate later in response to external cues (e.g., morphogen gradients, signals –or lack thereof - from the stem cell niche, or contact with the basement membrane). 2) A mother cell becomes polarized before division such that each daughter cell inherits distinct fate determinants, typically located on the cell cortex or in the cytoplasm, which then steers them or their descendants towards different fates. *C. elegans* is an excellent model system for the study of both types of ACD; however, we will mostly focus here on the second type, sometimes called cell-intrinsic ACD (Horvitz and Herskowitz, 1992).

1.1 The first unequal cleavage of the *C. elegans* zygote

The first division of the *C. elegans* zygote is a prime example of unequal ACD, which scientists studied for nearly four decades in exquisite detail. Many discoveries made in this ACD model system turned out to be conserved across the animal kingdom. The first division of the *C. elegans* zygote generates a larger anterior AB cell and a smaller posterior P1 cell, comprising ~60 % and ~40 % of the initial cell volume, respectively. Thereafter, AB and its descendants divide mostly symmetrically and with synchronous timing, while P1 undergoes three additional ACDs producing pairs of sister cells with asynchronous timing (**Figure 1**). Together, these four ACDs generate five somatic blastomeres – AB (pharynx, hypodermis, neurons), E (sole intestinal progenitor), MS (muscle, pharynx, neurons, somatic gonad), C (muscle, hypodermis, and neurons), D (muscle) and the germline blastomere P4 (Gönczy, 2008; Sulston et al., 1983).
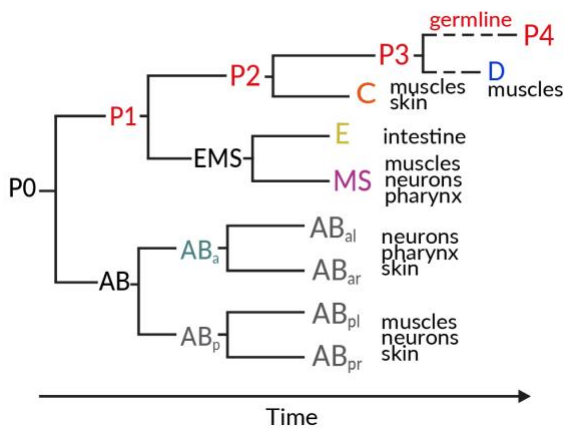
1.1.1 Polarity establishment

Polarization of the initially isotropic *C. elegans* zygote is jump-started by a component of the paternally-derived centrosomes (Cowan and Hyman, 2004; Sadler and Shakes, 2000). Proximity of these centrosomes to the plasma membrane leads to a local relaxation of the cortical actomyosin network at the presumptive posterior pole and a flow of cortical material towards the presumptive anterior side (Bienkowska and Cowan, 2012; Cowan and Hyman, 2004; Jenkins et al., 2006; Motegi et al., 2011; Srinivasan et al., 2003; Zonies et al., 2010). This cortical flow displaces the anterior PAR complex composed of aPKC-3/PAR-3/PAR-6 away from the posterior, allowing binding of PAR-1 and PAR-2 in that location, which then expand to eventually occupy ~50% of embryo length (Munro et al., 2004; Zonies et al., 2010; reviewed in Rose and Gönczy, 2014). Thereafter, polarity is maintained via a complex network of feedback loops, which fine-tune the association and dissociation rates of polarity proteins, resulting in two stable and mutually exclusive domains (**Figure 2A**) (reviewed in Hoege and Hyman, 2013).

1.1.2 Spindle positioning

Proper positioning of the mitotic spindle is essential for accurate segregation of fate determinants and correct arrangement of cells within embryos and tissues (reviewed in Dewey et al., 2015; Williams and Fuchs, 2013). In the one-cell stage embryo of *C. elegans*, the mitotic spindle first orients along the anterior-posterior (AP) axis specified by the PAR polarity proteins, and is then displaced slightly to the posterior during metaphase and anaphase (Colombo et al., 2003; Grill et al., 2003, 2001; Kemphues et al., 1988). Thereafter, the cleavage furrow forms so as to bisect the anaphase spindle, generating two daughter cells of unequal sizes, ensuring that DNA and cytoplasmic components are properly segregated between them (Bringmann and Hyman, 2005; Pacquelet et al., 2015; Schenk et al., 2010).
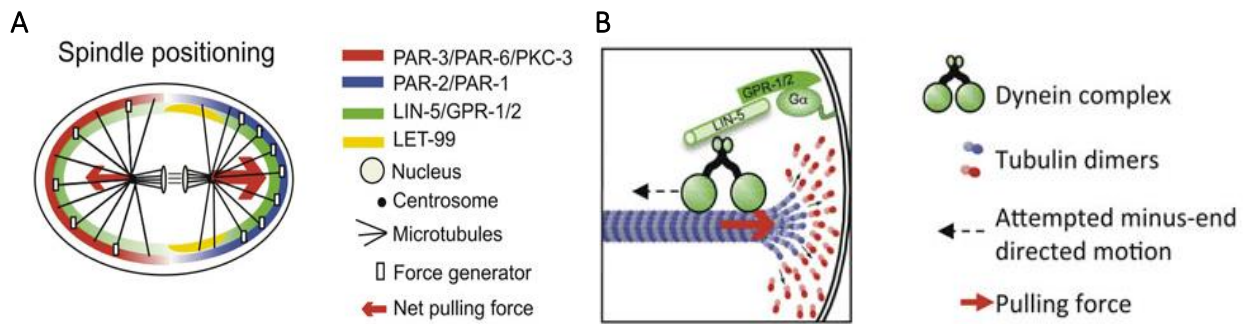
Figure 2 - Spindle positioning by cortical force generators

(A) In the one-cell *C. elegans* embryo, two cortical PAR polarity domains (blue and red) control the asymmetric localization of cortical force generators (squares) via enrichment of GPR-1/2/LIN-5 at the posterior cortex. This results in higher net pulling forces acting on astral microtubules at the posterior, which move the spindle off-center, closer to the posterior. (B) Cortical force generators comprise dynein-dynactin tethered to the cortex via interaction with a ternary complex comprising Gα-GDP/ GPR-1/2/LIN-5. See text for details. Adapted from Rose and Gönczy, 2014.

Asymmetric spindle positioning relies on a conserved ternary complex, composed of the membrane associated and partially redundant Gα proteins GOA-1 and GPA-16, of the two TPR and GoLoCo domain containing proteins GPR-1 and GPR-2 (referred to collectively as GPR-1/2), as well as of the long coiled-coil protein LIN-5, homologous to human NuMA and *Drosophila* MUD. This ternary complex anchors the microtubule-dependent motor-protein dynein to the cell cortex, where it contributes to the production of pulling forces positioning the spindle (Colombo et al., 2003; Gotta and Ahringer, 2001; Lorson et al., 2000; Nguyen-Ngoc et al., 2007; Werts et al., 2011). The precise mechanism by which cortically anchored dynein generates pulling forces on astral microtubules to position the spindle is not fully understood. Dynein alone directly recruited to the membrane is not able to exert pulling forces on astral microtubules in *C. elegans*, while LIN-5 tethered to the membrane is sufficient for recruitment and activation of dynein, suggesting that it serves an important regulatory role in addition to mechanical anchoring of dynein (Fielmich et al., 2018).

Unequal division of the one-cell *C. elegans* embryo stems from posterior displacement of the spindle during metaphase and anaphase, which is caused by asymmetric net cortical pulling forces acting on astral microtubules (Grill et al., 2003, 2001). It has been shown that GPR-1/2, and to a lesser extent LIN-5, become enriched on the posterior cortex in response to AP polarity cues (**Figure 2A**) (Colombo et al., 2003; Gotta et al., 2003; Grill et al., 2001; Park and Rose, 2008). Several additional proteins regulate the distribution and activity of cortical force generators. Among them, the DEP protein LET-99 prevents localization of GPR-1/2 in a posterior lateral band and thus contributes to asymmetry and directionality of net pulling force (Tsou et al., 2003, 2002).

Importantly, mutants in *par* genes or in genes encoding ternary complex components, such as *lin-5*, or *gpr-1/2*, produce embryos that divide equally during the first cleavage. Such mutant embryos are, however, early embryonic lethal due to the complete lack of AP polarity or impaired divisions in subsequent cell divisions, respectively (Gotta and Ahringer, 2001; Kemphues et al., 1988; Lorson et al., 2000; Srinivasan et al., 2003).

1.1.3 Asymmetric distribution of fate determinants

So-called "polarity mediators" respond to cortical polarity, forming cytoplasmic gradients along the AP axis and regulating the distribution of fate determinants – maternal proteins and mRNAs - in the blastomeres after division (reviewed in Griffin, 2015; Rose and Gönczy, 2014). Typically, polarity mediators are RNA binding proteins (RBPs), which regulate translation and degradation of maternally provided mRNAs by binding to their 3'UTRs in a combinatorial fashion. Among them, the RBPs MEX-5 and a redundant paralogue MEX-6 are enriched in AB after the first division (Griffin et al., 2011; Schubert et al., 2000). MEX-5/6 promote somatic fates through ZIF-1-dependent proteasomal degradation of germline fate determinants (e.g. PIE-1, MEX-1, POS-1 and SKN-4 (Guedes and Priess, 1997; Mello et al., 1996; Ogura et al., 2003)) in the AB lineage (DeRenzo et al., 2003; Reese et al., 2000). In contrast, germline determinants in the P lineage are prevented from such degradation by the RBP POS-1, which binds the *zif-1* mRNA and inhibits its translation (Oldenbroek et al., 2012; Reese et al., 2000). PIE-1 acts as a global transcriptional repressor in the nuclei of P lineage cells, where it prevents phosphorylation and activation of RNA polymerase II, thus keeping germline cells transcriptionally silent (Mello et al., 1996; Seydoux et al., 1996; Seydoux and Dunn, 1997). In addition, polarity mediators directly affect distribution of factors regulating cell cycle and thus contribute to setting up asynchronous pace between AB and P1. MEX-5 has been shown to physically interact with a mitotic kinase PLK-1, which is thus enriched in AB where it accelerates mitosic entry (Budirahardja and Gönczy, 2008; Han et al., 2018; Rivers et al., 2008). Furthermore, PLK-1 plays a critical role in relaying the anterior gradient to the opposing posterior gradient of POS-1 by its phosphorylation, which increases POS-1 mobility at the anterior half of the embryo likely due to POS-1 unbinding from cytoplasmic RNA (Han et al., 2018)

In conclusion, the founder blastomeres are specified sequentially by combinatorial interactions of maternally-provided fate determinants, localized translation, and protein degradation, leading later to the activation of the zygotic transcription and synthesis of new proteins, starting substantially at the 26-cell stage with the onset of gastrulation (Powell-Coffman et al., 1996; Schauer and Wood, 1990; Zacharias and Murray, 2016).

1.2 Unequal cell divisions in other model systems

Importantly, ACD and spindle positioning in other organisms often relies on homologous proteins and analogous mechanisms to those of *C. elegans* described above, highlighting the value of this model for the study of ACD (reviewed in Gönczy, 2008; Thompson, 2013; Yassin and Russell, 2016). I will briefly describe three examples from other model systems to illustrate similarities and interesting differences.

Embryonic and larval neuroblasts in Drosophila divide unequally along the apicobasal axis and produce a small ganglion mother cell (GMC), which later terminally divides to give rise to two neurons, and a larger apical neuroblast, which repeats the same unequal ACD multiple times to generate more GMCs (reviewed in Gönczy, 2008). The NB is polarized before division by mutually exclusive apical and basal complexes containing homologs of *C. elegans* polarity network and cortical force generators, and additional proteins. The apical complex contains atypical kinase C (DaPKC), the polarity protein bazooka that is homologous to PAR-3 and DmPar6, similar to the anterior PAR complex in *C. elegans*. In addition, Inscuteable, taking the role of *C. elegans* GPR-1/2, and partner of Inscuteable (Pins), which inhibits GDP release from $G\alpha i$, also localize to the apical domain and restrict the homeodomain factor Prospero, essential for neurogenesis, and protein Numb to the basal side for inheritance by the GMC (reviewed in Gönczy, 2008). The mechanism ensuring unequal daughter cell sizes relies upon spindle displacement closer to the basal side and on the asymmetry of spindle geometry. The spindle half closer to the apical pole elongates during late anaphase under the activity of Pins, effectively placing the future midbody closer to the basal pole and thus contributing to the resulting size asymmetry (Cai et al., 2003; Kaltschmidt et al., 2000; Siller et al., 2006).
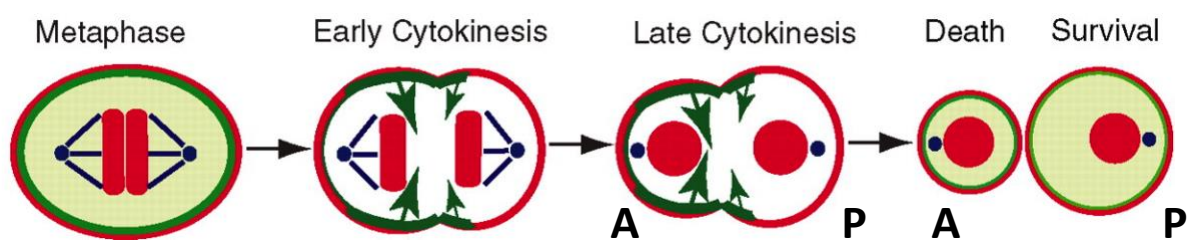
Figure 3 - Unequal cell division of Qa neuroblast

Adapted from (Ou et al., 2010). Unequal ACD of the Qa neuroblasts in *C. elegans* L1 larva. The spindle is positioned symmetrically in the center of the Qa neuroblast, but the anterior half of the dividing cell shrinks and pushes cytoplasm to the posterior half during anaphase. This is achieved by enrichment of contractile myosin-II at the anterior cortex of the dividing neuroblast. The smaller anterior cell then undergoes apoptosis, while the larger posterior cell differentiates into PQ(R/L) neuron. Both cells survive whet myosin-II is inhibited and Qaa differentiates into additional neuron.

A second example is the unequal division of the eight-cell stage sea urchin embryo *Strongylocentrotus purpuratus* into micro- and macromeres, which relies on the asymmetric distribution of the LIN-5 orthologue spNuMa to the vegetal cortex of cells, resulting in asymmetric net pulling forces acting on the mitotic spindle, like during the first cleavage in *C. elegans.* spNuMa is recruited to the vegetal cortex downstream of the Pins/LGN orthologue AGS and of $G\alpha_i$ (Poon et al., 2019). Interestingly, physical interaction of $G\alpha_i$ with spNuMa and the fate determinant Vasa depends on the mitotic kinase PLK-1 being inactive. Furthermore, the authors showed that asymmetric distribution of AGS/$G\alpha_i$ and, therefore, Vasa is critical for acquisition of organizer function by micromeres and successful gastrulation (Poon et al., 2019).

Another interesting example is an unequal division of *C. elegans* Q neuroblasts at the L1 larval stage. *C. elegans* has two pairs of Q neuroblasts on the left and right side of the body along the AP axis (reviewed in Rella et al., 2016). While the posterior neuroblasts divide by a similar mechanism to that of the zygote, the anterior Qa neuroblasts employ a very different mechanism (**Figure 3**). Qa neuroblasts divide terminally to produce a smaller anterior cell that will undergo apoptosis and a larger posterior that differentiates into a neuron. The spindle in Qa neuroblast remains in the center of the cell; instead, asymmetrically localized cortical non-muscle myosin NMY-II, enriched at the anterior cortex, triggers contraction of the anterior half of the dividing neuroblast during anaphase to push cytoplasm into the larger posterior daughter (Ou et al., 2010). Inhibition of cortical myosin results in equalized Qa division, and to the survival of the anterior daughter, which then ectopically divides, producing extra neurons (Ou et al., 2010).

Conversely, there are many cases where having equal division is important. For example, the unequal size of blastomeres in early human embryos (e.g. at the 4-cell) was shown to correlate with reduced implantation success during *in vitro* fertilization. Such defective human embryos often harbor chromosomal aberrations, likely reflecting imbalance of pulling forces during mitosis, and are therefore excluded during visual screening in clinical settings (Hardarson et al., 2001).

1.3 *C. elegans* embryogenesis

John Sulston and coworkers described the invariant lineage of *C. elegans* in their pioneering work nearly 40 years ago (Sulston et al., 1983). In doing so, they discovered that worm development is highly reproducible in terms of cell cycle timing, cell positions, resulting in exactly the same number of cells with precisely controlled fates. These observations were later supported by an array of quantitative analyses enabled by 3D fluorescence timelapse microscopy and advanced image analysis (Bao et al., 2006; Hench et al., 2009).

Early experiments revealed that development in *C. elegans* is mosaic; i.e., blastomeres killed by a laser beam do not get replaced by their neighbors, and the resulting larva will thus lack all cells and tissues generated by the descendants of the killed cell (Sulston et al., 1983). Removing any of the very early blastomeres results in embryonic lethality (Sulston et al., 1983). The mosaic development mode is in stark contrast to the regulative development in most studied organisms, in which early cells are typically replaceable, differentiate in response to morphogen gradients, and grafting of cells or tissues between parts of an embryo is possible. The blastomere ablation experiment in *C. elegans* also revealed that most cell fates arise through a lineal, mostly cell-autonomous program, which integrates the inputs from the neighboring cells by direct cell-cell interactions (Priess and Thomson, 1987; Sulston et al., 1983).

1.3.1 Establishment of embryonic axes

Despite its tubular body shape, *C. elegans* belongs to bilateral animals, having three principal body axes, and exhibits internal left-right (LR) asymmetry, similar to many other animals, including humans. Fist, the AP axis is specified upon fertilization by PAR proteins, as described above (Goldstein and Hird, 1996). Then, the dorsoventral (DV) axes is determined by the skewed division of AB, ensuring that blastomeres at the four-cell stage will asumme rhomboid (diamond-like) geometry, which will place EMS on the future ventral side (Sulston et al., 1983). The two AB cells then divide in the LR orientation with a leftward spindle skew due to an inherent chirality of the actomyosin network that generates counter-rotating cortical flows resulting in a torque acting on the dividing AB cells (Naganathan et al., 2014). This skewed division positions the left ABal and ABpl cells more anteriorly in comparison to their sisters.

1.3.2 Embryonic inductions and spindle positioning in later stages of embryogenesis

I will mention briefly some of the events occurring during early embryogenesis that are most relevant to this work. The posterior polarity mediator POS-1 activates translation of some maternal mRNAs and represses that of others; such maternal mRNAs encode components crucial for diversification of cell fates in four-cell stage embryos (Ogura et al., 2003; Oldenbroek et al., 2013, 2012; Reese et al., 2000;

reviewed in Rose and Gönczy, 2014). Thus, in the P2 cell, POS-1 enables translation of the Delta ligand APX-1 and the Wnt ligand MOM-2.

EMS becomes polarized in response to redundant Wnt and Src signaling from P2 (Bei et al., 2002; Berkowitz and Strome, 2000; Schlesinger et al., 1999; Walston et al., 2004; Zhang et al., 2008). These two signaling pathways trigger enrichment of the dynein/dynactin complex at the contact site between the two cells. Surprisingly, cortical localization of dynein in EMS is independent of GPR-1/2; instead, dynactin interacts directly in this cell with the activated Wnt receptor (Schlesinger et al., 1999; Zhang et al., 2008). Ultimately, the EMS spindle is positioned closer to P2, resulting in the unequal cleavage of EMS into a larger MS cell and a smaller E cell.

Another important function of POS-1 is to restrict production of GLP-1, a Notch family receptor for APX-1, exclusively to AB cells. POS-1 binds to the 3'UTR of the *glp-1* mRNA, preventing its translation in P2 and EMS (Evans et al., 1994; Ogura et al., 2003; Priess et al., 1987). Only the posterior AB daughter ABp, which is in contact with the APX-1-presenting P2 cell, can thus activate the Notch pathway, resulting in the induction of different cell fates than those derived from its anterior sister ABa (Priess et al., 1987). The mechanism of asymmetric spindle positioning in P2 involves GPR-1/2, which gets enriched on the membrane adjacent to EMS through active dissociation from the P2-ABp interface (Werts et al., 2011).

1.3.3   Gastrulation in *C. elegans*

Gastrulation in *C. elegans* begins at the 26-cell stage, with ingression of the two endodermal progenitors Ea and Ep (referred to collectively as E2 hereafter) and continues for several hours with the sequential and precisely timed ingression of another 66 cells (reviewed in Goldstein and Nance, 2020; Nance and Priess, 2002; Sulston et al., 1983). In contrast to mammalian gastrulation, there is no empty blastocoel cavity into which gastrulating cells would move in the worm. Instead, all cells at the 26-cell stage share basolateral membrane interactions and have their apical side in contact with eggshell. Thereafter, the internal endoderm and mesoderm germ-layers are formed through sequential ingression of gastrulating cells, a process characterized by the constriction of apical actomyosin cortex, which induces cell-shape change and internalization, away from the eggshell (Lee and Goldstein, 2003) (**Figure 4**). Apical constriction is a conserved mechanism employed in gastrulation of other organisms as well as other processes such as neurulation in chordates (Nikolopoulou et al., 2017; Sullivan-Brown et al., 2016). Thus, study of *C. elegans* gastrulation can provide insights into mechanisms employed during development across the animal kingdom.

Apical constriction in E2 cells is induced by Wnt signaling, which activates actomyosin cortical contractions (Chisholm, 2006; Marston et al., 2016) and induces the formation of lateral tight junctions, which are also essential for this process (Roh-Johnson et al., 2012). In addition, MSpp helps promote E2

ingression by actively migrating along the eggshell towards P4, which is tightly bound to Ep, ultimately resulting in the complete internalization of the intestinal precursors before their next mitosis (reviewed in Goldstein and Nance, 2020) (**Figure 4**).

Gastrulation is accompanied by a major wave of zygotic genome activation (ZGA), starting first in E2 cells and causing a delay of their cell cycle by about ~20 min compared to their MS cousins (Hashimshony et al., 2015; Powell-Coffman et al., 1996; Wong et al., 2016). Ingression of E2 cells fails to initiate in embryos subjected to RNAi-mediated knockdown of AMA-1, the large subunit of RNA polymerase II, despite earlier development proceeding normally, demonstrating the critical role of ZGA, i.e. transcription for gastrulation (Powell-Coffman et al., 1996).

Internalization of ingressing cells is aided by planar divisions of ectodermal cells mostly originating from the AB lineage that remain on the outside of the embryo to form skin and neurons. These planar divisions oriented along the AP axis are thinning the outer sheet of ectoderm, thus making space for ingressing endo- and mesodermal cells of E, MS, C, and D lineages, which internalize in this order. Unlike E2 cells, other blastomeres activate zygotic transcription later on, when the embryo comprises ~100 cells (Bao et al., 2008; Hashimshony et al., 2015; Powell-Coffman et al., 1996).
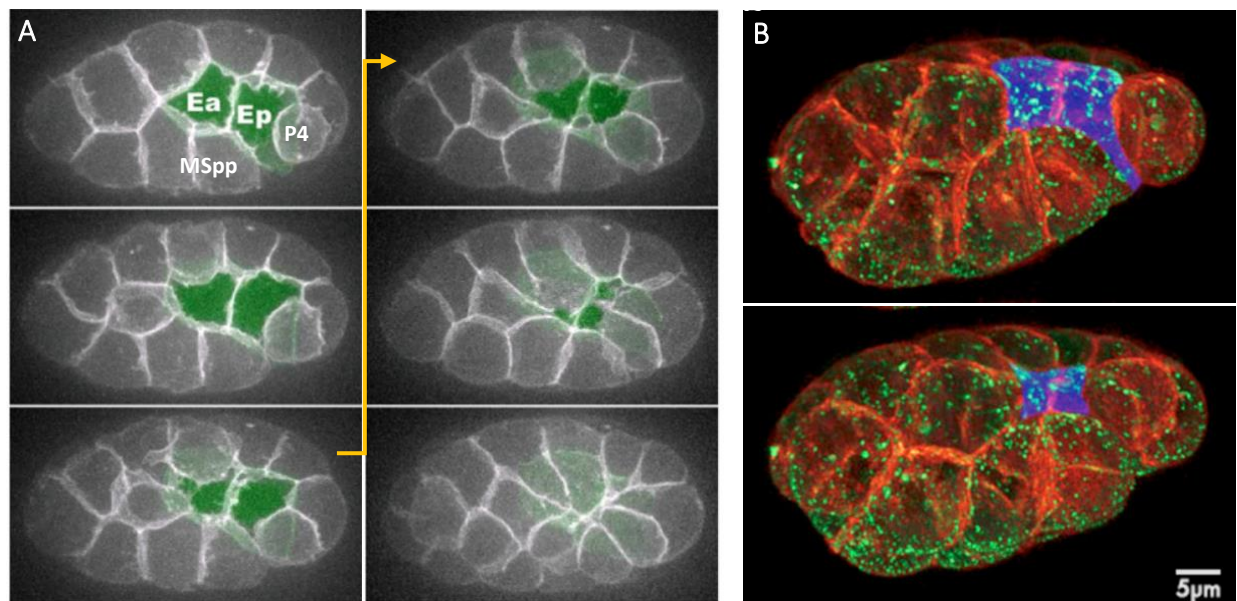
Figure 4 - Ingression of endoderm
(**A**) Six frames from a timelapse movie of *C. elegans* gastrulation beginning at the 26-28 cell stage with the internalization of the two endodermal precursors Ea and Ep (E2, coloured in green) on the ventral side of the embryo (shown are maximum intensity projections of the first 10 microns of the ventral surface). In this sequence, E2 cells gradually constrict their apical cortex, causing a shape change driving their internalization. Surrounding cells gradually crawl over the apical surface of E2 cells to entirely seal them away from the eggshell, before they divide inside the embryo. E2 yields cells that eventually differentiate to form the entire intestine. Gastrulation continues for several hours by internalization of the surrounding cells. (**B**) Projection of two frames 340 s apart from the Bessel beam SPIM time-lapse of embryos during gastrulation of E2 cells with membrane in red and contractile cortical myosin NMY-II, in green. Clearly visible are larger cortical puncta of NMY-II on the cortical surface in E2 cells undergoing apical constriction (pseudo colored in blue). Adapted from (Goldstein and Nance, 2020)

Finally, ingressing mesodermal cells are followed by the partial internalization of neuroblasts of the ABprp and ABplp lineages, which subsequently guide epiboly of ectodermal cells from the lateral sides over the ventral surface during the process of ventral closure. This final gastrulation event seals the embryo in a continuous epidermal layer that provides mechanical support and actively contributes to the morphogenesis of what until now was ball of cells into a worm-like tubular body plan.

1.4   Developmental robustness

Animal development is fascinating in many aspects, starting with the fact that an elaborate three-dimensional body plan arises from a one-dimensional set of instructions encoded in the DNA, to the stunning reliability with which embryos develop into a conserved form despite environmental factors, genetic variability, and transcriptional noise. The latter has also been called developmental robustness (Keller, 2002; Levy and Siegal, 2012).

The British biologist and philosopher C. H. Waddington was the first to report that organisms found in the wild, evolving under the influence of natural selection, tend to produce less variable offspring, in comparison to isolated genetic mutants or selectively bred variants of the same species, whose offspring is more sensitive to perturbations and environmental stress (Waddington, 1942). He later proposed his famous theory of epigenetic landscape and the term canalization, which describes how cells acquire their distinct fates during development by following pre-existing branching valleys in this imaginary downhill landscape. The valleys and ridges defined in the genetic code and shaped by evolution to robustly guide (or canalize) and restrict the transcriptional program of the cell during differentiation despite environmental noise or external perturbations. Besides, ridges between valleys in Waddington's landscape prevent cells from direct transdifferentiation from one fate to another (reviewed in Mestek Boukhibar and Barkoulas, 2016).
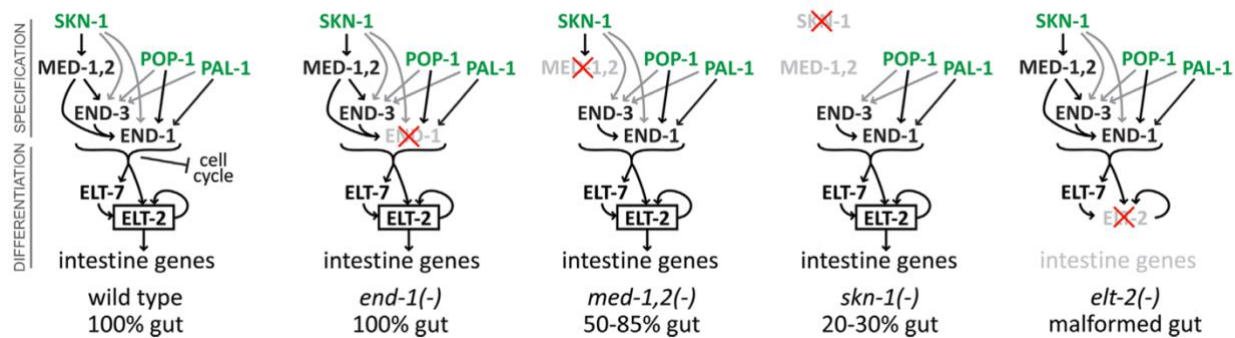
Figure 5 - The transcriptional network specifying C. elegans intestine
Redundant network specifying the worm gut (endoderm). Green proteins are maternal factors. The success of gut differentiation upon knock-out of a single component within the network (red cross) is indicated below the scheme. See main text for more details. Adapted from Maduro 2015.

Several mechanisms contribute to developmental robustness. Firstly, networks of transcription factors essential for the fate specification are often redundant (Fievet et al., 2013; Maduro, 2015; Masel and Siegal, 2009; Sawyer et al., 2011), ensuring reliable outcomes even if a part of the network is perturbed, e.g., by mutation or epigenetic silencing. Another mechanism at play, experimentally demonstrated in *Drosophila*, is the existence of shadow enhancers that can substitute the function of the primary gene enhancer upon its inactivation, and therefore provide redundancy for activation of a required gene product (Hong et al., 2008; Perry et al., 2010).

The specification of the *C. elegans* intestine is an excellent example of a redundant network. It occurs over three rounds of divisions by serial activation of three tiers of GATA transcription factors starting in the EMS blastomere at the 8-cell stage by the expression of MED-1 and MED-2 under the control of the maternal transcription factors POP-1, and SKN-1, as well as the caudal family homeobox protein PAL-1 (Bowerman et al., 1992; Hunter and Kenyon, 1996; Lin et al., 1998). This is followed at the 26-cell stage by downstream activation of END-1 and END-3 in the sole gut precursor E (Maduro et al., 2005; Zhu et al., 1997). END-1 and END-3 gradually accumulate throughout the next cell cycle in the two daughters of E, where they activate the expression of the GATA factors ELT-2, ELT-4 and ELT-7 (Baugh et al., 2003; Fukushige et al., 1998). Moreover, ELT-2 - the only essential TF from the above mentioned trio - activates itself in a feed-forward feedback loop, sealing the enterocyte fate (Fukushige et al., 1999; McGhee et al., 2009). The entire endoderm specification network is remarkably robust thanks to redundancies and feedback loops (**Figure 5**). Removing any single factor from the network, except for ELT-2, does not cause a complete gut specification failure, but rather manifests itself in less penetrant defects (Maduro, 2015). Mutations impairing SKN-1 function lead to incompletely penetrant defects in endoderm specification, whereby only a subset of 20 larval intestinal cells gets specified in about 25% of all embryos as judged by the expression of ELT-2 (Raj et al., 2010). This work also revealed that a certain threshold number of *end-1* transcripts must to be present for the sustained expression of ELT-2 (Raj et al., 2010).

The last two paragraphs focus on genetic redundancy as a mechanism conferring developmental robustness. Embryos are often able to cope with a range of environmental factors and still produce consistent form. Temperature is one of the frequently changing external factors that every organism has to cope with. Every species has its optimal thermal range, in which it can not only survive, but also successfully reproduce (Begasse et al., 2015; Neves and Priess, 2005; Pörtner et al., 2006). Previous work from our laboratory revealed that *C. briggsea* and *C. elegans* are able to cope with changing temperature at their respective thermal limits by characteristic changes in embryo size and shape, reflecting an adaptive response to the non-linear characteristics of the energy production via cellular respiration. Beyond thermal limits, aerobic metabolism fails to match the demands of developing

embryos, leading to increased lethality (Neves et al., 2015). In conclusion, nematode embryogenesis is robust to changes in temperature within a given thermal range.

As mentioned previously, the second division of *C. elegans* embryos is asynchronous, with AB dividing about 2 minutes before P1 at 25°C. Since cell cycle duration as well as *C. elegans* embryogenesis scale with temperature according to Arrhenius kinetics (Begasse et al., 2015), it should be possible to alter timing of individual blastomeres by subjecting them to differential temperatures. Indeed, this has been accomplished in a recent publication by heating P1 with an infrared laser to accelerate the P1 cell cycle, and thus to synchronize the division of P1 with that of AB (Choi et al., 2020). Interestingly, the authors found that such synchronization had little effect on the survival of manipulated embryos, suggesting that *C. elegans* embryogenesis is robust against this perturbation of the second division timing.

Another case where embryos can cope with a perturbation of temperature and still produce consistent form occurs during *Drosophila* embryo development (Lucchetta et al., 2005). Here, the embryo placed into a laminar flow inside a microfluidic device experienced a dramatic temperature step function along its long axis. Given that the pace of cell divisions, as well as the overall developmental rate, scale with environmental temperature both in worm and flies, authors expected a misalignment of development at the anterior and posterior portions of the embryo. Indeed, after 2.5 hours at 17/27°C step, nuclei on the warmer half of embryo were two cell cycles ahead. Despite this, embryos left afterward at a uniform temperature developed into healthy larvae with the right amount of body segments, suggesting the existence of a compensation mechanism that can bring the two halves of the embryo back in synchrony and ensure proper segmentation. The authors demonstrated that segmentation precision monitored by Even-skipped distribution was normal, despite an altered temporal sequence at which Even-skipped stripes resolved, but were not able to identify the compensation mechanism occurring later. Nonetheless, the fact that embryos developed into healthy larvae under such unnatural conditions underscores the remarkable developmental robustness of *Drosophila* embryos.

In addition to temperature, developing systems must cope with external forces or geometries of the egg imposed by the mother. Several reports quantitatively characterized the response to altered shape and/or size in sea urchin, ascidian, mouse, zebrafish, and worm embryos (Dan, 1979; Gray et al., 2004; Hertwig, 1884; Niwayama et al., 2019; Pierre et al., 2016; Yamamoto and Kimura, 2017). Many studies focused on spindle positioning during early cleavages in cells with changed 3D shape, revealing that, in the absence of dominant cell polarity, spindles will orient along the longest axis of the cell, which can change upon compression (Minc et al., 2011).

One study in *C. elegans* took a step further and compared the development of compressed and wild-type embryos using cell lineage tracing (Jelier et al., 2016). This study revealed that a distorted LR axis in compressed embryos gets corrected at around the ~100-cell stage, close to the wild-type geometry by a coordinated movement of many cells. Furthermore, the authors were able to identify a single cell on the dorsal surface of embryo called ABarppap that generates forces necessary for this coordinated movement by changing its shape. This example illustrates one of many not fully understood mechanisms employed during metazoan embryogenesis to cope with environmental variability to generate viable and remarkably uniform embryos robustly.

1.5   Objectives of the thesis

Early metazoan embryogenesis is characteristic by rapid cell cycles alternating between DNA replication (S phase) and cell divisions, or cleavages (M phase), without intervening gap (G1, G2) phases and growth. Therefore, ACDs should be tightly controlled to generate blastomeres of appropriate sizes, at the right time and in the correct arrangement to allow for proper morphogenesis within the confined space of the eggshell (e.g., in nematodes), the vitelline membrane (e.g., in amphibians), or the zona-pellucida (in mammals). While in some organisms, this constrained environment is relieved during embryogenesis, potentially allowing embryos to correct errors in cell size, in other cases, including in nematodes, this is not possible because embryos develop in isolation from the outside world until hatching as a fully-formed larva.

However, the possible importance of unequal cell volumes for faithful development is still somewhat hypothetical and poorly studied. The *C. elegans* embryo appears to be an excellent model to study this subject since it exhibits a series of early unequal cleavages during its stereotypic development. Several lines of evidence suggested that unequal cell volumes of AB and P1 stemming from the first division might be important for *C. elegans* embryogenesis. First, the volume asymmetry between AB and P1 is tightly controlled and has a very low variation (3.5%) between embryos (Kemphues et al., 1988). Second, the asymmetric size of AB and P1 is a feature shared among many related nematode species in the *Rhabditidae* genus (Brauchle et al., 2009).

Therefore, we decided to manipulate AB/P1 volume asymmetry to address the following general questions:

1. Is there a requirement for precise cell size control in early *C. elegans* embryogenesis?
2. If so, what are the limits beyond which developmental programs can no longer handle such alterations?
3. How do embryos cope with altered AB/P1 blastomere volumes?
4. What are the consequences of changed AB/P1 cell volumes for developing embryos in terms of cell cycle timing, cell positions, and fate?

2 Results

2.1 Manipulation of size asymmetry using *lin-5(ev571)*

To test whether cell size asymmetry between AB and P1 arising during the first division of the *C. elegans* zygote is important for development, we envisaged two methods to render the first division equal in size, while preserving anterior-posterior polarity cues.

The first method took advantage of the previously described temperature sensitive *lin-5(ev571)* allele, which encodes a mutant LIN-5 protein. In the wild-type, LIN-5 tethers the molecular motor dynein to the cell cortex and is therefore essential for cell-size asymmetry of the first embryonic division (Fisk Green et al., 2004; reviewed in Rose and Gönczy, 2014). The LIN-5 variant encoded by *lin-5(ev571)* carries a three amino acid insertion in its coiled-coil domain, which perturbs the heptad repeat register required for homodimerization, likely underlying its temperature sensitivity (Fisk Green et al., 2004) (**Figure 6**).
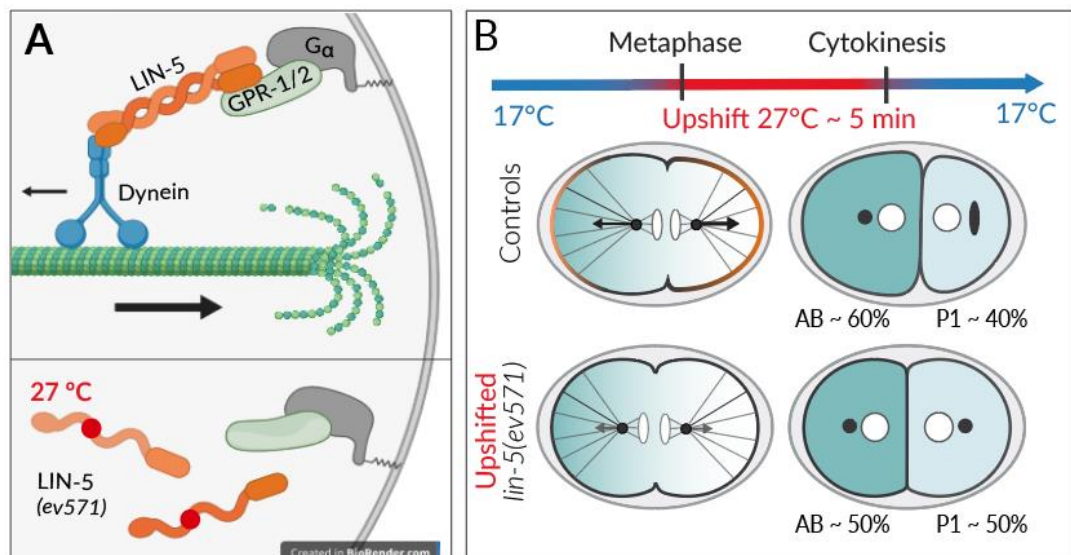
Figure 6 - Scheme of the transient temperature upshift experiment using lin-5(ev571) embryos

(**A** - top) The cortical ternary complex comprised of Gα, GPR-1/2 and LIN-5 tethers cytoplasmic dynein to the plasma membrane and mediates pulling forces acting on astral microtubules, resulting in extension and posterior displacement of the mitotic spindle. (**A** - bottom) The Temperature sensitive *lin-5(ev571)* allele encodes a LIN-5 protein with a 3-amino acid insertion in the coiled-coil domain (red circles), which at the restrictive temperature destabilizes self-dimerization, impairing cortical force generation. (**B**) (top) Scheme of transient metaphase upshift of control and *lin-5(ev571)* embryos. Embryos were upshifted after nuclear envelope breakdown (NEBD), or at metaphase, for strains with fluorescently labelled histones, until completion of cytokinesis (~5 minutes) and then reverted back to the permissive temperature of 17°C to restore LIN-5 function. Development of such embryos was followed to score the resulting phenotypes. (**B** - bottom) Control embryos divide unequally due to enrichment of LIN-5 at the posterior cortex (orange shading) producing a larger net pulling force towards the posterior pole of embryo (black arrows, length indicates amount of net pulling forces), displacing the mitotic spindle towards the posterior pole. The cytokinetic furrow then bisects the spindle midway, resulting in a larger anterior AB and a smaller posterior P1 cell. Pulling forces are globally diminished upon upshift of *lin-5(ev571)* to 27°C, resulting in an equalized (EQ) division, producing AB and P1 cells with similar sizes. Embryos are oriented with the anterior pole to the left in this and all following figures.

15

Figure 7 - Upshift of lin-5(ev571) embryos results in equalized first cell division
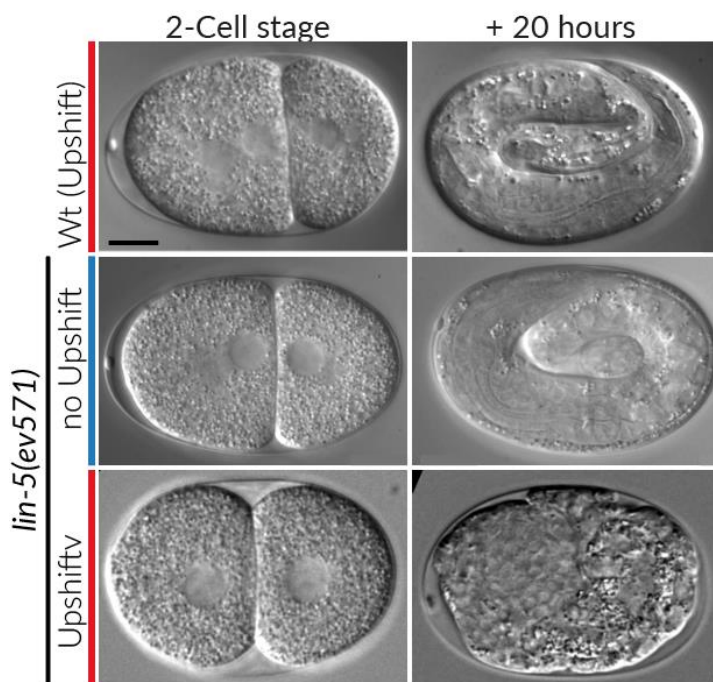
Frames from timelapse DIC series showing 2-cell stage embryos after a transient upshift to 27°C and outcome of development 20h at 17°C after the first mitosis. Wild-type embryos divide unequally in spite of the upshift and develop into 3-fold larvae that later hatch. The *lin-5(ev571)* mutants imaged at the permissive temperature (17°C) divide unequally and develop into normal 3-fold larvae that later hatch. Transient upshift of *lin-5(ev571)* embryo during the first division leads to equalized division of AB and P1 (see Figure 8 for distribution of cell sizes). Equalized cell volumes lead to embryonic lethality in about 65% of such embryos. Scale bar: 10 μm.

Inactivation of *lin-5* by RNAi or by permanent upshift of *lin-5(ev571)* to the restrictive temperature of 25°C leads to equalized (EQ) cell sizes after the first cleavage, but also to perturbation of all following divisions, resulting in fully penetrant embryonic lethality (Fisk Green et al., 2004; Horvitz and Sulston, 1980; Srinivasan et al., 2003).

Fortunately, we found that *lin-5(ev571)* is a fast-acting temperature-sensitive allele. Transient upshift of *lin-5(ev571)* one-cell embryos to 27°C for ~5 minutes from metaphase until the completion of cytokinesis inhibited cortical pulling forces that would normally cause posterior spindle displacement during anaphase. LIN-5 inactivation manifested itself through a lack of spindle rocking and the absence of anaphase posterior spindle displacement (**Figure 6B, Figure 7, Movie S1-3**). Consequently, the cleavage furrow bisected the centrally positioned spindle, producing two relatively equally sized AB and P1 cells (mean relative AB size 51.2 ± 2.8 %, **Figure 8A, Figure 7, Movie S3**). After completion of the first cleavage, embryos were reverted back to the permissive temperature of 17°C to restore LIN-5 function allowing subsequent divisions to proceed[1]. Note that upshifted wild-type N2 (WT) embryos divided unequally (AB size 59.3% ± 2.0 SD), and the temporary higher temperature treatment had no obvious deleterious effects on their development (**Figure 8A-B, Movie S1**).

We conclude that transient upshift of *lin-5(ev571)* zygotes during the first mitosis enables us to obtain embryos with relatively equally sized AB and P1 cells.

---

[1] Note that we chose a slightly higher temperature of 17°C compared to the originally described permissive temperature of 15°C to speed up experiments, as embryonic development is faster at this temperature, as well as to facilitate cooling of equipment and microscopes during long-term imaging experiments.
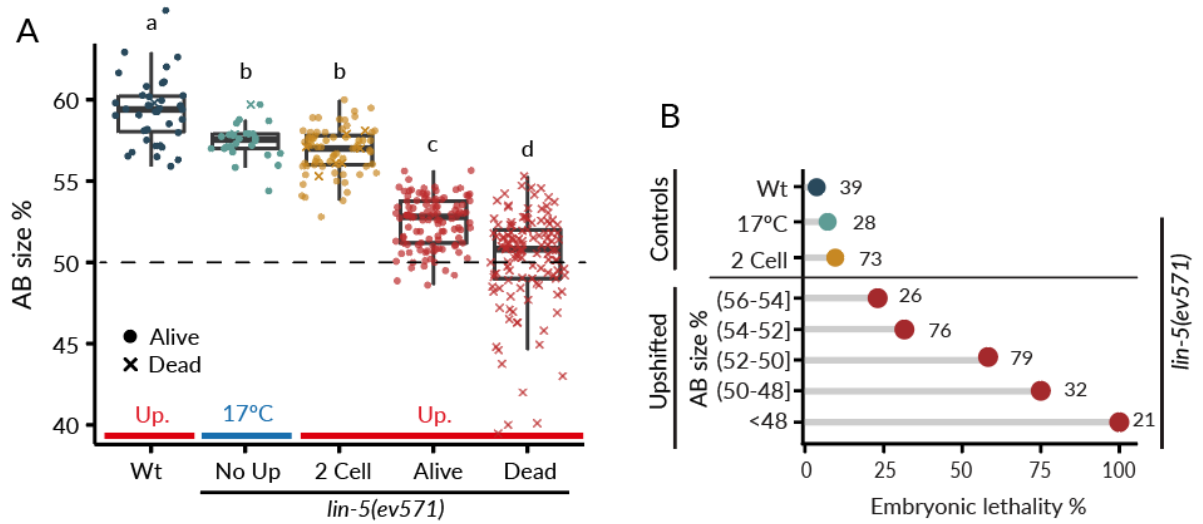
Figure 8 - Cell size distribution and lethality in upshifted embryos

(A) Distribution of relative AB sizes (at the mid-plane) after metaphase upshift (Up.). "2 Cell" indicates a control upshift of *lin-5(ev571)* embryos early at 2-cell stage, No Up indicates that embryos were kept at 17°C for the entire duration of the experiment. Wild-type (Wt) embryos were upshifted during the first division in the same way as *lin-5* embryos. Dashed line indicates equal size of AB and P1. Two groups are significantly different (p < 0.05, Tukey HSD) if they have a different letter above the boxplot. (B) Embryonic lethality of embryos from panel A. Lethality of equalized *lin-5(ev571)* embryos increases with decreasing size of AB. Upshifted embryos were split in 2% bins, values indicate total number of recorded embryos in each bin.

2.1.1 Inversion of the size-asymmetry results in complete embryonic lethality

We then followed development of upshifted embryos using combined DIC and fluorescence time-lapse microscopy to analyze phenotypes arising from equalized cell sizes. Moreover, we assessed whether embryos reached a morphologically normal, motile, 3-fold stage. Such upshifted embryos, as well as equalized embryos that hatched, were categorized together as equalized alive (EA); the remaining embryos were categorized as equalized dead (ED).

To assess the importance of cell size asymmetry of the first division, we first correlated the incidence of lethality in upshifted *lin-5(ev571)* embryos versus relative AB size (**Figure 8B**). We observed that lethality gradually increased as AB and P1 became closer in size. Furthermore, all embryos with AB smaller than 48% of the total embryonic volume died (hereafter referred to as inverted, or INV, since AB is smaller than P1), establishing the existence of a size-asymmetry threshold for successful embryogenesis and, thus, for viability.

Interestingly, we noted that about 40% of embryos with equalized cell size (alive and dead considered together, EQ) were able to complete embryonic development despite the lack of substantial size asymmetry after the first cleavage (**Figure 8B**). We will focus on understanding possible differences between equalized embryos that survive and those that die later in this thesis.

2.1.2   Control upshift of unequal *lin-5(ev571)* embryos causes only a negligible lethality

Next, to exclude possible unspecific effects of *lin-5(ev571)* on embryonic lethality unrelated to equalization, we upshifted unequal *lin-5(ev571)* embryos early at the two-cell stage for ~5 minutes (the same duration as for the metaphase upshift) and determined their lethality. We observed only a slightly elevated lethality (9.6%, n=73) in comparison to non-upshifted *lin-5(ev571)* embryos imaged at 17°C (7.1%, n=28), suggesting that there is no drastic effect of *lin-5(ev571)* at the permissive temperature later in embryogenesis. This notion is supported also by the reported on-plate embryonic lethality for *lin-5(ev571)* of ~3% at 15°C (Fisk Green et al., 2004) and by our own on-plate measurement showing 2.5% lethality at 17°C (n=394). These measurements are comparable to the 2.6% on-plate embryonic lethality of WT embryos (n=427). The mild increase of lethality among imaged embryos in comparison to embryos laid on plates can possibly be attributed to dissection, handling, phototoxicity and embryo compression due to mounting on the agarose pads or between coverslips separated by plastic beads (see Methods). Note that the *lin-5(ev571)* strain used for the majority of experiments expressed in addition the plasma membrane marker GFP::PH and mCherry::H2B labeling nuclei, exhibiting on plate lethality of 4.7% (n=829), closer to that of the imaged embryos above (i.e. 7.1%,).

2.2   Terminal phenotypes of equalized embryos

Interestingly, we found that equalized and inverted *lin-5(ev571)* embryos that will eventually die <u>never elongate</u> into a worm-like tubular shape (0/ ~150 dead embryos examined). This phenotype reflects a failure of ventral epidermal closure, eventually resulting in extrusion of gut and mesodermal tissues due to lateral compressive forces acting on the embryo as muscles start contracting (**Figure 9, Movie S8** and **S9**, n > 20 dying embryos filmed during ventral closure). Differentiated intestine, pharynx, and neuronal tissues were apparent by DIC microscopy 20 hours post-fertilization. Besides, deformed embryos were always twitching, suggesting that at least some muscles had differentiated (**Movie S9**). Similar phenotypes were reported for cadherin and catenin mutants with impaired mechanical integrity of adherent junctions (reviewed in Michaux et al., 2001), or mutants failing to complete ventral closure due to defective differentiation of ventral neuroblasts (Chin-Sang et al., 1999). Since ventral closure represents the very last step of *C. elegans* gastrulation, we can only speculate about the underlying reason for this phenotype, which occurs after nearly 10 rounds of division at the ~570 cell stage. Because of the countless number of potential causes for such failure of ventral epidermal closure, we did not investigate this late phenotype in depth, but rather attempted to understand earlier events following the first equalized cleavage.
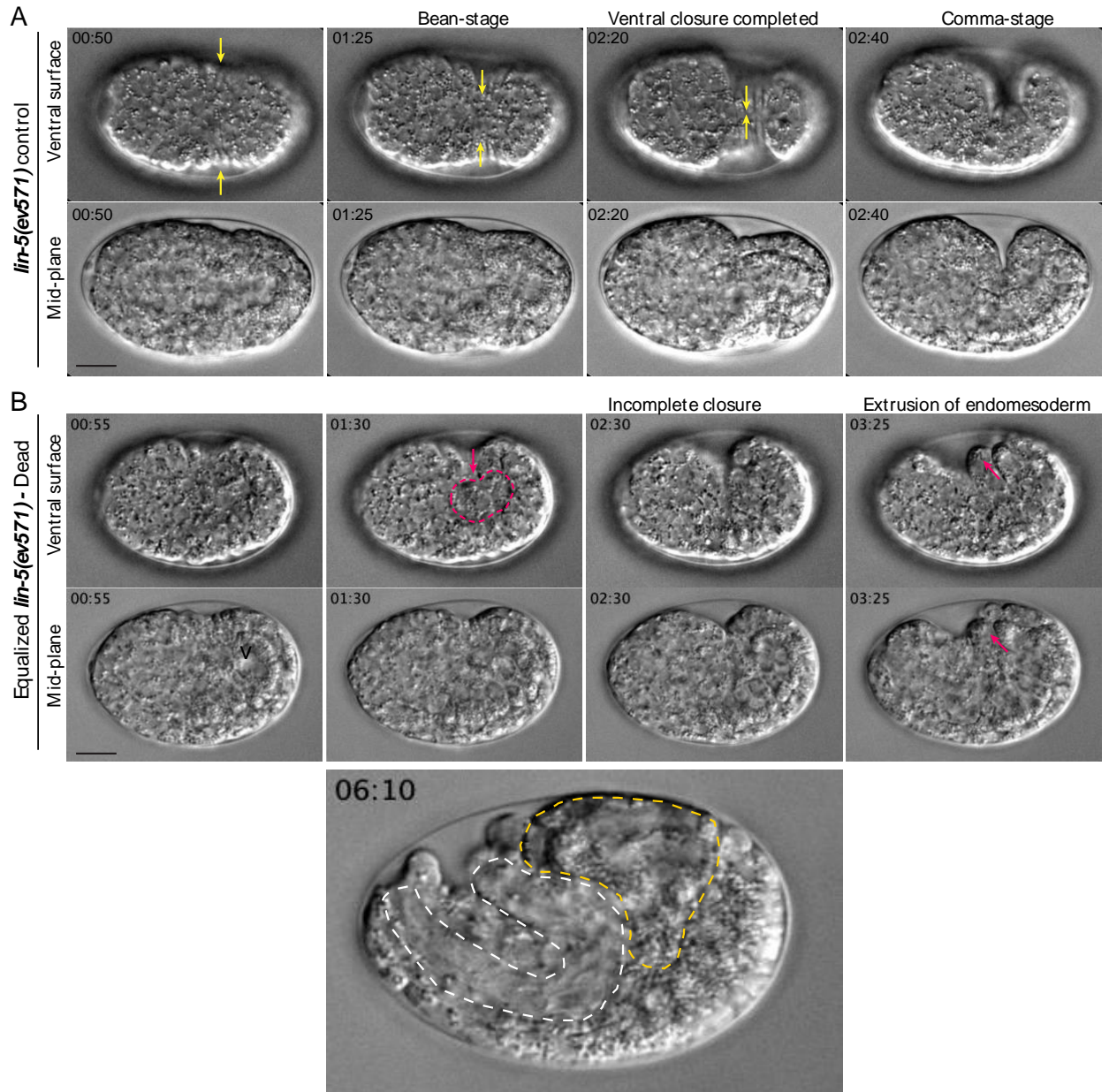
Figure 9 – Failure of ventral epidermal closure in equalized embryos

(A) Four frames from time-lapse DIC recording of ventral closure of hypodermis (skin) in control unequal embryo. Hypodermal cells migrate from both sides of the embryo towards the ventral midline (yellow arrows indicate movement), where they meet and seal the embryo in a continuous skin layer. Completed epidermis closure is essential for embryo elongation from a "ball" of cells into a tubular worm-like. Embryo flips on the side at the comma stage as the elongation phase of morphogenesis begins. **(B)** Incomplete ventral closure in equalized embryo (red dashed area), leading to the extrusion of internal tissues (red arrows) due to opening in the skin. The resulting phenotype at 06:10 shows an embryo with a visible part of the pharynx (white dashed area) and gut tissue (orange dashed area) squeezed outside of the body cavity. Scale bar: 10 μm, time in hours::minutes. Time 0 corresponds to about 6 hours after the first cleavage at 17°C when the first lateral movements of ectoderm begin and become visible as a mild lateral contraction of embryo.

2.3 Embryos equalized by optogenetic recruitment of LIN-5 to the anterior cortex display a similar lethality profile to *lin-5(ev571)* upshifted embryos

The second approach for equalizing the first division relied on a targeted optogenetic recruitment of LIN-5 to the anterior cortex during mitosis to counteract the larger posterior pulling forces, and, thus, maintain the spindle in the center of the embryo. While the transient *lin-5(ev571)* upshift temporarily inhibited cortical force generation globally, this optogenetic approach maintains normal cortical pulling forces at the posterior cortex, but introduces ectopic balancing force generation at the anterior cortex. The aim of this alternative method was to validate the observation of embryonic lethality in equalized *lin-5(ev571).*

To achieve equalization of the first division with optogenetics as described above, we used a system allowing to recruit LIN-5 to ectopic locations in the *C. elegans* zygote (Fielmich et al., 2018). This optogenetic system relies on LOV::PH::GFP permanently bound to the plasma membrane by the phosphoinositide binding PH domain and on endogenously tagged LIN-5::ePDZ::mCherry, which can be recruited to a desired portion of the membrane by localized induction of LOV<-> ePDZ interaction with 488 nm light (**Figure 10A**). To render the first division equal, we ectopically recruited LIN-5::ePDZ::mCherry to a small region of the anterior cortex to balance posterior pulling forces from NEBD until the end of mitosis (**Figure 10B-E, Movie S4**). This method worked relatively reliably allowing us to obtain a range of AB/P1 sizes. One embryo (a single outlier in **Figure 10B**), however, seemed irresponsive to anterior recruitment of LIN-5, perhaps due to overall spurious activation of the ePDZ<->LOV by ambient light prior to imaging, as evidenced by vigorous spindle oscillations already at the beginning of the experiment (not shown). Similar to the *lin-5(ev571)* upshift experiment, we followed the outcome of development in optogenetically manipulated embryos. We observed a similar trend of increased lethality with decreasing relative AB size and detected the same threshold of 48% AB size below which all embryos failed to develop (**Figure 10D**).

Despite the fact that both methods that we used to equalize the first division relied on manipulating either LIN-5 function or distribution, they nonetheless provide partially independent evidence pointing to a critical role of cell size asymmetry for the *C. elegans* embryogenesis.

Next, we set out to investigate the underlying mechanisms of lethality in manipulated embryos in greater detail. Our questions included:

1) What are the differences during embryogenesis in equalized embryos in comparison to controls?

2) What distinguishes equalized embryos that live from those that die?

We used the *lin-5(ev571)* mutant strain for all the remaining experiments presented in this thesis as this was the first method available at the start of this project, and because *lin-5(ev571)* was easy to cross with strains carrying fluorescent markers, in contrast to the optogenetic strain in which the LOV and ePDZ fluorescent fusions already occupied both GFP and mCherry channels, respectively.

Figure 10 - Equalization of the first division by optogenetic recruitment of LIN-5 *to the anterior cortex.*
(A) Scheme of optogenetic-mediated LIN-5::ePDZ::mCherry recruitment to the cortex by activation of PH::eGFP::LOV (Fielmich et al., 2018) using a 488 nm laser. A helix in the PH::LOV domain unfolds upon illumination with blue light, allowing binding of ePDZ (B, C) Relative AB size in embryos equalized by optogenetic recruitment of LIN-5::ePDZ::mCherry to the anterior cortex (blue rectangle in C) during metaphase/anaphase to balance posterior pulling forces generated due to enrichment of endogenous ternary complex at the posterior (orange). (D) Lethality following optogenetic equalization, same data as in B. Note that inverted embryos with AB < 48% always died, in agreement with the *lin-5(ev571)* upshift data. The category "Plates" refers to unimaged embryos that were scored for hatching after being laid on agarose plates by young hermaphrodites during one day. (E) Sequence from timelapse recording of optogenetically equalized embryo (AB size 48.7%). LIN-5::ePDZ::mCherry was recruited to the anterior cortex from metaphase until completion of cytokinesis by scanning of the 488 nm laser in the rectangular region (white dashed rectangle). Note that LIN-5 localizes to the spindle and centrosomes independently of its cortical function through its microtubule binding activity and that LIN-5 is encoded by an endogenous allele with an in frame insertion of ePDZ::mCherry, hence resulting in the fusion protein localizing to the posterior cortex during anaphase as in the wild-type, see Movie S4. Scale bar 10 μm.

A

LOV::PH::GFP

LIN-5::ePDZ::mCh

+ 488 nm
LOV ↔ ePDZ
interaction

B Optogenetic recruitment
LIN-5::EPDZ, LOV::GFP::PH

AB size %

- Alive
- Dead

No light   Anterior
Recruitment

C

+488 nm

Recruited
LIN-5::ePDZ   Endogenous
LIN-5

force balance

D

AB size %

Plates   299
(60-56]   6
(56-52]   8
(52-50]   7
(50-48]   6
<48   5

Embryonic lethality %

E

	Transmitted light	LIN-5::ePDZ::mCherry	PH::EGFP::LOV
NEBD	00:00	LIN-5 cytoplasmic	488 nm OFF
Anaphase	01:30	Anterior LIN-5 recruitment	488 nm ON
Cytokinesis	05:00		488 nm ON
2 Cell	06:50		488 nm OFF
late 2 Cell	13:30	LIN-5 cytoplasmic	

22

2.4   AB and P1 in equalized embryos are polarized nearly normally

Symmetry of the initially unpolarized *C. elegans* zygote is broken in response to a sperm component after fertilization (Goldstein and Hird, 1996; Sadler and Shakes, 2000). As a result, mutually exclusive cortical domains of PAR polarity proteins are established along the long axis of the embryo, thus defining the first principal embryonic AP axis (reviewed in Rose and Gönczy, 2014). The *par* mutants, as well as mutants of downstream cytoplasmic polarity mediators such as *mex-5/6*, result in fully penetrant embryonic lethality as both AB and P1 assume either completely anterior or posterior fates, depending on which gene of the polarity network is perturbed (Draper et al., 1996; Kemphues et al., 1988; Schubert et al., 2000).

To verify that upshifted *lin-5(ev571)* embryos were polarized normally in spite of dividing equally, we investigated the distribution and intensity of the key polarity protein PAR-2, which is normally enriched at the posterior cortex, and of the cytoplasmic polarity mediator MEX-5. First, we imaged embryos expressing endogenously tagged GFP::PAR-2 and measured the total intensity of GFP in the cytoplasm and at the cortex in AB and P1, serving as a proxy for total protein amount. We expressed the data as mean pixel intensity, which should correspond to the average concentration of total PAR-2 in each cell. We did not detect a significant difference in GFP::PAR-2 intensity in AB or P1 between unequal control and upshifted *lin-5(ev571)* embryos, nor in the P1/AB ratio of GFP::PAR-2 (**Figure 11A-C**).

Next, we imaged the distribution of the RNA-binding zinc-finger polarity mediator MEX-5, which is normally enriched in the anterior cytoplasm prior to the first division (Schubert et al., 2000). We discovered that MEX-5 still distributes in a graded fashion along the AP axis of equalized *lin-5(ev571)* embryos, indicating that PAR-dependent AP polarity cues responsible for such a graded distribution are functional. Interestingly, in addition, we found that the intensity of endogenously tagged mCherry::MEX-5 was elevated by about 8% in P1 of upshifted embryos in comparison to unequal *lin-5(ev571)* controls (**Figure 11F**). This difference can be likely explained by the positioning of the cytokinetic furrow closer to the anterior pole in upshifted embryos, which consequently bisects the MEX-5 gradient more anteriorly than in the unequal controls. Thus, P1 in equalized embryos inherits part of AB destined cytoplasm raising the final MEX-5 concentration in this blastomere.

We conclude that equalized *lin-5(ev571)* embryos display nearly normal polarity. While there is no difference of cytoplasmic PAR-2 concentration in AB and P1 in equalized embryos, MEX-5 seems to be mildly, but significantly increased in P1, as expected from the altered cleavage furrow position in such embryos.
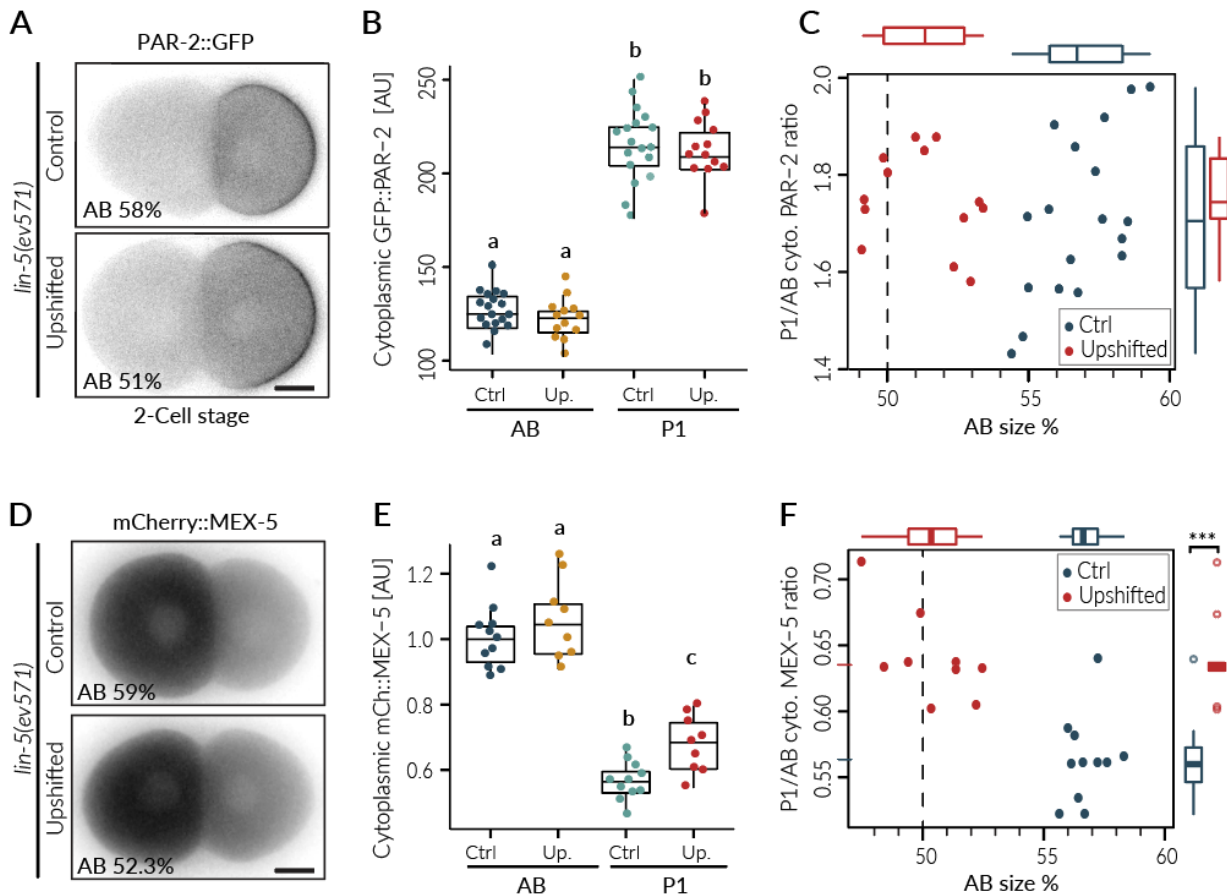
Figure 11 - Polarity in equalized embryos

(A) Localization and intensity of endogenously tagged GFP::PAR-2 in equalized (Upshifted) and unequal control *lin-5(ev571)* embryos. Scale bar: 10 μm (B) Quantification of mean cytoplasmic GFP::PAR-2 intensity in AB and P1 cells in embryos such as those shown in panel A. (C) Same data as in panel B expressed as the P1/AB fluorescence intensity ratio. (D) The polarity mediator MEX-5::mCherry is enriched in AB. A strain carrying endogenously tagged *mex-5* allele was used. Scale bar: 10 μm. (E) Quantification of cytoplasmic MEX-5::mCherry fluorescence intensity in AB and P1 cells (data from panel D). Fluorescence intensity was normalized to the mean AB intensity in control embryos for every experimental batch due to the high variability in absolute intensity levels between batches. (F) Relative amounts of endogenously tagged GFP::PAR-2 with respect to mean fluorescence in AB. Multiple comparisons in B and E were performed using Anova and Tuckey honest significant difference (HSD) post-hoc test. Two boxplots that do not share the same letter are significantly different from each other with $p < 0.05$. Cytoplasmic intensity ratios in panels C and F were compared with the Welsh two sample *t*.test. Vertical dashed lines in C and F indicate equal size of AB and P1.

2.5 Decreased asynchrony of the second division in equalized embryos

The second embryonic division of *C. elegans* was shown previously to display tightly controlled asynchrony, whereby AB divides ~120 seconds before P1 at 25°C (reviewed in Budirahardja and Gönczy, 2009), and ~210 s before P1 at 17°C (our data). The unequal sizes of AB and P1 in combination with the asymmetric localization of several factors controlling cell cycle progression, including PLK-1, were shown to underpin this division asynchrony.

Previous experiments using RNAi-mediated knockdown of *lin-5* or *gpr-1/2* revealed the cell-size dependence of this asynchrony (Brauchle et al., 2003; Budirahardja and Gönczy, 2008). Depletion of these proteins renders the first division equal but also impairs all following cell divisions, as discussed above. We set out to verify that the asynchrony between AB and P1 is recapitulated in equalized *lin-5(ev571)* embryos obtained through an acute temperature upshift. Using this method, we obtained a range of AB/P1 sizes in *lin-5(ev571)* embryos carrying fluorescent histone fusion H2B::mCherry and determined the delay between metaphase to anaphase transition in AB and P1. We found a strong correlation of this delay with the initial size asymmetry (**Figure 12A**, Pearson correlation r=0.81,
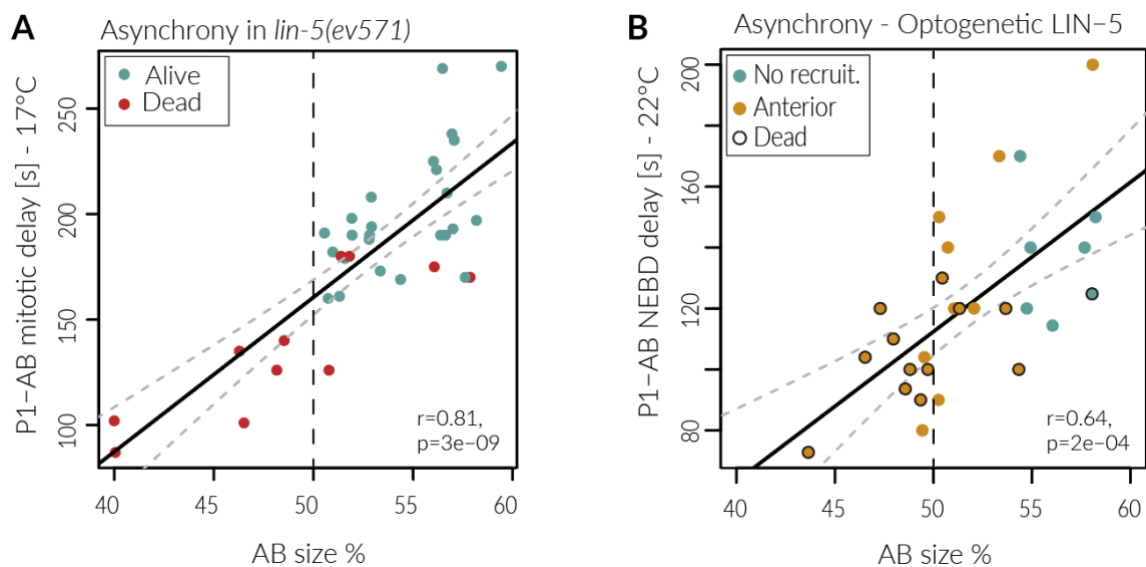
Figure 12 - Asynchrony of the second division correlates with cell size asymmetry.
(**A**) Division asynchrony in *lin-5(ev571)* embryos as a function of relative AB size quantified as a delay between metaphase to anaphase transition in P1 versus AB in embryos expressing mCherry::H2B. Embryos were upshifted to 27°C for ~5 min either at metaphase or in the early two-cell stage, and shifted back to 17°C for the rest of the experiment. (**B**) A similar correlation between AB size and asynchrony of the second division was observed in optogenetically equalized embryos, as determined by the delay between AB and P1 nuclear envelope breakdown; this plot includes unequal controls not exposed to blue light. r indicates Pearson correlation coefficient, p-value was determined based on Student's t-distribution for Pearson's correlation coefficient. Dashed lines indicate 95% confidence interval for the fitted linear function. Vertical dashed line indicates equal sizes of blastomeres. Note that the two experiments were performed at different temperatures, hence the absolute timing is not the same. Residual asynchrony in equal embryos is due to differential regulation of cell cycle pace by PLK-1 and other factors.

P=3e-9). Interestingly, even inverted embryos (AB smaller than P1) displayed residual asynchrony, indicating that they were still polarized, and that cell size is only one of several factors underlying asynchronous division (**Figure 12A**). We obtained similar results by measuring the difference in timing of nuclear envelope breakdown (NEBD) between AB and P1 in optogenetically manipulated embryo, whereby LIN-5::ePDZ was recruited to the anterior cortex to equalize the first division (**Figure 12B**, r=0.64, P=1.8e-4, same embryos as in **Figure 10**).

We conclude that the unequal cell size of AB and P1 contributes to cell division asynchrony, in agreement with previously published results from our laboratory (Brauchle et al., 2003).

2.6 Restoration of AB/P1 asynchrony does not rescue lethality in equalized embryos

We hypothesized that the accelerated cell cycle of P1 in equalized embryos could contribute to embryonic lethality. For example, a perturbed division timing in different lineages could lead to a physical interference of neighboring cells during division and result in an abnormal cell positioning or cell-cell contacts. If the sole reason for the lethality of equalized embryos was the accelerated P1 cell cycle, we would expect to obtain a higher survival in equalized embryos with restored asynchrony.

Therefore, we attempted to slow P1 back to its normal pace in equalized embryos by exposing its nucleus to 405 nm laser light during early S-phase. This method was used previously in *C. elegans* to slow down the cycle of endodermal cells (Lee et al., 2006). First, we determined a non-lethal irradiation regime in WT embryos that delayed P1 mitosis by an additional ~120 seconds compared to normal timing, while still allowing treated embryos to develop (see Methods for details). We found that the same 405 nm laser light dose applied to P1 in equalized embryos was indeed able to bring AB/P1 asynchrony back to the timing of unequal Ctrl and WT embryos (**Figure 13A**). However, we did not observe any rescue of embryonic lethality in equalized embryos with restored asynchrony, suggesting that accelerated P1 cell cycle progression is not the sole cause of lethality. We noticed that the extent of slow down induced by the 405 nm laser correlated with AB/P1 asymmetry (**Figure 13B**). In other words, a smaller P1 in unequal embryos gets slowed down by about 1.5-times more with the same light dose in comparison to P1 in equalized embryos. This observation is in line with the increased DNA replication checkpoint sensitivity of P1 as a function of cell size reported previously (Brauchle et al., 2003).

In addition, we observed that deceleration of the cell cycle induced in P1 propagated to its P2 and EMS daughters (**Figure 14B**), both in WT and EQ, indicating that more than a single cell cycle is needed to relieve activated replication checkpoint.
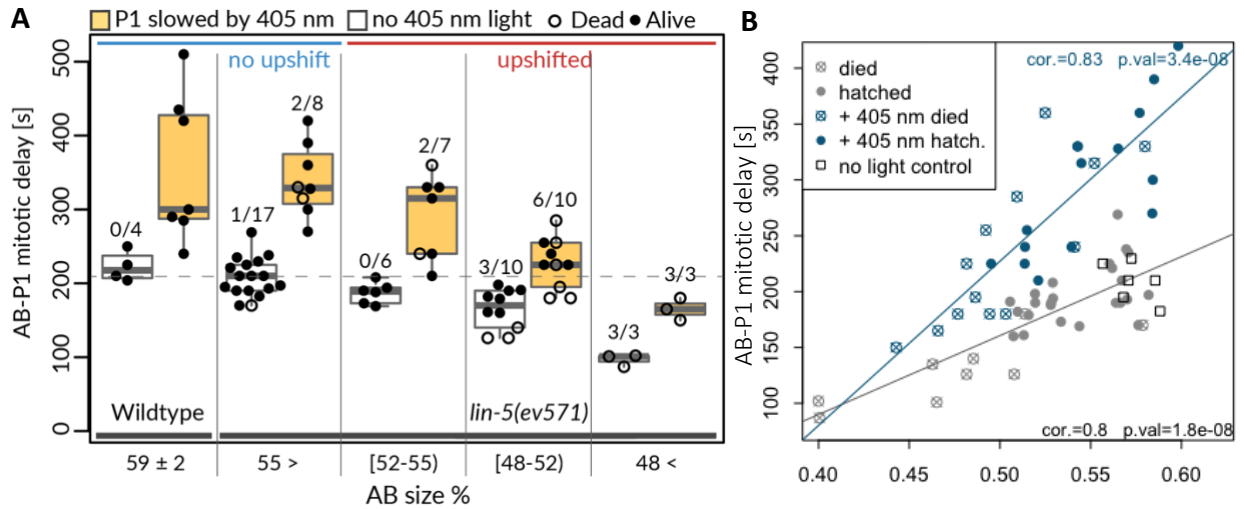
Figure 13 - *Restoring AB-P1 asynchrony in equalized embryos does not rescue embryonic lethality.*

(A) The P1 nucleus was continuously illuminated with the high intensity 405 nm laser light for 250 s following the first division to slow P1 cell cycle progression. This treatment delayed the P1 cell cycle by an additional ~140 seconds in both wild-type (WT) and unequal *lin-5(ev571)* control (Ctrl) embryos in comparison to untreated embryos. Embryos are displayed according to the treatment, genotype, and relative size of the AB cell, as indicated. Note that despite restoring asynchrony between AB and P1 to the control duration of ~210 s in illuminated EQ embryos (bin 48-52%), their lethality was of ~60%, comparable to the global lethality of ~63% in EQ embryos (see Figure 8). Numbers above boxplots indicate dead/total number of embryos imaged in each bin. (B) Same data as in A, showing the mitotic delay as a function of relative AB size. This plot highlights different slopes of the fitted linear regressions, indicating that the sensitivity of the embryo to a damage induced in P1 by 405 nm irradiation depends on the relative asymmetry, as the smaller P1 in control embryos is slowed down more so than in equalized embryos.
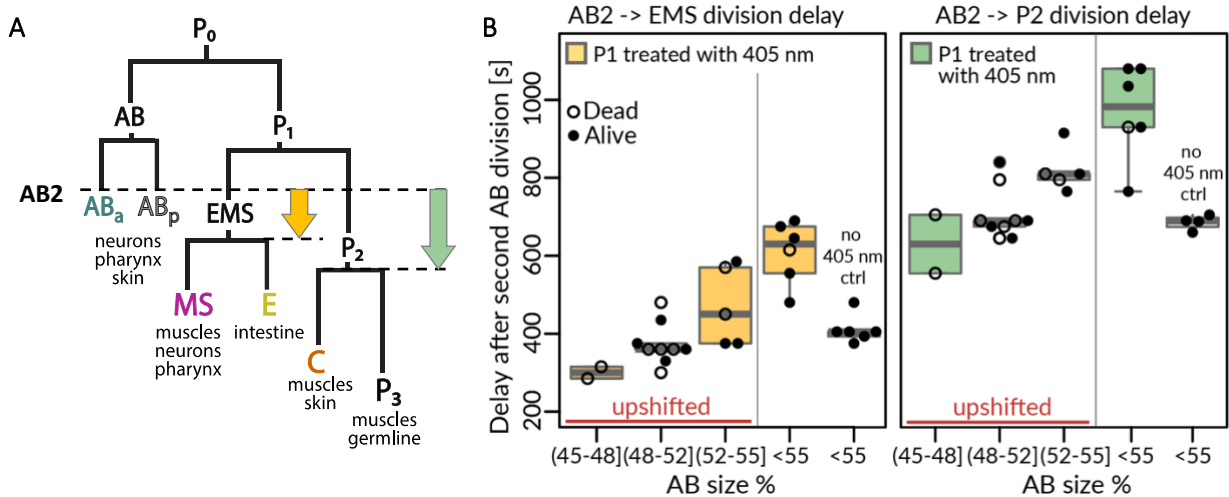
Figure 14 – *Delay induced in P1 propagates to its daughters EMS and P2 in equalized embryos*

(A) Cell lineage scheme of a WT embryo with highlighted timing delays measured in panel B. Time between ABa division and EMS, or P2 divisions (yellow, and green arrows, respectively) was measured in embryos from Figure 14 following P1 slowdown with the 405 nm laser at the early two cell stage. (B) Both EMS and P2 are substantially decelerated after irradiation of the P1 nucleus with 405 nm in equalized *lin-5(ev571)* embryos depending on the degree of initial AB/P1 size asymmetry. around 60% of all upshifted embryos died, in spite of EMS and P2 timing being restored close to the control division pace. Note that not all embryos from Figure 14 were imaged past the second division, hence counts of embryos in some AB size bins do not correspond.

2.7 Defective cell positioning at the four-cell stage in some equalized embryos

In WT embryos, the second division results in a characteristic rhomboid arrangement of the four cells with the most posterior P2 cell being in contact with its sister EMS and one of the AB daughters called ABp. The AB division is symmetrical, yet ABp ultimately acquires a different fate than its anterior sister ABa thanks to Delta/Notch (GLP-1/APX-1) induction from P2 that shares a membrane contact only with ABp (Shelton and Bowerman, 1996) (**Figure 15** – top, and **Figure 16**).

Interestingly, we observed that the second division occasionally resulted in an abnormal four-cell stage configuration in a small fraction of equalized *lin-5(ev571)* embryos, with cells organized in a T-like arrangement (~8%, 9/~120 equalized *lin-5(ev571)* embryos imaged beyond the four-cell stage; 1/20 in optogenetically equalized embryos). In these cases, P2 had no physical contact with ABp and, by inference, the Delta/Notch instructive signaling between these two cells must have been impaired (**Figure 16**, **Movie 5**). All of these embryos were either very close to equal or inverted at the two-cell stage, seemed more elongated, and - without exception - failed to develop into normal larvae (N=10).
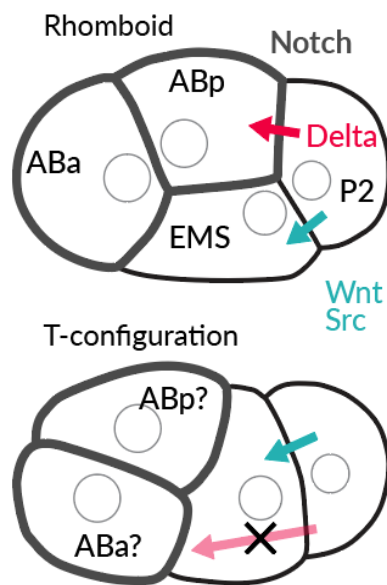
Figure 15 - Four-cell stage geometry and inductive signaling.

(top) Typical rhomboid four-cell stage arrangement critical for differentiation of ABp induced via Delta/Notch signaling from P2, as well as for the polarization of EMS that normally gives rise to the mesoderm lineage MS and to the sole endoderm precursor E through Wnt/Src signaling. **(bottom)** A scheme of an abnormal T-like four cell geometry that occurs in a small fraction of equalized *lin-5(ev571)* embryos and likely prevents instructive signaling between ABp and P2 (see Figure 16 and Movie 5)

Possibly, equal AB and P1 cell sizes in combination with decreased asynchrony might contribute to this rare phenotype. Normally, AB divides well before P1, and the elongation of its mitotic spindle in the transverse direction induces sliding of the posterior pole along the eggshell into a more oblique position, ensuring the rhomboid four-cell stage configuration to come. In some equalized embryos, however, both AB and P1 spindles start extending nearly at the same time, preventing sliding of either cell as forces of elongating spindles balance out (Figure 16, bottom, Movie 5). The same T-like cell geometry was reported for embryos entirely lacking the eggshell and vitelline membrane (Schierenberg and Junkersdorf, 1992). These embryos loose the spatial guidance required to position blastomeres correctly, leading to complete failure of normal cell positioning and eventual death.
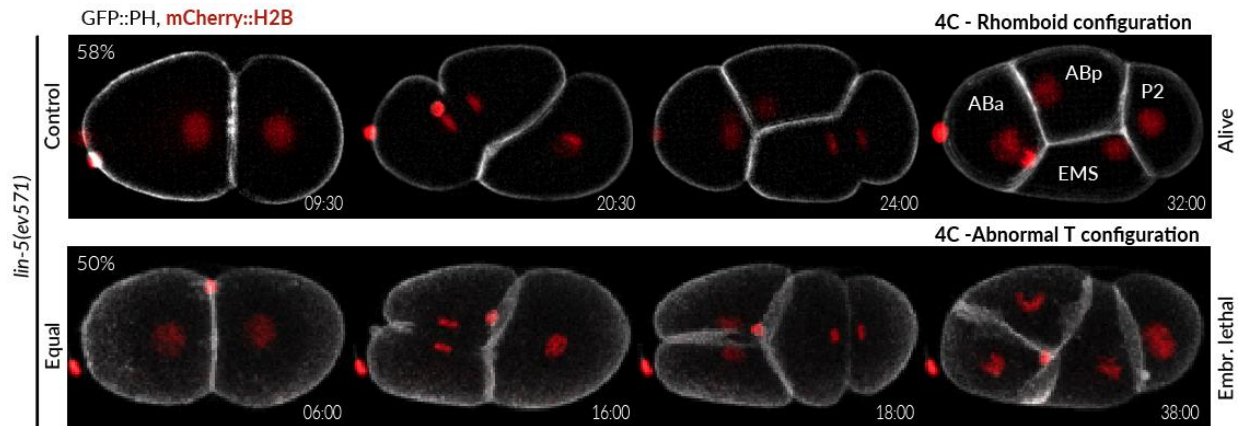
Figure 16 - Aberrant blastomere arrangement at the four-cell stage

(top) During the second round of embryonic divisions, AB normally divides before P1 and skews into an oblique position as its spindle extends, ultimately resulting in the characteristic four-cell rhomboid conformation. **(bottom)** In contrast, AB and P1 divide more synchronously in equalized embryos (embryo shown had AB size 50%), both spindles have similar sizes, and in rare cases, forces generated by dividing cells balance each other out, preventing the lateral skew of AB division, leading to the "T-conformation" whereby P2 has no contact with ABp. All such embryos die (10/10). See also Movie S5.

In conclusion, a small cohort of ED embryos exhibited an early cell positioning defect leading to an abnormal four-cell stage geometry that prevents the essential physical contact between P2 and ABp required for Delta/Notch-mediated ABp induction (**Figure 15**, bottom).

2.8 Cell lineage tracing in equalized embryos

To obtain a more comprehensive understanding of phenotypes arising later in embryogenesis following equalization of the first division, we turned to cell lineage tracing using a *lin-5(ev571)* strain expressing mCherry labelled histone (Bao et al., 2006; Krüger et al., 2015). We aimed to address two principal questions: 1) Are there systematic differences in equalized embryos (EQ) in comparison to unequal controls in terms of cell cycle timing, cell positioning, and cell division orientation? 2) What distinguishes alive equalized embryos (EA) from those that fail to develop and eventually die (ED)?

We lineaged 10 WT, 19 unequal controls (Ctrl), and 62 EQ embryos (25 EA and 37 ED) up to the ~120 cell stage to systematically assess differences between these groups. This work was done in collaboration with professor Rob Jelier from KU Leuven, Belgium, who kindly shared his software and invaluable advice.

First, we analyzed physical variables such as embryo shape (aspect ratio - AR), size, and compression during time-lapse microscopy (**Figure 17**). We used 20 μm polystyrene beads as spacers between the cover slips to maintain compression of embryos constant. However, polystyrene beads are deformable, and depending on the amount of liquid and concentration of beads, sample height varied between 16-27 μm assessed based on the embryo margins visible in the 3D stacks (**Figure 17**).

We noticed that ED embryos tended to be rounder and larger in size, as determined by their 2D cross-sectional surface, and that embryo size was strongly anticorrelated with compression (r= -0.57, p < 2e-09, **Figure 18**). The AR, however, did not correlate with compression, despite a mild correlation with embryo size (r= -0.31, p = 0.003), suggesting that embryo shape is affected by embryo size independently of compression. We assume that greater compression leads to an apparent increase in the 2D size of the embryo at the mid-plane when embryos are flatter (**Figure 18**). The degree of compression that lineaged embryos experienced was compatible with normal development of all lineaged unequal WT and unequal *lin-5(ev571)* Ctrl embryos (N=10, and 29, respectively).

Importantly, we found a significant difference in the amount of compression experienced by EA and ED embryos (22 μm, versus 19.8 μm, respectively, p = 0.002, **Figure 17**), suggesting that compression somehow sensitizes equalized embryos and increases their propensity to die (see Discussion).
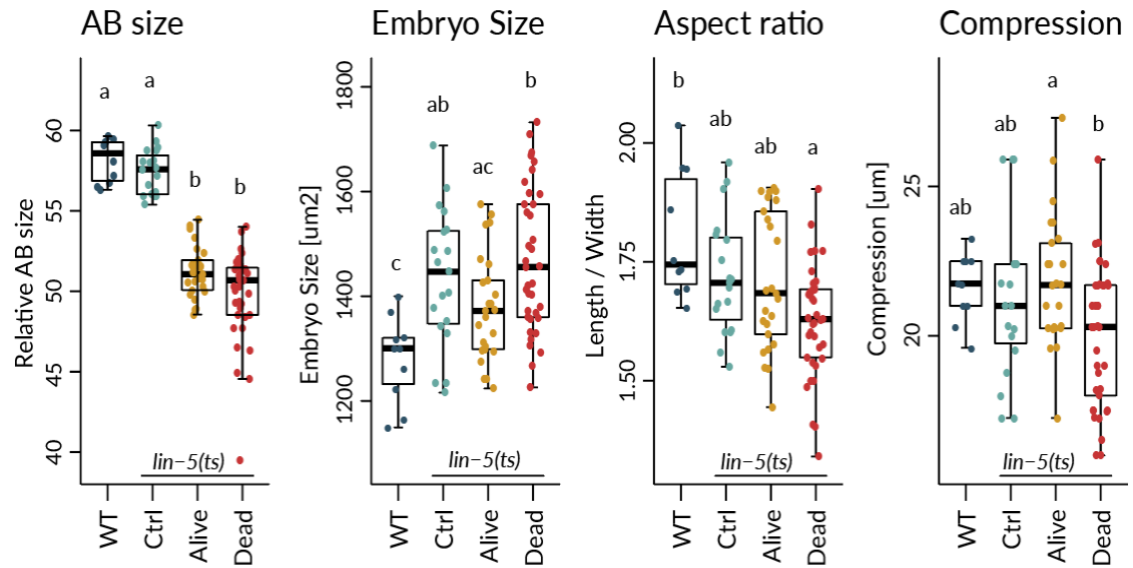
Figure 17 - *Physical parameters of lineage traced embryos*

Asymmetry, size, and aspect ratio and compression in embryos used for lineage tracing. Notably, ED embryos were larger in comparison to EA embryos, likely due to the higher degree of compression. Comparisons were performed using Anova and Tuckey honest significant difference (HSD) post-hoc test. Two boxplots that do not share a letter are significantly different from each other with p < 0.05.
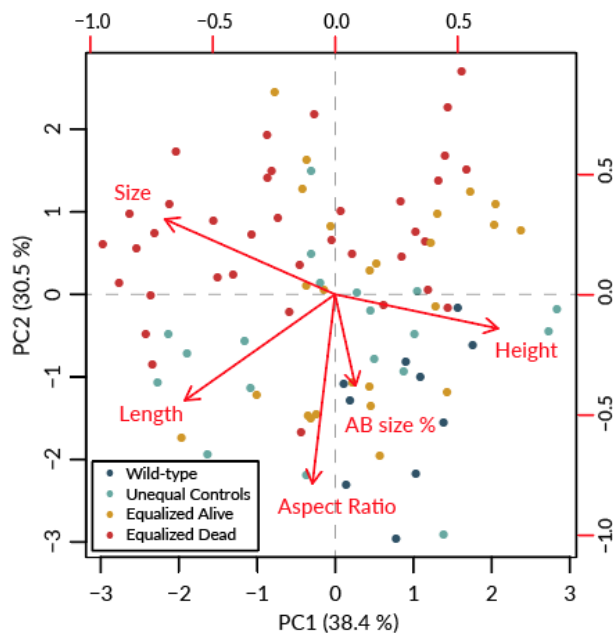
Figure 18 - *PCA of physical parameters*

Principal component (PC) analysis showing relationships between physical parameters in lineaged embryos. Secondary (red) axes indicates loadings (i.e., relative contributions) for the PC1 and PC2. Red arrows indicate contributions of each variable to the respective principal component. Same or opposite direction of two arrows indicates high degree of correlation, or anticorrelation, respectively, between two variables. The embryo 2D size and sample compression (Height), are significantly anticorrelated (Pearson r= -0.57, p < 2e-09) having the exactly opposite direction in the PC1/PC2 projection. The PC2 separates embryos mostly according to the AB size and aspect ratio.

31

Figure 19 - Cell cycles are accelerated in most P1 descendants in equalized embryos.
(A, B) Cell counts in the AB and P1 lineages during development, starting at the four-cell stage, indicating that cells proliferate faster in the P1 lineage, but not in the AB lineage of equalized embryos (time 0 is aligned to ABa division time). Dotted lines and shading in the zoomed region indicate standard deviation. Rectangular region is enlarged on the right **(C)** Graphical depiction of cell-cycle acceleration in individual cells at the 28-cell stage mapped on the control 3D nuclei model. The color scale indicates cell cycle acceleration in equalized embryos relative to unequal *lin-5(ev571)* control timing. The selected timepoint is relevant since it coincides with the onset of gastrulation whereby Ea and Ep cells, which are among the cells whose timing is most affected, start ingressing into the blastocoel. AB and P1 lineage cells are shown separately for clarity. **(D)** Cell cycle duration correlates with initial size asymmetry in most P1 lineage cells (orange), but rarely in AB lineage cells in equalized *lin-5(ev571)* embryos (blue). Note that this analysis included all upshifted and control *lin-5(ev571)* embryos to obtain a reliable correlation of cell cycle duration with the initial size asymmetry. Vertical lines indicate 95% confidence interval for correlation coefficient value. Cells with significant Pearson correlation are indicated by full circle ($p < 0.05$, corrected for multiple testing with the Bonferroni-Hochberg method).

2.8.1 Acceleration of most P1 descendants in equalized embryos.

Next, we investigated cell cycle timing in detail amongst lineaged embryos. First, we plotted the time evolution of AB and P1 lineage cells separately. Strikingly, we observed an apparent divergence between the curves of unequal controls and EQ embryos only in the P1 lineage (**Figure 19A, B**).

Accordingly, we found that most descendants of the enlarged P1, but not those of smaller AB in EQ embryos, experienced significantly accelerated cell cycles in EQ embryos compared to unequal controls (**Table 1, Figure 19C,** and **Appendix Figure S1**).

The vast majority of significantly accelerated cells with shorter cell cycles ($p < 0.05$) were descendants of P1, with P4 being accelerated to last 68% of the normal cell cycle duration (-34 min), D to 86% (-8 min), Ea/Ep and their descendants to ~88% (-8 minutes) of the time taken in unequal *lin-5(ev571)* controls (**Table 1, Appendix Figure S1**). These cell cycle accelerations were highly correlated with the extent of the asymmetry of the first division in many P1 descendants (**Figure 19D**). After adjusting comparisons between groups by Bonferroni-Hochberg (BH) correction to account for false discovery rate, 16/170 tested cells had significantly different cell cycle duration, with 13/16 significant cells originating from the posterior P1 lineage, while only 3/16 originating in the AB lineage. Moreover, the first cell of the AB lineage ABplaa with significantly different cell cycle duration appeared only at the 26-cell stage, while posterior cells were significantly accelerated already at the division of P1, and in all subsequent stages (**Figure 12, Table 1**).

Table 1 – Cell cycle duration in lineaged embryos

Cell	Average cell cycle [min]						Change + Welsh t-test adjusted					Coefficient of variation						Number of embryos					
	WT	C	EQ	EA	ED	INV	EQ/C		ED/EA	ED/C		WT	C	EQ	EA	ED	INV	WT	C	EQ	EA	ED	INV
ABa		24.1	24.8	24.1	25.6		103%		106%	106%			0.08	0.05	0.04	0.06			7	13	7	6	
ABp		24.4	24.8	24.4	25.2		101%		103%	103%			0.07	0.04	0.03	0.05			7	13	7	6	
EMS		27.3	25.8	25.3	26.3		94%		104%	96%			0.06	0.05	0.06	0.04			7	13	7	6	
P2		31.8	30.2	30.1	30.3		95%		101%	95%			0.06	0.05	0.04	0.06			7	13	7	6	
Abal	26.4	26.1	26.2	26.2	26.2	24.8	100%		100%	100%		0.04	0.04	0.04	0.04	0.04	0.04	10	19	46	19	27	7
Abar	26.4	26.0	25.9	25.8	25.9	25.1	99%		100%	100%		0.04	0.04	0.05	0.04	0.05	0.04	10	19	46	19	27	7
ABpl	26.1	26.6	25.9	25.8	26.0	25.4	97%		101%	98%		0.05	0.04	0.05	0.04	0.05	0.05	10	19	46	19	27	7
Abpr	26.4	26.5	26.1	26.1	26.1	25.1	98%		100%	98%		0.05	0.04	0.05	0.04	0.05	0.04	10	19	46	19	27	7
MS	31.2	29.8	28.0	28.0	28.0	26.5	94%	**	100%	94%	**	0.04	0.04	0.06	0.05	0.06	0.06	10	18	46	19	27	7
E	33.6	31.4	29.0	28.7	29.1	27.8	92%	***	102%	93%	**	0.06	0.03	0.07	0.04	0.08	0.07	10	18	46	19	27	7
C	33.8	32.3	30.9	31.3	30.7	30.0	96%	**	98%	95%	**	0.03	0.03	0.05	0.03	0.05	0.04	10	18	46	19	27	7
P3	45.6	41.7	38.5	38.8	38.3	34.8	92%	***	99%	92%	***	0.06	0.05	0.06	0.06	0.07	0.09	10	17	45	18	27	7
Abala	31.9	32.3	32.5	32.5	32.6	33.0	101%		100%	101%		0.04	0.05	0.05	0.03	0.06	0.02	10	16	41	18	23	6
Abalp	31.9	31.0	30.9	30.8	31.0	31.4	100%		101%	100%		0.04	0.04	0.04	0.04	0.04	0.05	10	17	41	18	23	6
ABara	31.4	31.6	32.2	32.1	32.2	32.6	102%		100%	102%		0.04	0.04	0.04	0.03	0.04	0.06	10	17	41	18	23	6
ABarp	31.2	30.7	30.9	30.9	30.9	31.8	101%		100%	101%		0.04	0.04	0.04	0.04	0.05	0.07	10	17	41	18	23	6
ABpla	30.9	30.2	30.8	30.7	30.9	32.3	102%		101%	102%		0.03	0.03	0.03	0.04	0.03	0.05	10	17	41	18	23	6
Abplp	32.1	31.2	31.7	31.7	31.7	31.8	101%		100%	101%		0.04	0.04	0.04	0.04	0.05	0.03	10	16	41	18	23	6
ABpra	30.9	30.5	31.1	30.8	31.4	31.9	102%		102%	103%		0.03	0.04	0.04	0.03	0.04	0.04	10	17	41	18	23	6
Abprp	32.1	31.7	31.9	31.9	32.0	32.6	101%		100%	101%		0.04	0.05	0.04	0.03	0.04	0.04	10	17	41	18	23	6
Msa	36.0	36.5	35.7	35.3	36.1	33.8	98%		102%	99%		0.03	0.05	0.07	0.05	0.09	0.06	10	14	39	17	22	6
MSp	36.0	36.5	35.5	34.8	36.1	34.2	97%		104%	99%		0.03	0.05	0.08	0.05	0.10	0.07	10	14	39	17	22	6
Ea	65.4	66.2	58.4	58.8	58.1	52.4	88%	***	99%	88%	***	0.04	0.04	0.07	0.07	0.07	0.11	10	14	36	14	22	6
Ep	69.8	69.7	60.5	61.1	60.2	55.2	87%	***	98%	86%	***	0.04	0.04	0.08	0.07	0.08	0.09	10	14	36	14	22	6
Ca	39.6	39.9	39.5	39.2	39.7	37.8	99%		101%	99%		0.04	0.03	0.07	0.05	0.07	0.10	10	14	36	14	22	6
Cp	39.6	40.7	39.1	39.4	38.9	37.3	96%		99%	96%		0.04	0.04	0.06	0.05	0.07	0.08	10	14	36	14	22	6
D	59.0	56.4	48.5	49.3	48.0	43.2	86%	***	97%	85%	***	0.05	0.07	0.08	0.09	0.08	0.09	10	14	36	14	22	6
P4	123.7	103.9	70.6	74.3	68.3	51.3	68%	***	92%	66%	***	0.05	0.18	0.18	0.18	0.17	0.17	10	12	36	14	22	5

Length of the cell cycle in individual cells up to the 16-cell stage embryo. WT – wild-type, lin-5(ev571): C – Control, EQ – equalized alive and dead together, EA – equalized alive, ED – equalized dead, INV – inverted. Pairwise comparisons were performed with Welsh two sample test with Bonferroni-Hochberg correction for multiple comparisons. Asterisk indicate statistical significance, * P <0.05, ** P < 0.01, *** P < 0.001. Variation coefficient was adjusted for number of embryos by multiplication with (1+1/(4*N)).The blue-red gradient (low-> high) encodes the magnitude of change between compared groups. Similarly, the coefficient of variation is color-coded in a green-yellow-red gradient for easier visual interpretation

2.8.2 Aberrant division sequence in equalized embryos

The accelerated cell cycle of P1-derived cells in EQ embryos had an effect on the global temporal sequence with which individual cells divided during embryogenesis (**Figure 20**).The shorter cell cycles of individual P1 lineage cells accumulated across division cycles and, in consequence, resulted in the division of several cells, including Ea/Ep, D, Da and P4, before the corresponding AB division rounds (red arrows in **Figure 20**). While we detected significantly different cell cycle duration in less than 10% of cells in EQ embryos in comparison to unequal controls, small changes in cell cycle duration accumulated over time and were magnified in times of division of individual cells during embryogenesis. We found 47/170 of the tested cells that divided at significantly different time in EQ compared to Ctrl embryos. Of those, only 4 come from the late AB lineage, supporting the notion that the P1 lineage is affected much more and earlier by equalization of the first division (**Table 2, Figure 20**).

We were interested in specific differences between equalized embryos that died in comparison to those that lived to possibly uncover processes leading to embryonic lethality. To this end, we compared only "truly" equalized embryos in the AB size range 48-52.5%, so that there was no significant difference in their AB sizes (Welsh *t-test*, p=0.95, mean size in EA 50.55% vs 50.57% in ED, N=20 and 27 respectively). We therefore excluded inverted embryos and embryos that were only partial equalized with AB > 52.5%. We chose this uneven interval in order not to reject several lineages that were close to 52% and thus maintain statistical power. The comparison of division times between EA and ED embryos, however, did not reveal any cell that would be significantly different, especially after applying Bonferroni-Hochberg correction. This suggests that timing of divisions is not a major factor behind the lethality of equalized embryos, in line with the inability to rescue lethality by slowing down P1.
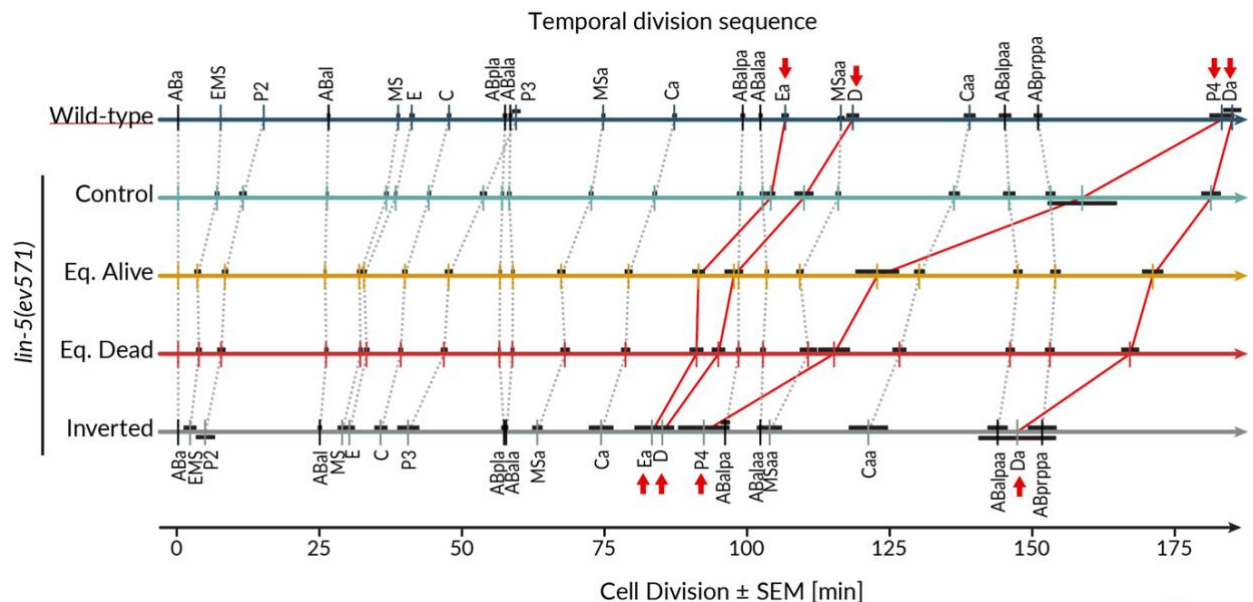
Figure 20 - Altered temporal division sequence in equalized embryos

Division sequence in wild-type, and in *lin-5(ev571)* control, equalized alive (Eq. Alive), equalized dead (Eq. Dead), and inverted embryos. Shown are average division times in each group for indicated cells. Timing of embryogenesis was aligned (0 min) to the division of the ABa cell. Note accelerated cell cycles of the P1 lineage cells in equalized embryos, leading to altered division sequence, in Ea, P4, D, and D (highlighted by solid red connecting lines and by red arrows) with respect to divisions of AB lineage cells Not all AB cells are shown due to space constrains; however, the first and last AB cell in a given division round of the AB lineage are indicated. Dark horizontal bars indicate standard error of the mean.

Table 2 – Cell division times in lineaged embryos

Cell	Average division time [min]						Effect size							Coefficient of variation						Number of embryos					
	WT	CTRL	EQ	EA	ED	INV	EQ/C		ED/EA	EA/C		ED/C		WT	C	EQ	EA	ED	INV	WT	EQ	CTRL	EA	ED	INV
ABp		0.4	0.0	0.3	-0.3																7	13	7	6	
EMS		6.8	3.5	3.4	3.6		52%	***	106%	50%	**	53%	**		0.16	0.40	0.48	0.35			7	13	7	6	
P2		11.4	7.9	8.2	7.6		70%	**	92%	73%	*	67%	*		0.16	0.20	0.18	0.24			7	13	7	6	
ABal	26.4	26.1	26.2	26.2	26.2	24.8	100%		100%	100%		100%		0.04	0.04	0.04	0.04	0.04	0.04	10	19	46	19	27	7
ABar	26.4	26.0	25.9	25.8	25.9	25.1	99%		100%	99%		100%		0.04	0.04	0.05	0.04	0.05	0.04	10	19	46	19	27	7
ABpl	26.4	26.6	25.8	25.9	25.7	25.1	97%		99%	97%		97%		0.04	0.04	0.05	0.04	0.06	0.05	10	19	46	19	27	7
ABpr	26.6	26.5	26.0	26.2	25.8	24.8	98%		99%	99%		97%		0.04	0.05	0.05	0.04	0.06	0.04	10	19	46	19	27	7
MS	38.6	36.5	31.9	31.9	31.9	28.8	87%	***	100%	87%	***	87%	***	0.03	0.05	0.06	0.07	0.06	0.08	10	19	46	18	27	7
E	41.0	38.1	32.8	32.6	33.0	30.0	86%	***	101%	86%	***	87%	***	0.04	0.03	0.07	0.06	0.08	0.08	10	19	46	18	27	7
C	47.5	44.0	39.3	39.7	39.0	35.5	89%	***	98%	90%	***	89%	***	0.02	0.03	0.06	0.05	0.06	0.09	10	19	46	18	27	7
P3	59.3	53.4	46.9	47.4	46.6	40.4	88%	***	98%	89%	***	87%	***	0.04	0.05	0.07	0.07	0.07	0.13	10	18	45	17	27	7
ABala	58.3	58.2	58.6	58.6	58.6	57.6	101%		100%	101%		101%		0.02	0.03	0.03	0.02	0.03	0.01	10	18	41	16	23	6
ABalp	58.3	57.0	56.9	56.9	57.0	56.0	100%		100%	100%		100%		0.02	0.02	0.02	0.02	0.02	0.03	10	18	41	17	23	6
ABara	57.8	57.6	57.9	57.9	57.9	57.5	101%		100%	101%		101%		0.02	0.02	0.02	0.02	0.02	0.02	10	18	41	17	23	6
ABarp	57.5	56.6	56.6	56.7	56.6	56.7	100%		100%	100%		100%		0.02	0.02	0.02	0.02	0.02	0.03	10	18	41	17	23	6
ABpla	57.3	56.7	56.4	56.6	56.4	57.1	100%		100%	100%		99%		0.02	0.02	0.02	0.02	0.02	0.02	10	18	41	17	23	6
ABplp	58.5	57.6	57.3	57.5	57.2	56.7	100%		99%	100%		99%		0.02	0.03	0.02	0.02	0.02	0.03	10	18	41	16	23	6
ABpra	57.6	56.8	56.9	56.9	56.9	56.4	100%		100%	100%		100%		0.02	0.02	0.02	0.02	0.02	0.01	10	18	41	17	23	6
ABprp	58.7	58.0	57.7	58.0	57.5	57.1	100%		99%	100%		99%		0.03	0.02	0.02	0.01	0.03	0.02	10	18	41	17	23	6
MSa	74.5	72.7	67.5	67.2	67.8	63.0	93%	***	101%	92%	***	93%	***	0.01	0.02	0.05	0.05	0.06	0.04	10	17	39	14	22	6
MSp	74.5	72.6	67.3	66.7	67.8	63.3	93%	***	102%	92%	***	93%	***	0.01	0.02	0.05	0.04	0.06	0.05	10	17	39	14	22	6
Ea	106.4	104.1	91.0	91.4	90.7	83.1	87%	***	99%	88%	***	87%	***	0.02	0.03	0.06	0.05	0.07	0.09	10	14	36	14	22	6
Ep	110.8	107.6	93.1	93.6	92.8	85.9	87%	***	99%	87%	***	86%	***	0.03	0.03	0.06	0.05	0.07	0.08	10	14	36	14	22	6
Ca	87.0	83.6	78.6	78.9	78.4	74.2	94%	***	99%	94%	***	94%	***	0.02	0.02	0.04	0.04	0.05	0.07	10	14	36	14	22	6
Cp	87.0	84.4	78.2	79.1	77.7	73.7	93%	***	98%	94%	***	92%	***	0.02	0.02	0.04	0.04	0.04	0.06	10	14	36	14	22	6
D	118.3	109.5	95.6	96.9	94.7	84.9	87%	***	98%	89%	***	87%	***	0.03	0.05	0.06	0.07	0.06	0.06	10	14	36	14	22	6
P4	183.0	156.8	117.6	121.9	114.9	92.2	75%	***	94%	78%	***	73%	***	0.04	0.13	0.12	0.13	0.12	0.11	10	14	36	12	22	5
ABalaa	102.1	102.8	102.8	103.2	102.5	102.2	100%		99%	100%		100%		0.01	0.02	0.02	0.01	0.02	0.02	10	14	36	14	22	5
ABalap	101.4	101.4	102.0	102.0	101.9	100.8	101%		100%	101%		101%		0.01	0.02	0.02	0.02	0.03	0.02	10	14	36	14	22	5
ABalpa	99.0	98.5	98.2	98.1	98.2	95.9	100%		100%	100%		100%		0.01	0.02	0.02	0.01	0.02	0.02	10	14	36	14	22	5
ABalpp	100.0	99.1	97.9	98.0	97.9	95.9	99%		100%	99%		99%		0.01	0.02	0.02	0.02	0.02	0.02	10	14	36	14	22	5
ABaraa	99.2	99.8	100.8	100.1	101.3	100.2	101%		101%	100%		102%		0.01	0.02	0.02	0.01	0.02	0.03	10	14	36	14	22	5
ABarap	99.5	99.5	100.0	99.3	100.5	100.2	100%		101%	100%		101%		0.01	0.01	0.02	0.01	0.02	0.01	10	14	36	14	22	5
ABarpa	100.9	99.8	99.3	99.2	99.3	100.2	99%		100%	99%		99%		0.01	0.01	0.02	0.02	0.02	0.03	10	14	36	14	22	5
ABarpp	102.1	101.1	100.0	100.3	99.7	99.7	99%		99%	99%		99%		0.01	0.01	0.02	0.01	0.02	0.02	10	14	36	14	22	5
ABplaa	98.1	97.1	98.6	98.7	98.5	98.8	102%	*	100%	102%	*	102%		0.01	0.02	0.02	0.01	0.02	0.01	10	14	36	14	22	5
ABplap	97.3	97.2	98.2	98.0	98.3	98.8	101%		100%	101%		101%		0.01	0.02	0.02	0.02	0.02	0.02	10	14	36	14	22	5
ABplpa	99.5	99.4	99.0	99.8	98.5	97.3	100%		99%	100%		99%		0.01	0.01	0.02	0.02	0.02	0.02	10	14	36	14	22	5
ABplpp	101.1	100.4	100.0	100.4	99.8	98.2	100%		99%	100%		99%		0.02	0.02	0.02	0.02	0.02	0.02	10	14	36	14	22	5
ABpraa	98.0	97.4	97.9	97.8	98.0	97.4	101%		100%	100%		101%		0.01	0.01	0.02	0.01	0.02	0.02	10	14	36	14	22	5
ABprap	97.3	97.8	98.3	98.2	98.3	98.8	101%		100%	100%		101%		0.01	0.02	0.02	0.01	0.02	0.01	10	14	36	14	22	5
ABprpa	99.7	100.4	100.0	100.8	99.4	99.3	100%		99%	100%		99%		0.01	0.02	0.02	0.02	0.02	0.03	10	14	36	14	22	5
ABprpp	100.4	100.4	100.9	101.4	100.6	99.3	100%		99%	101%		100%		0.01	0.01	0.02	0.01	0.02	0.03	10	14	36	14	22	5
MSaa	116.2	116.2	109.9	109.0	110.5	103.7	95%	***	101%	94%	***	95%	*	0.02	0.02	0.06	0.02	0.07	0.05	10	13	35	14	22	5
MSap	120.3	120.7	113.9	113.1	114.3	106.6	94%	***	101%	94%	***	95%	*	0.02	0.02	0.06	0.03	0.08	0.04	10	13	35	14	22	5
MSpa	116.7	115.4	109.7	109.0	110.2	103.3	95%	***	101%	94%	***	95%	*	0.01	0.01	0.05	0.03	0.07	0.06	10	13	35	14	22	5
MSpp	120.3	118.9	113.7	112.0	114.7	107.1	96%	**	102%	94%	***	96%		0.02	0.02	0.07	0.03	0.08	0.05	10	13	35	14	22	5
Caa	138.8	136.1	127.7	129.8	126.5	121.0	94%	***	97%	95%	***	93%	***	0.02	0.02	0.04	0.03	0.05	0.07	10	13	35	12	22	5
Cap	148.6	143.9	136.1	137.9	135.1	126.4	95%	**	98%	96%	*	94%	**	0.02	0.04	0.05	0.04	0.05	0.09	10	13	34	11	21	5
Cpa	136.4	133.5	126.2	128.1	125.2	120.7	95%	***	98%	96%	*	94%	***	0.02	0.03	0.04	0.04	0.04	0.08	10	13	35	13	22	5
Cpp	144.1	142.8	134.8	137.0	133.4	127.3	94%	**	97%	96%	*	93%	***	0.02	0.03	0.04	0.04	0.04	0.08	10	13	34	11	21	5
ABaraap	144.5	145.5	149.5	149.8	149.3	149.0	103%	***	100%	103%	***	103%	**	0.02	0.01	0.02	0.01	0.03	0.03	10	13	33	11	20	4
ABplaaa	144.3	146.1	149.4	149.2	149.5	152.1	102%	*	100%	102%		102%	*	0.02	0.02	0.02	0.02	0.02	0.03	10	13	33	11	20	4
ABplaap	141.7	142.6	145.2	146.1	144.7	145.5	102%	*	99%	102%	*	101%		0.02	0.02	0.02	0.02	0.02	0.03	10	13	33	11	20	4
Eal	177.8	178.0	156.1	157.6	155.1	138.8	88%	***	98%	89%	***	87%	***	0.03	0.03	0.07	0.03	0.09	0.14	10	13	33	9	20	4
Ear	178.7	178.0	156.2	157.6	155.4	141.4	88%	***	99%	89%	***	87%	***	0.03	0.03	0.07	0.03	0.08	0.13	10	13	33	9	20	4
Epl	185.1	183.4	159.3	161.6	157.8	143.6	87%	***	98%	88%	***	86%	***	0.03	0.04	0.07	0.04	0.09	0.13	9	13	33	9	20	4
Epr	186.0	183.4	159.6	160.7	158.9	143.1	87%	***	99%	88%	***	87%	***	0.03	0.04	0.07	0.04	0.08	0.12	8	13	33	9	20	4
Da	184.8	181.1	168.3	170.4	166.9	147.1	93%	***	98%	94%	**	92%	***	0.02	0.03	0.04	0.04	0.04	0.10	8	13	33	8	20	4
Dp	185.7	181.8	167.6	168.8	166.9	146.1	92%	***	99%	93%	***	92%	***	0.03	0.02	0.04	0.04	0.05	0.10	8	13	33	8	20	4

Division time of individual cells in indicated groups of embryos. For the encoding of experimental groups and statistics see the legend of Table 1 above.

The fact that there were no significant differences between alive and dead equalized embryos regarding cell cycle duration prompted us to investigate timing variability in addition. As mentioned before, normal *C. elegans* development is highly stereotypical, including cell cycle timing that has particularly low variability. The average variation coefficient of cell cycle duration in WT embryos was 4.2% for 170 measured cells. Cell cycles in Ctrl *lin-5(ev571)* were only about 1% more variable (5.1%, p<0.001 in comparison to the WT). Interestingly, EA embryos had a comparable variability of timing to *lin-5* controls (4.9%, p=0.3), while ED embryos exhibited a significant increase in cell cycle timing variability (6.2%) in comparison to their alive peers (p < 2e-8). In addition, the P1 lineage cells exhibited a significantly greater variation coefficient in cell cycle timing than AB lineage cells in equalized embryos (5.6% vs 6.9%, p<0.001), while there was no difference in the same comparison in control embryos (5.2% for both AB and P1 cells, p=0.98). These findings again strongly support the notion that the P1 lineage is much more affected by equalization of the first division than the AB lineage.

We then split cells from wild-type, control, EA, ED, and INV *lin-5(ev571)* embryos into four groups by developmental stage (8 cells, 16 cells, 28 cells, and Late –comprising all subsequent stages) and compared the variation in timing at each stage in greater detail among these groups (**Figure 21**). We found an apparent trend of increased variability amongst ED and INV embryos in comparison to wild-type, control, or EA embryos at all developmental stages in the three measured features: cell cycle duration, time of division during embryogenesis, and asynchrony of sister cells. Sister cell asynchrony
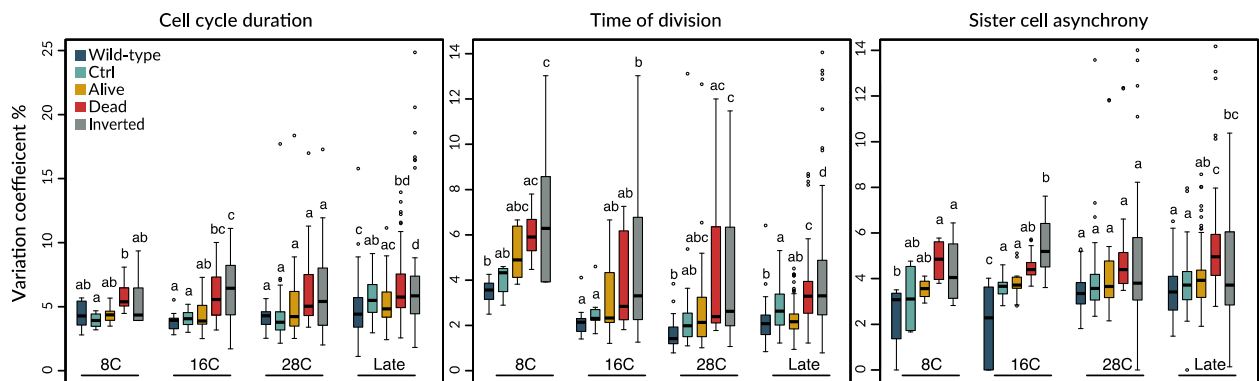
Figure 21 - Variation in the timing of cells during embryogenesis

We calculated the coefficient of variation for cell cycle duration, time of division, and sister cell asynchrony for the 5 indicated groups of embryos at the 8 cells stage (8C), 16 cells stage (16C), 28 cells stage (28C), and thereafter –comprising all subsequent stages up to the ~120 cell stage. Each data point used for a given boxplot represents the variation coefficient for a single cell calculated for embryos within each group. Therefore, boxplots for the 8-cell stage contain 8 data points (cells), etc. Comparisons between groups were performed using Anova and Tuckey honest significant difference (HSD) post-hoc test. Two boxplots that do not share the same letter are significantly different from each other with p < 0.05.

can be used to assess differentiation of various lineages, since fate decisions are often accompanied by differential cell cycle duration between sister cells. Therefore, low variance of this metric indicates that embryos within a given category behave similarly to each other and follow a shared stereotypical developmental trajectory. By contrast, large variance amongst equalized embryos, and in particular amongst EA and INV embryos, suggests that the differentiation program was not followed tightly. Furthermore, this data suggest that the changes induced by equalization of the first division did not lead to a uniform phenotype, which would manifest itself as a systematic change in timing of particular cells without increasing the variability within each experimental group.

In conclusion, our data strongly suggest that the lack of size asymmetry in the first division results in a global acceleration of cell cycles within the P1 lineage, leading to an altered temporal sequence of divisions. In addition, embryos that are to die have significantly larger variation in cell cycle timing. This likely reflects stochastic defects in fate acquisition. This might be, indeed, the reason why we were not able to find any systematic differences between EA and ED embryos when looking for change in the average timing, because test we used are losing power with increasing variance.

2.8.3   Ectopic divisions in the germline

The conserved embryonic lineage of *C. elegans* allows one to identify fate transformations and ectopic division based on the topology and branch lengths of reconstructed lineage trees. First, we observed that the sole germline precursor cell, P4, which normally divides only once during embryogenesis, underwent at least one additional divisions in 37% (n=43) of upshifted *lin-5(ev571)* embryos (**Figure 22**). We never observed this phenotype in unequal *lin-5(ev571)* Ctrl or WT lineages (**Figure 22**, n=21). This phenotype was more frequent in embryos that died (44%, n=27) than in those that lived (25%, n=16, **Figure 22B**). However, as our data clearly indicate, this phenotype does not perfectly correlate with the outcome of development in equalized embryos.

In addition to the ectopic P4 divisions, we observed signs of lineage transformation of D into a C-like division pattern in a few inverted embryos (**Figure 22**, INV embryo). We cannot exclude the possibility of additional fate transformations or ectopic divisions in other lineages because we typically lineaged embryos only up to ~120 cells, at least two division rounds before full differentiation of most cells.
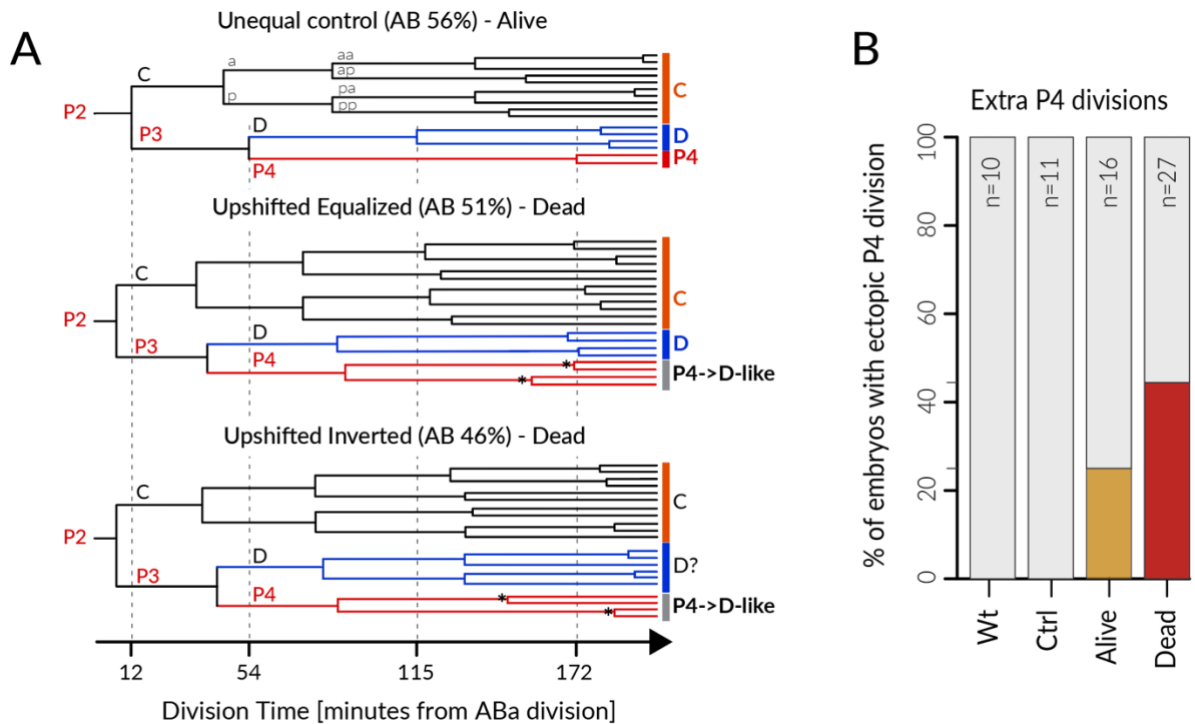
Figure 22 - Ectopic divisions in the germline in equalized embryos

(A) The P4 cell normally divides only once, producing the Z2 and Z3 germline precursors that remain quiescent until hatching (control embryo on the top, red P4 branch). In some equalized and inverted embryos, P4 divides more than once, producing extra cells, suggesting a fate transformation to a D-like state or repetition of the P3 fate. Note acceleration of the cell cycle in C, D and P4 lineages in equalized and inverted embryos in comparison to the normal division timing in control (dashed lines). All shown embryos are *lin-5(ev571)*, the control embryo was upshifted during early two-cell stage. (B) Frequency of embryos with one or more extra divisions within the P4 lineage in control and equalized embryos. Extra divisions happened nearly in 44% (n=27) of the dead embryos and were never observed in control embryos or in the wild-type (n=21).

2.9   Cell volumes following the first equalized cleavage

C. elegans development involves many size-asymmetric divisions, in particular within the germline branch stemming from P1, which undergoes three subsequent unequal divisions producing smaller P2, P3, and P4, and the larger somatic cells EMS, C, and D (see **Figure 1**).

We hypothesized that EA and ED embryos could differ in the extent of asymmetry of some of these unequal divisions, perhaps reflecting a compensatory mechanism allowing some equalized embryos to develop and hatch. In particular, we envisaged that the appropriate volume of blastomeres that contribute to different embryonic layers might be essential during gastrulation when their progeny organizes into organs and tissues. Altered blastomere volumes in ED embryos could physically preclude correct movements, prevent or establish aberrant instructive cell-cell interaction, or affect the concentration of important fate determinant, which are normally split asymmetrically during unequal divisions.

To test these hypotheses, we measured cell volumes in EQ, *lin-5(ev571) Ctrl,* as well as in wild-type embryos up to the 16-cell stage. We used a watershed-based segmentation pipeline to extract cell volumes from image stacks enhanced by the Noise2Void machine learning pipeline (Krull et al., 2019) for better signal to noise and improved membrane continuity (see Methods, **Figure 23**, **Figure 24A**). We then reconstructed the cell lineage of these embryos to obtain the identity of segmented cells before measuring cell volumes and calculating sister volume ratio to assess the extent of division asymmetry.

The vast majority of cells in EQ embryos had a significantly different relative volume in comparison to cells in unequal *lin-5(ev571)* Ctrl (**Figure 24B, C**). In fact, all posterior cells had different volumes in EQ embryos compared to unequal controls, except for C and its daughters Ca and Cp (**Table 3**). It was relatively unexpected to find any cell with unchanged volumes given that equalized embryos start with quite dramatically changed sizes of AB and P1. Indeed, P3/C sister volume ratio, and thus P2 division asymmetry was different in EQ in comparison to Ctrl embryos, explaining why EQ embryos can have same sized C as in the controls. This also leads to P3 being about 1.3 larger that in controls.

We were interested in finding differences in division volumetric asymmetries between EA and ED embryos that could point us to possible compensation mechanisms in alive embryos. However, there were no cells with significantly different relative volume among equalized embryos after applying BH correction. Without correcting for false discovery, the MSa cell, which is ~10% larger than normal, would come to p=0.031, and Abplpa, which is ~9% smaller, to p=0.0507 in ED compared to EA embryos.

Regarding the division volumetric asymmetry, less cells were significantly different between unequal Ctrl and EQ embryos (**Table 4**). We found that divisions of P2 and EMS (reported as ratios of their daughters P3/C and MS/E) were significantly less asymmetric comparing EQ to Ctrl embryos (**Figure 24C**). Importantly, we found that division of Abpr (ABpra/Abprp) and ABpl (ABpla/Abplp) are unequal in controls, but loose or decrease division asymmetry in particular in dying embryos (**Table 4, Figure 24C**). The division of EMS (E/MS), and Abpr (ABpra/Abprp) were the only two that differed significantly between EA and ED embryos, suggesting that there is no obvious compensation mechanism for volume reallocation by differential asymmetric divisions operating in EA embryos up to the 16-cell stage.

Surprisingly, P3 and P4 divided less asymmetrically and were slightly larger even in unequal *lin-5(ev571)* control embryos than in the wild-type embryos, most likely due to partially impaired LIN-5 function even at the permissive temperature (**Figure 24C**).

This dataset also allowed us to address the relationship between cell volume and the pace of the cell cycle up to the 15-cell stage. Interestingly, we observed that cell cycle was anticorrelated with cell volumes in most P1 lineage cells, but not in anterior AB derived lineage cells (**Figure 24D, E**). This again supports the notion that the P1 lineage is far more affected and sensitive to equalization of the first division and that AB lineage cells might be saturated with cell cycle promoting factors, such as PKL-1.
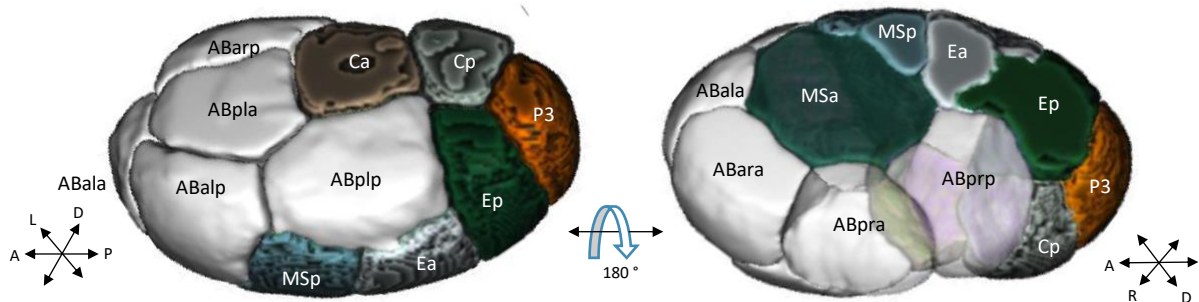
Figure 23 – Results of volumetric segmentation

Example of segmentation of an equalized embryo at the 15-cell stage. We were able to obtain pleasing segmentation results that allow for reliable volumetric measurements evidenced by minimal variability (<5%) between segmentation of identical cells at different timepoints (not shown).
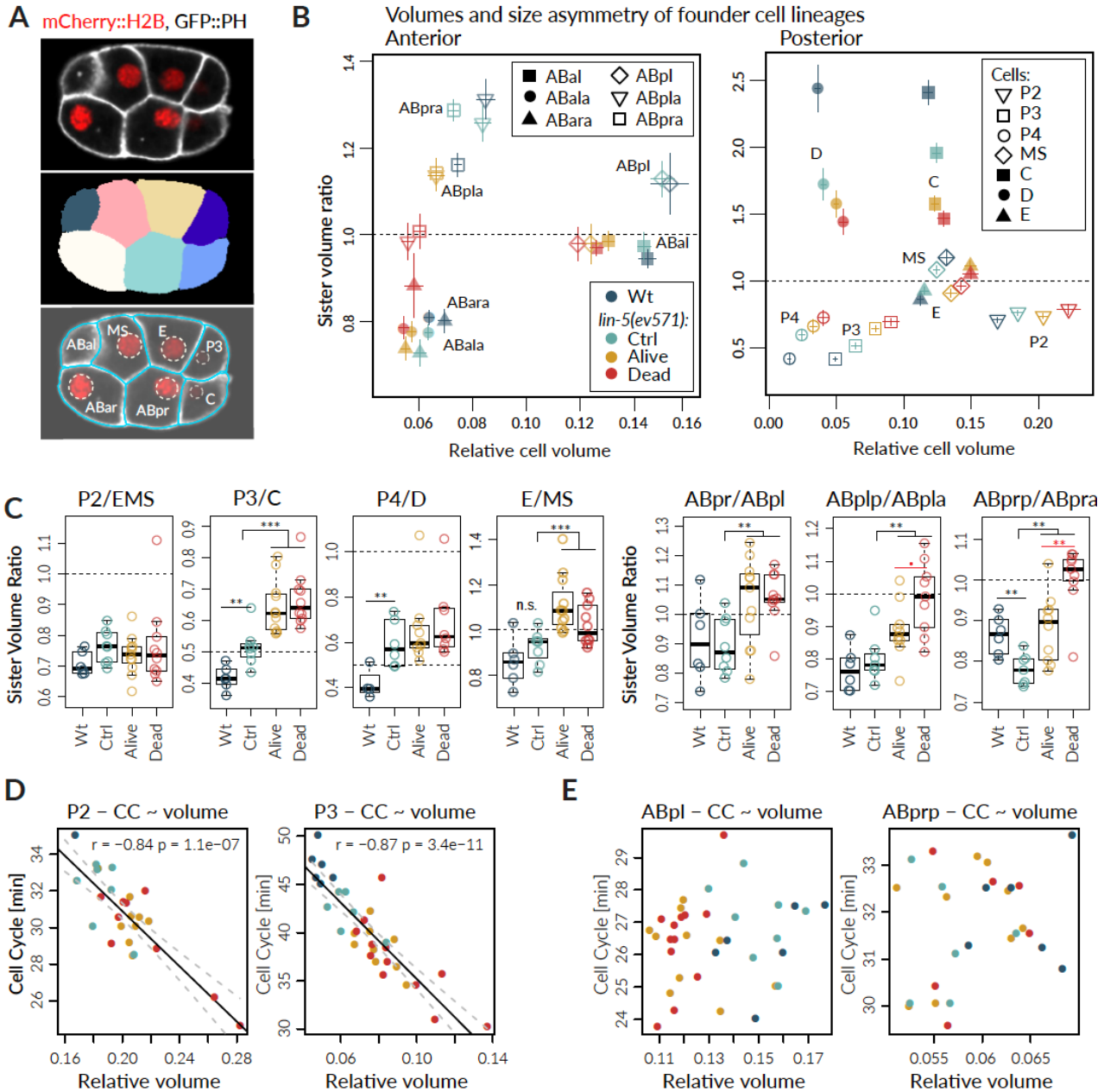
Figure 24 - *Some cell volumes and size asymmetries are affected in equalized lin-5(ev571) embryos.*
(A) Cell lineage was traced using 3D timelapse recordings of embryos co-expressing histone mCherry∷H2B to label all nuclei, and GFP∷PH to mark the plasma membranes. Shown is a single slice from the timelapse movie. Cell volumes were segmented for several embryos using the membrane signal (bottom two panels); blue lines indicate cell boundaries resulting from the automatic segmentation pipeline. **(B)** Scatterplot of sister volume ratio versus relative cell volume in control (wild-type, 2-cell stage upshifted *lin-5(ev571)*) and equalized alive and equalized dead *lin-5(ev571)* embryos -blue and red points, respectively). Dashed line indicates equal cell size of sister cells. Germline cells (P2, P3, P4) are clearly larger in equalized embryos. Only selected anterior cells showing notable differences from controls are displayed for readability. EMS cell is also not shown for the same reason. Vertical and horizontal lines indicate standard error of mean. **(C)** Sister volume ratio for cells showing significant differences in the germline and in anterior cells (same data as in C). **(D,E)** Cell cycle duration correlates with cell volume in germline cells **(D)**, but not in the AB lineage. **(E)** ABpl and ABprp were chosen as representative example. The color code is the same as in B and C.

Table 3 – Relative volumes of cells in control and equalized embryos

Cell	Average volume %					Change + Welsh t.test (BH)						Var. coeficient					N of embryos				
	WT	C	EQ	EA	ED	C/WT	EA/C		ED/C		ED/EA	WT	C	EQ	EA	ED	WT	C	EQ	EA	ED
AB		57.8	51.0	51.0	51.0		88%	***	88%	***	100%		0.03	0.02	0.03	0.02		6	13	7	6
P1		42.3	49.0	49.0	49.0		116%	***	116%	***	100%		0.04	0.03	0.03	0.02		6	13	7	6
ABa	30.6	29.1	25.9	26.0	25.8	95%	89%	***	89%	***	99%	0.04	0.05	0.03	0.04	0.03	6	8	17	9	8
ABp	28.7	28.3	25.2	25.3	25.1	99%	90%	***	89%	***	99%	0.03	0.04	0.03	0.04	0.03	6	8	17	9	8
EMS	23.9	24.2	28.0	28.1	27.7	101%	116%	***	115%	**	99%	0.04	0.05	0.06	0.04	0.08	6	8	17	9	8
P2	16.9	18.4	20.9	20.5	21.4	109%	111%	**	116%	**	104%	0.06	0.07	0.08	0.05	0.10	6	8	17	9	8
ABal	14.5	14.4	12.9	12.8	13.0	99%	89%	***	90%	**	101%	0.06	0.05	0.04	0.04	0.05	6	8	17	9	8
ABar	15.3	14.8	13.1	13.1	13.1	97%	88%	**	88%	**	100%	0.04	0.08	0.05	0.06	0.04	6	8	17	9	8
ABpl	15.3	15.0	12.1	12.2	12.0	98%	81%	***	80%	***	99%	0.11	0.08	0.07	0.08	0.07	6	8	17	9	8
ABpr	13.8	13.4	12.7	12.7	12.6	97%	95%		94%	*	100%	0.05	0.06	0.05	0.06	0.04	6	8	17	9	8
MS	13.1	12.4	13.9	13.6	14.2	95%	110%	*	114%	*	104%	0.09	0.06	0.10	0.10	0.10	6	8	17	9	8
E	11.2	11.5	14.8	15.3	14.3	103%	133%	***	125%	**	94%	0.06	0.08	0.09	0.07	0.10	6	8	17	9	8
C	11.8	12.4	12.4	12.2	12.6	105%	98%		101%		103%	0.07	0.07	0.08	0.07	0.09	6	8	17	9	8
P3	4.9	6.4	8.3	8.0	8.6	131%	125%	**	134%	**	107%	0.08	0.15	0.14	0.11	0.17	6	8	17	9	8
ABala	6.4	6.3	5.7	5.7	5.7	100%	90%	**	90%	**	100%	0.07	0.06	0.07	0.07	0.07	6	7	15	8	7
ABalp	7.8	8.2	7.2	7.3	7.1	105%	89%	**	87%	**	97%	0.05	0.07	0.07	0.06	0.08	6	7	15	8	7
ABara	6.9	6.0	5.8	5.5	6.0	87%	91%		100%		110%	0.09	0.10	0.14	0.11	0.16	6	7	15	8	7
ABarp	8.7	8.3	7.1	7.3	6.9	96%	88%	***	83%	**	94%	0.02	0.04	0.07	0.04	0.08	6	7	15	8	7
ABpla	8.5	8.4	6.0	6.3	5.7	99%	76%	***	69%	***	91%	0.10	0.10	0.10	0.10	0.09	6	7	15	8	7
ABplp	6.5	6.7	5.7	5.7	5.7	103%	86%	*	85%	**	99%	0.07	0.10	0.06	0.07	0.07	6	7	15	8	7
ABpra	7.4	7.3	6.4	6.6	6.1	98%	91%	*	84%	**	92%	0.04	0.07	0.09	0.09	0.08	6	7	15	8	7
ABprp	6.4	5.7	5.9	5.9	6.0	88%	103%		106%		103%	0.07	0.07	0.08	0.09	0.07	6	7	15	8	7
MSa	6.5	6.3	7.1	6.7	7.5	97%	106%		118%	**	111%	0.06	0.08	0.10	0.08	0.09	6	7	15	8	7
MSp	6.6	6.3	7.0	6.8	7.2	95%	107%		114%	*	107%	0.11	0.06	0.11	0.10	0.11	6	7	15	8	7
Ea	5.9	5.9	7.6	7.9	7.3	100%	135%	***	124%	**	92%	0.13	0.07	0.10	0.07	0.13	6	7	15	8	7
Ep	5.5	6.0	7.4	7.6	7.2	110%	127%	***	119%	*	94%	0.08	0.07	0.11	0.11	0.11	6	7	15	8	7
Ca	5.8	6.1	6.2	6.2	6.3	106%	101%		102%		102%	0.08	0.09	0.10	0.11	0.10	6	7	14	7	7
Cp	6.3	6.2	6.4	6.4	6.5	98%	103%		105%		102%	0.10	0.04	0.08	0.06	0.10	6	7	14	7	7
D	3.6	4.0	5.1	5.0	5.2	112%	126%	**	130%	**	104%	0.11	0.13	0.08	0.08	0.09	4	6	13	7	6
P4	1.5	2.4	3.6	3.5	3.8	161%	144%	*	160%	*	111%	0.18	0.26	0.28	0.23	0.35	4	6	13	7	6

Statistical comparisons were performed using Welsh two sample t-test with BH correction. There was no significantly different cell volume between control (C) and wild-type (WT), or equalized dead (ED) and alive (EA) embryos. Variation coefficient was adjusted for number of samples by multiplication with (1+1/(4*N)).

Table 4 – Sister-cell volumetric asymmetry and statistical comparisons

Cell	Volume ratio of sister cells					Change + Welsh t.test								Var. coeficient					N embryos				
	WT	C	EQ	EA	ED	C/WT		EA/C		ED/C		ED/EA		WT	C	EQ	EA	ED	WR	C	EQ	EA	ED
AB		1.37	1.04	1.04	1.04			76%	***	76%	***	100%			0.07	0.05	0.06	0.04		6	13	7	6
P1		0.73	0.96	0.96	0.96			131%	***	131%	***	100%			0.07	0.05	0.06	0.04		6	13	7	6
ABa	1.07	1.03	1.03	1.03	1.03	96%		100%		100%		100%		0.05	0.04	0.04	0.05	0.04	6	8	17	9	8
ABp	0.94	0.97	0.97	0.97	0.97	104%		100%		100%		100%		0.05	0.04	0.04	0.05	0.04	6	8	17	9	8
EMS	1.42	1.31	1.35	1.38	1.31	93%	*	105%		100%		95%		0.05	0.07	0.12	0.08	0.16	6	8	17	9	8
P2	0.71	0.76	0.75	0.73	0.78	108%	*	96%		102%		107%		0.06	0.07	0.14	0.07	0.19	6	8	17	9	8
ABal	0.95	0.97	0.99	0.98	0.99	103%		101%		102%		101%		0.06	0.09	0.07	0.08	0.06	6	8	17	9	8
ABar	1.06	1.03	1.02	1.02	1.01	97%		99%		98%		99%		0.06	0.09	0.07	0.08	0.05	6	8	17	9	8
ABpl	1.12	1.13	0.96	0.96	0.95	101%		85%	*	84%	**	99%		0.16	0.11	0.11	0.12	0.11	6	8	17	9	8
ABpr	0.91	0.89	1.05	1.05	1.06	98%		117%	**	118%	**	101%		0.16	0.11	0.10	0.12	0.09	6	8	17	9	8
MS	1.18	1.08	0.94	0.89	0.99	92%		83%	***	91%	*	111%	*	0.12	0.08	0.11	0.11	0.09	6	8	17	9	8
E	0.86	0.93	1.08	1.13	1.01	108%		122%	**	109%	*	90%	+	0.13	0.08	0.12	0.12	0.09	6	8	17	9	8
C	2.41	1.96	1.52	1.54	1.49	81%	**	79%	***	76%	***	97%		0.10	0.11	0.12	0.13	0.13	6	8	17	9	8
P3	0.42	0.52	0.67	0.66	0.68	123%	**	128%	**	132%	**	103%		0.10	0.12	0.13	0.13	0.14	6	8	17	9	8
ABala	0.81	0.78	0.79	0.78	0.80	96%		101%		103%		103%		0.05	0.06	0.11	0.09	0.13	6	7	15	8	7
ABalp	1.24	1.29	1.28	1.29	1.26	105%		100%		98%		98%		0.05	0.06	0.10	0.09	0.13	6	7	15	8	7
ABara	0.80	0.73	0.81	0.75	0.88	91%		103%		121%	+	118%		0.09	0.12	0.20	0.12	0.23	6	7	15	8	7
ABarp	1.25	1.39	1.27	1.35	1.18	111%	+	97%		85%		88%		0.09	0.12	0.18	0.13	0.24	6	7	15	8	7
ABpla	1.31	1.26	1.06	1.10	1.01	96%		88%	**	81%	**	92%		0.09	0.09	0.11	0.07	0.13	6	7	15	8	7
ABplp	0.77	0.80	0.95	0.91	1.00	104%		114%	**	125%	**	110%		0.09	0.09	0.11	0.08	0.13	6	7	15	8	7
ABpra	1.16	1.29	1.08	1.13	1.02	111%	**	88%	**	79%	***	90%	*	0.06	0.05	0.11	0.10	0.10	6	7	15	8	7
ABprp	0.86	0.78	0.94	0.89	0.99	90%	**	114%	**	127%	***	111%	*	0.06	0.05	0.11	0.10	0.09	6	7	15	8	7
MSa	0.99	1.00	1.02	1.00	1.04	101%		100%		104%		104%		0.07	0.09	0.09	0.06	0.12	6	7	15	8	7
MSp	1.01	1.00	0.99	1.00	0.97	99%		100%		97%		97%		0.07	0.09	0.09	0.06	0.11	6	7	15	8	7
Ea	1.07	0.98	1.03	1.04	1.02	91%	*	107%		104%		98%		0.08	0.07	0.07	0.08	0.06	6	7	15	8	7
Ep	0.94	1.03	0.97	0.96	0.98	109%	*	94%		96%		102%		0.08	0.07	0.07	0.08	0.07	6	7	15	8	7
Ca	0.92	0.99	0.97	0.97	0.97	108%		98%		98%		101%		0.10	0.07	0.08	0.08	0.09	6	7	14	7	7
Cp	1.10	1.01	1.04	1.04	1.04	92%		103%		102%		100%		0.11	0.07	0.08	0.08	0.09	6	7	14	7	7
D	2.44	1.72	1.48	1.51	1.45	71%	*	88%		84%		96%		0.15	0.17	0.20	0.20	0.22	4	6	13	7	6
P4	0.42	0.59	0.71	0.69	0.72	143%	*	116%		122%		105%		0.17	0.18	0.25	0.27	0.26	4	6	13	7	6

Statistical comparisons in this table were performed with Welsh *t*-test and are reported without any correction. Encoding of groups and significance is the same as in the Table 1

2.10 Early gastrulation and differentiation defects in endoderm

Following our observations of altered cell cycle timing and minor defects in division asymmetry in relatively early embryogenesis, we decided to investigate downstream effects on gastrulation. As mentioned in the introduction, *C. elegans* gastrulation begins with ingression of the endoderm cells Ea and Ep (hereafter referred to as E2 collectively for simplicity) arising from the sole gut precursor cell E (**Figure 1**). E2 ingression is accompanied by a nearly two-fold lengthening of the E2 cell cycle as compared to the sister MS lineage (**Figure 25A, B**). This cell cycle delay is concomitant with the first wave of zygotic genome activation in E2 cells (Powell-Coffman et al., 1996). The E2 ingression is characterized by a dramatic cell shape change dependent on Wnt/Src signaling from neighboring P3/P4 cells that triggers apical constriction of E2 cells close to the embryo periphery, driving their inward movement (Chisholm, 2006; Pohl et al., 2012) (**Figure 4, Figure 25A, E**).

We observed a significant reduction of the E2 cell cycle in equalized *lin-5(ev571)* embryos (**Figure 25C**), confirming our observation from the lineaging dataset. Dying embryos had markedly shorter E2 cell cycle duration (58.9 ± 4.5 min, n=12) compared to *lin-5(ev571)* unequal controls (76.6 ± 9.9 min, n=23) or EA embryos (67 ± 4.8 min, n=6, **Figure 25D**). Accelerated E2 cells in equalized embryos often divided before completing the ingression into the blastocoel in contrast to control *lin-5(ev571)* embryos, in which E2 cells were completely covered by neighboring cells before dividing (**Movie S7, Figure 25E**). The average length of the trajectory that E2 nuclei travelled before dividing was significantly shorter in equalized embryos and correlated with cell cycle duration, suggesting that ingression requires certain time to be completed (**Figure 25D**). In line with this notion, E2 descendants continued ingressing right after E2 division, followed by P4, and MS lineage cells later (**Movie S7**).

As mentioned in the introduction, proper differentiation of the E lineage is a prerequisite for faithful gastrulation. The *C. elegans* gut is specified by a cascade of GATA-family transcription factors that are sequentially activated over three division rounds of the E lineage (Maduro and Rothman, 2002). First, the expression of the redundant GATA factors END-1 and END-3 is induced in E under a combinatorial control of maternal factors (Introduction). END-3 expression peaks at late E2 stage (28-44 cell stage) shortly before mitosis and activates the next tier of redundant transcription factors ELT-2/ELT-7, which are detectable from the late E4-stage (~96-cell stage) onwards. ELT-2 is a key transcription factor that remains active until adulthood and activates a large set of genes required for gut differentiation and physiology (Maduro et al., 2005).

A

Ea Ep

Ea Ep P4
MSpp

B

EMS

MS — E

MSa MSp Ea Ep

E2

E4

C

E2 delay after MSp [min]

Ctrl   Alive   Dead

***

*

D

E2 trajectory [um]

r=0.64
p=3e−05

E2 cell cycle [min]

E2 trajectory [um]

Ctrl   Alive   Dead

***

n.s.   *

E

lin-5 (ev571)

	E2 stage 8 min before division	E4 stage 4 min post E2 division	Peak END-3:GFP expression at E2
Unequal control	END-3::GFP — 02:32	02:40	GFP intensity [A.U] 0 — 1500
Equalized	02:18	02:34	GFP intensity [A.U] 0 — 1500

F

E2 END-3::GFP expression [A.U.]

r=0.78
p=1.6e−08

E2 cell cycle [min]

***

n.s.

G

	WT Control - AB 58%	AB 54% - Alive	AB 50.8% - Dead
2-cell GFP::PH	00:03:30		
E8 stage ELT-2::GFP	04:09:00		
3-fold stage + 20 hours			08:15:00

lin-5 (ev571)

H

% embryos with abnormal ELT-2::GFP pattern at E8

8   13

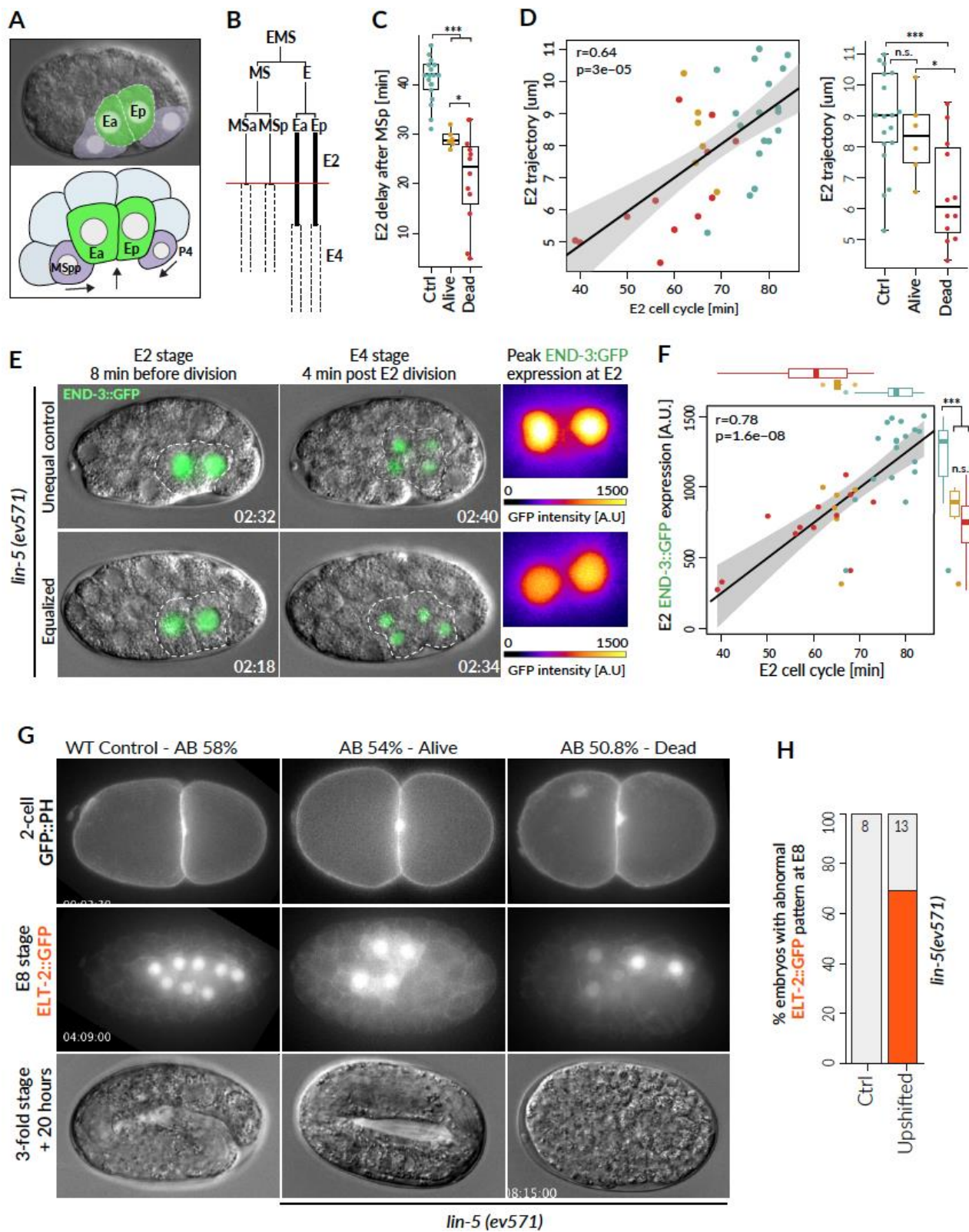Ctrl   Upshifted

lin-5(ev571)

46

Figure 25 - Defective endodermal fate acquisition in equalized lin-5(ev571) embryos

(A) Gastrulation in *C. elegans* begins with ingression of Ea and Ep (E2) cells. **(B)** Gastrulation is accompanied by a nearly 2-fold lengthening of the E2 cell cycle in comparison to that of their MSa/p cousins. The E2 cells divide once completetly internalized after MSpp and P4 came to contact them. **(C)** E2 cells in equalized *lin-5(ev571)* embryos have accelerated cell cycles and divide precociously. Graph shows E2 division delay after the division of their MSp cousin cell. **(D)** E2 ingression (nuclear trajectory) is significantly reduced in equalized embryos and correlates with E2 cell cycle duration. **(E)** Equalized embryos express less END-3**::**GFP in E2 cells (zoom view of the two E cells on the right shows the timepoint with the peak GFP expression). E2 cells in equalized embryos are noticeably larger, and begin dividing precociously close to the eggshell before completing ingression compared to the unequal control embryos (see Movie S7). Time is indicated in hh:mm, with time 0 being the time of the first cleavage. Unequal control was upshifted during the early 2-cell stage. **(F)** Quantification of END-3**::**GFP peak expression during the E2 cell cycle. Expression correlates with E2 cell cycle duration and initial size asymmetry at the two-cell stage. **(G, H)** Unequal controls express ELT-2::GFP in all 8 intestinal precursors at ~100-cell stage. The majority of equalized embryos exhibit variable defects in ELT-2**::**GFP expression at the E8 stage. Shown are two representative examples, one EA and one ED. Statistical comparisons were performed with Welsh two sample test with Bonferroni-Hochberg correction in case multiple comparisons were performed. Asterisk indicate statistical significance, * P <0.05, ** P < 0.01, *** P < 0.001.

To test whether the precocious E2 division and reduced ingression observed in equalized *lin-5(ev571)* embryos correlates with incomplete fate specification, we crossed fluorescent fusion markers of the GATA factors MED-1, END-3, and ELT-2 into the *lin-5(ev571)* background. We then investigated the corresponding expression patterns in control and equally dividing embryos using live imaging. Note that the END-3::GFP reporter becomes visible with one cell cycle delay in the E2 cells due to the time required for GFP maturation. Similarly, the ELT-2::GFP reporter becomes detectable at the E8 stage (~150-cell stage) in all 8 gut progenitors.

We observed that both the endomesoderm marker MED-1::GFP (n=8, data not shown), and END-3::GFP (n=18, **Figure 25F**) were always induced after the upshift only in MS2/E2, and E2 only, respectively. While MED-1::GFP pattern appeared normal in EQ embryos and we did not analyze it in any greater detail, the END-3::GFP was expressed significantly less in E2 cells of EQ embryos (62±19% of the control levels n=18 vs n=19 controls, P < 0.0001, **Figure 25E, F**). END-3::GFP expression levels correlated with the initial AB/P1 size asymmetry (r=0.75, p<0.0001, n=37, not shown), and with the mean duration of the E2 cell cycle (r=0.8, p<0.0001, n=37, **Figure 25F**).

Interestingly, the terminal endodermal differentiation marker ELT-2::GFP was not always expressed in all 8 intestinal progenitors as in the wild-type, but rather in a random pattern, suggesting that the correct fate might not be properly specified in all intestinal progenitors (**Figure 25G, H**, n=9/13). Indeed, we observed that some equalized larvae had a decreased number of ELT-2::GFP nuclei, indicating that embryos were not able to activate ELT-2 after the E8 stage (data not shown).
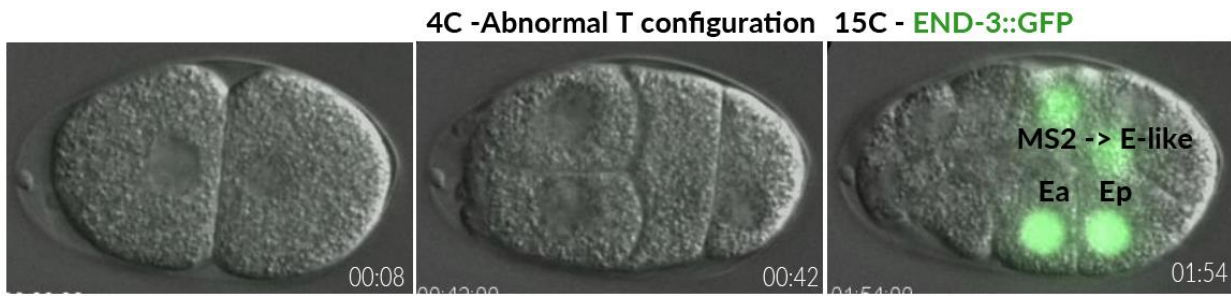
Figure 26 - Ectopic Induction of the gut fate in the MS lineage

Correct four-cell stage arrangement is critical for differentiation of ABp by Delta/Notch signaling from P2, as well as for the polarization of EMS that normally gives rise to the mesoderm lineage MS and to the sole endoderm precursor E expressing the GATA transcription factor END-3::GFP after the next division. Embryos with four-cell stage T-configuration undergo transformation of MS to E as illustrated here by 2 MS descendants expressing this endodermal marker.

Taken together, we conclude that in equalized embryos E2 cells have substantially shorter cell cycle and express lower levels of END-3::GFP, probably reflecting incomplete specification of the intestine. Moreover, ELT-2::GFP expression patterns are also abnormal in the majority of equalized embryos. However, some embryos with abnormal ELT-2::GFP expression patterns still hatched, ruling out aberrant endodermal differentiation as the sole cause of developmental failure.

Interestingly, in a few embryos with the T-configuration at the four-cell stage, both E and MS daughters expressed the endodermal marker END-3::GFP (n=3/3, **Figure 26, Movie S6**), clearly indicating that the MS lineage was transformed into an E fate. This was most likely caused by the transversal, instead of normal AP-directed EMS division orientation, changing EMS cell geometry. Wnt/Src signaling from P2 to EMS is required for the induction of the endodermal program in E (Maduro, 2017). Our observations suggest that the elongated EMS geometry along the AP axis might be required for appropriate polarization/induction of an endodermal program uniquely in the future E that is normally adjacent to P2, and not in MS, which is normally positioned closer to the anterior.

2.11 Spindle orientation and cell positioning in equalized embryos

We investigated cell positioning and division angles in greater detail in lineaged embryos (same data as in **Figure 17**) to reveal possible systematic changes in cell positioning following equalization of the first division, as well as to better understand the phenotypes of ED versus EA embryos. We compared cell positions at metaphase and division angles at anaphase to a reference model of embryogenesis based on unequal *lin-5(ev571)* embryos. We chose to use *lin-5(ev571)* control embryos as a suitable reference to equalized *lin-5(ev571)* embryos since they have the same genotype; nonetheless, we also report N2 wild-type statistics for completeness. We used the position of the MS cell at the end of the 12-cell stage to align embryos along the dorsoventral axis.
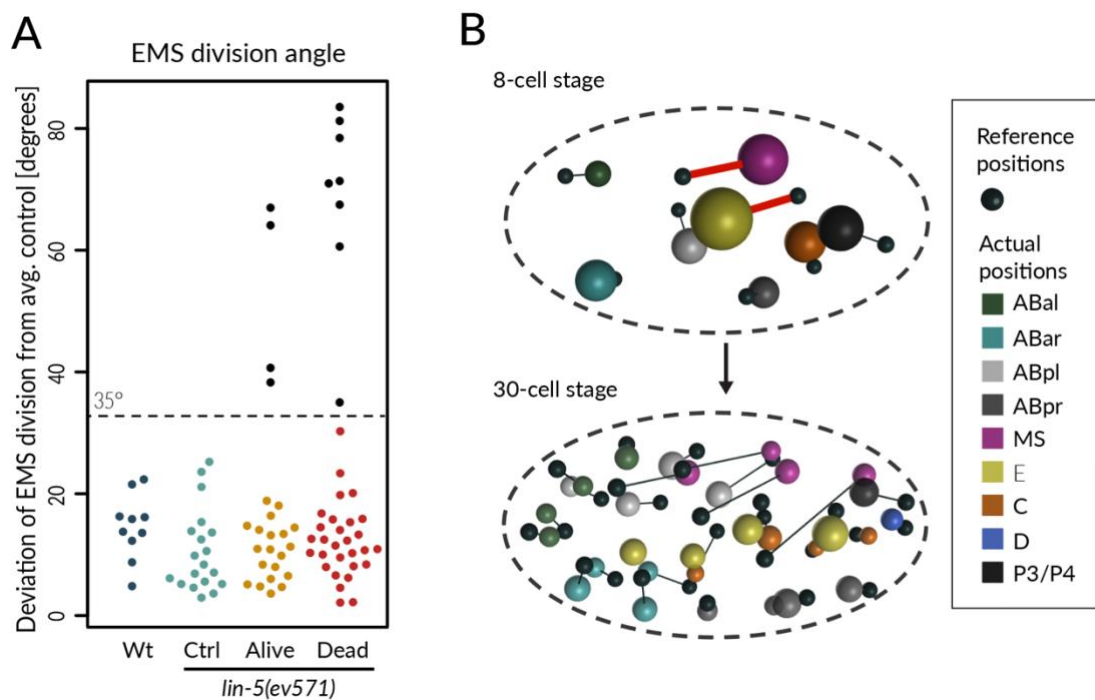
Figure 27 - Skewed EMS division leads to dramatic mispositioning of many cells

(A) Angular deviation of EMS division axis from normal AP orientation in average control *lin-5(ev571)* embryo. A skewed EMS division in some ED embryos with over 35° deviation resulted in mispositioning of many blastomeres later in embryogenesis as illustrated with one example in panel B. **(B)** 3D model of equalized embryo with dramatic mispositioning of E and MS following skewed EMS division (red lines connect the nuclei to their expected positions in the model control embryo). Colored spheres indicate position of nuclei in actual embryo, sphere sizes correspond to nuclear diameter; smaller black spheres mark the average cell positions in control embryos. Note that alive embryos with tilted EMS division shown in panel A were able to reposition E and MS cells to the correct positions post-division.

2.11.1 Aberrant orientation of the EMS division axis causes a dramatic shift in cell positions

First, we observed that the EMS division deviated more than 35° from its normal orientation in a fraction of equalized embryos within our lineaging dataset (n=12/61, **Figure 17A**). EMS normally divides along the AP axis in control embryos, resulting in MS being positioned more to the anterior and E closer to the posterior pole. A skewed EMS division was more frequent in ED embryos (n=8/37 in ED vs 4/25 in EA, **Figure 17A**), leading to a dramatic cell mispositioning in ED embryos already at the 8-cell stage, when E and MS cells assumed oblique positions (**Figure 17B**). This defect propagated over time, leading to severe perturbation in global cell organization (**Figure 17B**, bottom). Interestingly, by manual inspection of our data, we found that the four EA embryos with tilted EMS division corrected the E and MS positions quickly, while this was not the case in any of the ED embryos with the EMS skew (n=0/8).

EMS spindle orientation is under the control of Wnt/Src signaling from P2 (Liro and Rose, 2016; Zhang et al., 2008). The skewed EMS spindle in dying equalized embryos raises the possibility that either P2 did not provide sufficient signal (concentration, timing), or that EMS was not able to correctly respond to a normal incoming signaling. Both possibilities could be caused by defective fate acquisition of either P2, EMS, or both.

It appears that embryos with skewed EMS division that died represent a distinct phenotypic class, with early cell positioning defect leading to massive disruption of blastomere arrangement, resulting in failure of gastrulation and overall morphogenesis. We did not specifically investigate this class of embryos in any greater detail regarding the expression of lineage markers, since the EMS skew phenotype is relatively infrequent and therefore difficult to study. However, we provide some further analysis in **Chapter 2.12** using the same data set.

2.11.2 Unstable MS division orientation frequently results in the flip of MSa and MSp cells

Next, we analyzed spindle orientation in later divisions excluding embryos with the skewed EMS division. We found that the MS division axis in ED embryos had frequently a high angular deviation in comparison to anaphase spindle orientation in unequal Ctrl, ultimately leading to the mispositioning of MSa and MSp daughters in some ED embryos (**Figure** 28**A-C**). While the MS division was oriented with a ~23±10° (n=18) inclination from the AP axis in controls, it had a lower inclination of ~18±14° in EA embryos (n=23), and extremely variable orientation of 46±32° in ED embryos (n=28). Close inspection of equalized embryos before, during, and after the MS division in source movies revealed a highly unstable MS spindle position, whereby the spindle changed orientation during anaphase and through cytokinesis (**Figure** 28**D**). We scored the resulting position of MSa and MSp cells after MS cytokinesis was completed to assess the final orientation of these two cells. We found that MSa and MSp cells were frequently flipped in the LR axis, with MSa taking position on the right instead of the left ventral aspect (**Figure** 28**B, C**). Importantly, this "flipped" phenotype was significantly associated with death,

and never observed in unequal controls (**Figure** 28**B**). Surprisingly, we observed that eventhough MSa/p positions appeared initially relatively normal in some EQ embryos, they were prone to flipping even during the next division (**Figure** 28**D, E**). This might be due to the positioning of MSa/MSp almost perfectly along the AP axis in some EQ embryos, a situation that does not provide proper LR guidance for the following division (see **Figure** 28**E** for one such example).

Interestingly, MSa and MSp form nearly equivalent mesodermal tissues on the left and right side of the worm body, yielding notably body wall and pharyngeal muscles, as well as several neuroblasts. One of the asymmetries between MSa/MSp is the programmed cell death of MS**p**aapp that occurs on the right side of the embryo, whereas its contralateral homologue MS**a**aapp contributes to the pharyngo-intestinal valve (Sulston et al., 1983). Therefore, MS**p**aapp can be traced in equalized embryos to assess the impact of flipped MSa/p positions on fate. Moreover, this theoretically allows one to distinguish a cell-intrinsic differentiation program from an induced one, since the neighbors of the flipped cells do not vary in the same manner. In case of an induced fate, MS**a**aapp cell would be predicted to undergo apoptosis in the embryo with MSa/p flipped, whereas MSpaapp, which would normally die, would be expected to survive and take on the fate of MS**a**aapp on the left side. By contrast, in case of a cell autonomous program, the two cells would maintain their characteristic fate in flipped embryos, but die and differentiate, respectively, on the opposite sides of the body than they normally do.

We inspected only 2 embryos with such flip at the time of writing of this thesis. In one embryo, we observed that MS**p**aapp undergoes cell death on the left side instead of the right side as expected from the canonical lineage, supporting a cell-intrinsic mechanism. Moreover, both MSpaapp and MSaaap entered apoptosis in another flipped embryo, suggesting symmetrization of MSa/MSp fates in this case.
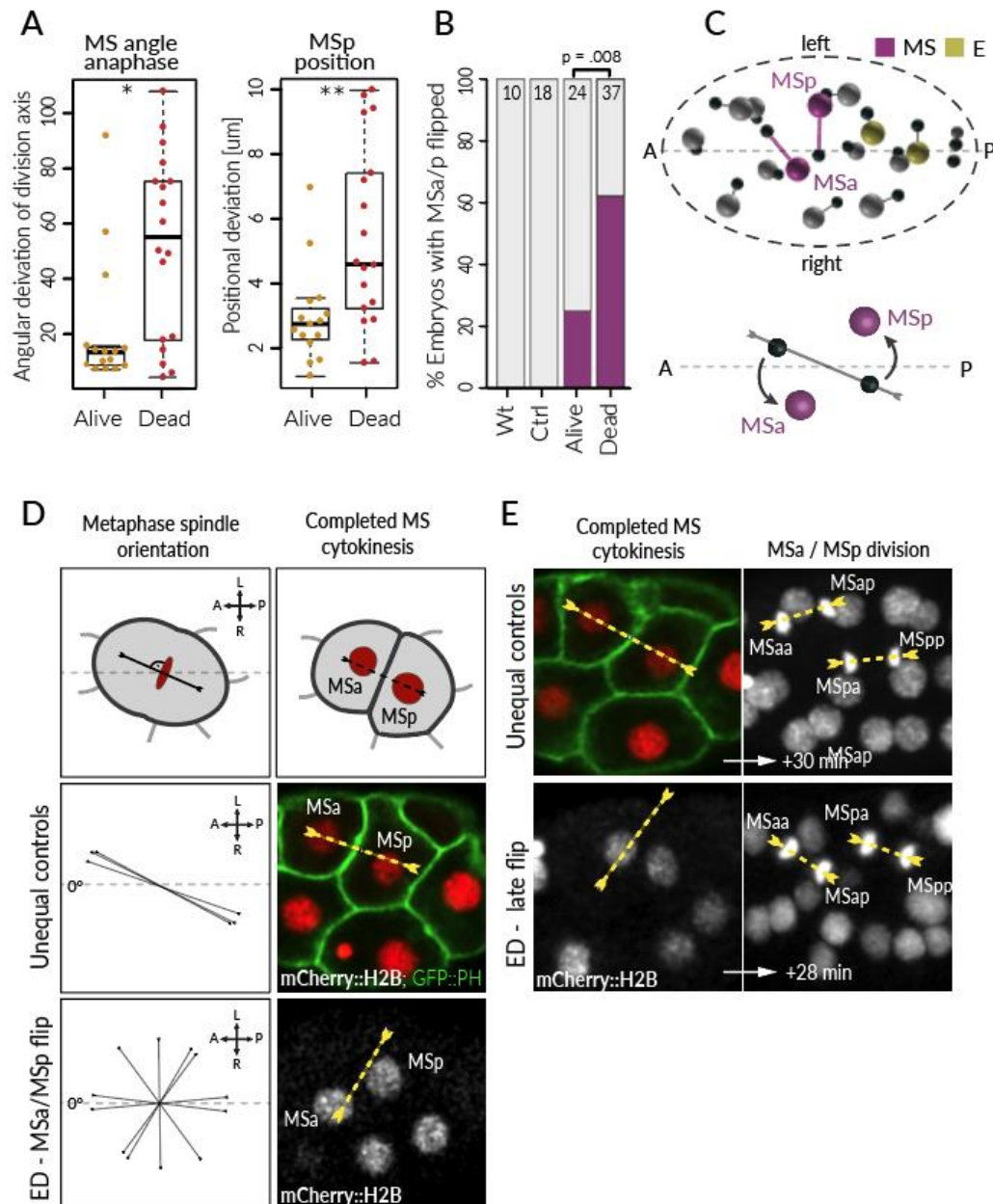
Figure 28 - *The MS spindle is frequently mispositioned leading to flipped positions of daughter cells*

(A) ED embryos had significantly increased angular deviation of the MS spindle in comparison to EA embryos, leading to mispositioning of MSp and MSa (not shown). Statistical comparisons were performed using Wilcoxon rank sum test. (B) MSa/p phenotype was significantly associated with the outcome of development in equalized *lin-5(ev571)* embryos (Fisher exact test). (C) 3D model of an equalized embryo with flipped MSa/p cells (magenta). Black spheres indicate cell positions in the unequal *lin-5(ev571)* control embryo model. Scheme below explains the MSa/p flip (D) Zoomed view on the ventral surface of control and EQ embryos showing (left) orientation of the MS spindle with respect to the AP axis at metaphase, indicated by black lines (determined by tracing a line orthogonal to the metaphase plate, shown in yellow in the right column). MS division was normally oriented ~25° to the left side from the AP axis in unequal Ctrl, while it was frequently misoriented in EQ embryos (bottom row), often leading to the flip of MSa/p cells. (right) MSa/p positions after MS cytokinesis was completed. (E) Some equalized embryos undergo the flip one division later. ED embryo shown on the second row initially appeared nearly normal, despite setting up MS spindle with high deviation (yellow arrow), but eventually flipped MSa/MSp division axes incorrectly in comparison to the control above.

2.11.3 Defects in pharynx induction in equalized embryos

The altered division of MS leading to the frequent MSa/MSp flip in EQ embryos raised the possibility of ectopic pharynx induction in ABa cells that are usually physically shielded from interacting with MS. The interaction of MS cells with adjacent ABalp and ABara cells is essential for Delta/Notch-mediated induction of the anterior portion of the pharynx (**Figure 29A**). All ABa cells express the GLP-1 Notch-family receptor and are sensitive to signaling from the MS cells that present the LAG-1 Delta ligand (reviewed in Mango, 2009). Unlike ABalp and ABara, the Aba descendants ABala and ABarp normally do not get induced because they share no or only minimal cell-cell contact with MS, respectively, due to their positions within the embryo (**Figure 29A**).

To investigate whether pharynx induction occurs normally in ABa cells in equalized embryos, we used the pharyngeal fate marker PHA-4::GFP. In control embryos, the expression of PHA-4::GFP became detectable at ~100-cell stage in both MS and ABalp/ABara cells differentiating into pharynx, but not in ABala or ABarp. Equalized embryos that developed had the expected number of 16-18 GFP positive nuclei at the 100-cell stage (5/5 EA embryos, **Figure 29B-D**).

D PHA-4::GFP expression pattern

Outcome	Alive N=5	Dead N=15					
# N embryos	5	8	1	1*	2*	2	1
ABalaaXX					🔴	🔴	🔴
ABalapaX						🔴	🔴
ABalpaXX	🟢	🟢	🟢	🟢	🟢	🟢	🟢
ABaraaXX	🟢	🟢	⚪	🟢	🟢	🟢	🟢
ABarapaX	🟢	🟢	⚪	🟢	🟢	🟢	🟢
ABarpaXX		🔴					
ABpraaXX					🔴		
ABprapaX					🔴		
ABprpaXX					🔴		
MSaaXX	🟢	🟢	🟢	🟢	🟢	🟢	⚪
MSpaaX	🟢	🟢	🟢	🟢	🟢	🟢	🟢
MSpapX	🟢	🟢	🟢	🟢	🟢	🟢	⚪
GFP⁺ cells total	18	18	16	28	22	24	18

🟢 Normal GFP expression
🔴 Ectopic GFP expression
⚪ GFP absent

A ABalp, MS Delta, ABala, ABara, ABarp, ABpra, ABprp — Notch (GLP-1)

B PHA-4::GFP ~100 cell stage 16-18 GFP positive / > 18 GFP positive — lin-5(ev571) — Equalized alive / Equalized dead

C % Embryos with aberrant PHA-4 expression — Alive (5) / Dead (15)

Figure 29 - Ectopic pharynx induction in dying equalized embryos
(A) The **MS** cell induces anterior pharynx in AB**alp** and AB**ara** lineages via Delta/Notch signaling. The GLP-1/Notch receptor (thick black lines) is expressed on the surface of all ABa cells, but ABala and ABarp normally have no physical contact with the signaling MS cells, and are therefore not induced (Mango, 2009). (B) Expression pattern of the pharyngeal marker PHA-4**::**GFP starting at ~100 cell stage. Control embryos display 16-18 GFP positive cells, while about half of ED embryos had either less (1/15) or more GFP positive cells (6/15) than controls. (C) Quantification of aberrant PHA-4::GFP expression pattern in B. (D) Detailed scoring of GFP positive cells at ~100 cell stage showing considerable variability of expression patterns. The normal pattern is in the second column for EA embryos; only a single embryo had some defect in the MS lineage in this case. AB64 and MS16 indicate that there are 64 AB cells and 16 MS at the time of scoring. Green fill color in the table indicates normal GFP positive cells, red indicates defects ectopic GFP expression. X in the cell names (e.g. MSpaaXX) stands for a/p, with XX comprising four cells: aa, ap, pa, pp.

In contrast, we observed abnormal expression pattern of PHA-4::GFP in 7/15 ED embryos (**Figure 29B**). There were more than 18 GFP positive cells in 6/15 ED embryos. We detected ectopic activation of PHA-4::GFP in four or more ABala lineage cells in 5/15 ED defective embryos, indicating that this otherwise physically forbidden induction between MS and ABala can occur in equalized embryos (**Figure 29D**).

In addition, a single ED embryo (1/15) expressed PHA-4::GFP in a few posterior AB cells (**Figure 29D**). Given present knowledge about pharynx specification (reviewed in Mango, 2007), this observation suggests that the Delta/Notch pathway was not correctly inhibited in ABp by signaling from P2 at the four cell stage. Normally, pharynx fate acquisition is prevented in the ABp lineage because Delta/Notch pathway is shut down and ABp cells, therefore, do not respond to Notch ligands presented by the MS cells (reviewed in Mango, 2007).

In conclusion, PHA-4 expression patterns varied among embryos (**Figure 29D**), suggesting - similarly to the case with ELT-2 expression patterns - that equalization of the first division does not lead to stereotyped phenotypes but instead promotes more stochastic defects in different embryos and in different lineages. Our findings indicate that at least some of these fate defects may be linked to spurious cell-cell interactions.

2.12 Cells in dying embryos diverge from normal positions

Next, we wanted to quantify overall cell misplacement during embryogenesis in EQ embryos, besides the early EMS division defect mentioned above. To this end, we calculated the Euclidian distance between equivalent cells in a given embryo and the reference model. We plotted the cumulative sum of this divergence measure over time (**Figure 30B**), as well as values normalized by the number of cells at any given time and compared the groups (**Figure 30A**). We found that equalized EA embryos showed a mild increase in positional divergence compared to unequal controls, but this difference remained mostly constant over time, indicating that cells maintained relatively normal spatial organization. In contrast, strikingly, cells in dead embryos (ED and INV) increasingly diverged over time and substantially deviated from both EA and controls embryos.
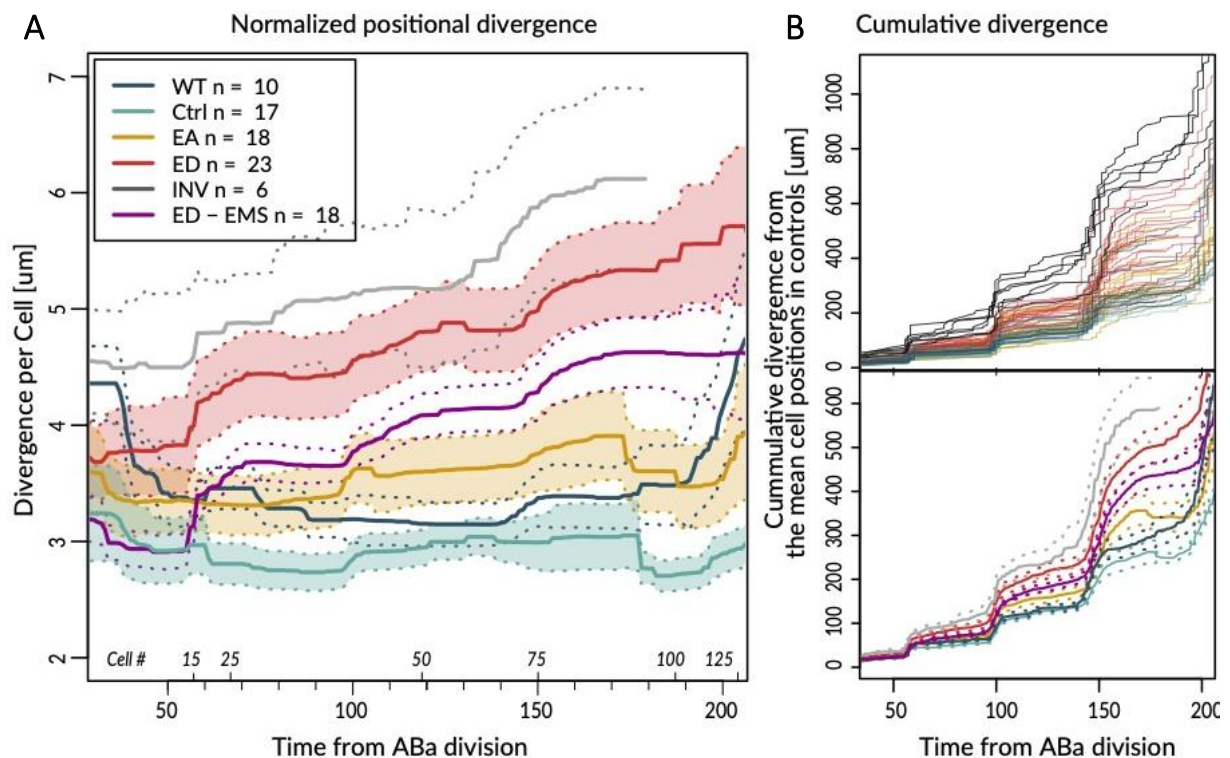
Figure 30 - *Divergence of cell positions over time*

Positional divergence in WT, *lin-5(ev571)* unequal Ctrl, EA and ED embryos (AB size in 48-52.5% range) and inverted (INV, AB size < 48%) embryos. Embryos were first aligned to the average Ctrl model embryo at the 8-cell stage using MS to define the ventral side and to correct possible rotation along AP axis. **(A)** Positional divergence was calculated as the Euclidian distance between actual nuclear position and position of the corresponding nucleus in the Ctrl model embryo just before division. The mean divergence per cell is plotted (i.e. the sum of Euclidian distances divided by cell number at any given time). INV and ED embryos exhibit greater positional divergence overall than Ctrl and EA embryos. **(B)** Plots of cumulative divergence (not normalized by cell number) for individual embryos (top) and group averages (bottom); color code as in panel A. Embryos with skewed EMS division (see Figure 27) exhibited by far the largest divergence (shown as black lines in panel B, top). Therefore, we plotted ED embryos excluding embryos with skewed EMS as well (purple line in panels A and B-bottom, ED – EMS). Dashed lines indicate SEM for each group.

Table 5 – Overall divergence of cell positions

Cell	Average deviation [um]						Change + Welsh t.test						Coefficient of variation						Number of embryos					
	WT	C	EQ	EA	ED	INV	EQ/C		ED/EA		ED/C		WT	C	EQ	EA	ED	INV	WT	C	EQ	EA	ED	INV
ABa	3.04	2.31	2.52	2.73	2.36	3.14	109%		86%		136%		0.40	0.48	0.54	0.53	0.55	0.14	10	19	47	20	27	7
ABp	3.20	2.84	3.64	4.08	3.32	6.31	128%		81%		222%		0.85	0.88	0.44	0.36	0.51	0.20	10	19	47	20	27	7
EMS	2.86	2.64	2.61	2.47	2.72	2.08	99%		110%		79%		0.30	0.68	0.54	0.56	0.54	0.32	10	19	47	20	27	7
P2	1.83	1.96	2.57	2.87	2.34	3.40	131%		82%		174%		0.37	0.62	0.40	0.29	0.49	0.45	10	19	47	20	27	7
ABal	3.25	2.40	2.88	2.46	3.18	3.28	120%		129%		137%		0.37	0.49	0.50	0.55	0.46	0.75	10	19	46	19	27	7
ABar	5.56	3.33	3.36	3.70	3.13	4.81	101%		84%		144%		0.22	0.70	0.50	0.56	0.44	0.70	10	19	46	19	27	7
ABpl	3.60	3.84	4.59	5.51	3.94	6.51	120%		72%		170%		0.37	0.64	0.60	0.52	0.65	0.51	10	19	46	19	27	7
ABpr	5.03	3.62	3.42	2.77	3.88	5.78	95%		140%		160%		0.48	0.57	0.57	0.57	0.54	0.32	10	19	46	19	27	7
MS	1.57	2.42	3.45	2.67	4.00	3.92	143%		150%		162%		0.45	0.55	0.83	0.64	0.84	0.34	10	18	46	19	27	7
E	2.52	2.47	4.08	2.85	4.95	5.61	165%	*	174%		227%	*	0.43	0.58	0.96	0.59	0.96	0.49	10	18	46	19	27	7
C	2.12	2.53	3.82	3.36	4.15	4.77	151%	*	123%		188%		0.63	0.50	0.68	0.45	0.77	0.75	10	18	46	19	27	7
P3	3.03	2.80	3.94	3.44	4.28	5.21	141%		125%		186%		0.43	0.51	0.76	0.36	0.88	0.74	10	17	45	18	27	7
ABala	2.20	2.94	3.40	2.89	3.80	3.06	116%		131%		104%		0.59	0.61	0.54	0.60	0.48	0.62	10	16	41	18	23	6
ABalp	2.28	3.69	3.76	3.31	4.11	3.51	102%		124%		95%		0.35	0.64	0.54	0.51	0.55	0.72	10	17	41	18	23	6
ABara	2.66	4.31	4.35	2.75	5.60	5.44	101%		204%	**	126%		0.63	0.63	0.57	0.57	0.42	0.27	10	17	41	18	23	6
ABarp	4.59	3.00	4.38	3.28	5.24	4.89	146%		160%		163%	*	0.41	0.58	0.67	0.40	0.68	0.51	10	17	41	18	23	6
ABpla	3.85	3.61	4.14	3.77	4.43	4.25	115%		117%		118%		0.26	0.53	0.41	0.52	0.32	0.36	10	17	41	18	23	6
ABplp	3.02	3.26	4.42	4.23	4.57	4.48	136%	*	108%		137%	*	0.23	0.32	0.52	0.60	0.46	0.46	10	16	41	18	23	6
ABpra	4.76	3.50	4.23	3.40	4.88	5.34	121%		143%		152%		0.45	0.47	0.66	0.56	0.67	0.47	10	17	41	18	23	6
ABprp	5.26	3.41	3.68	2.77	4.40	9.24	108%		158%		271%		0.24	0.45	0.63	0.45	0.62	0.47	10	17	41	18	23	6
MSa	1.92	2.07	4.98	3.61	6.05	6.76	241%	***	168%	*	327%	***	0.31	0.41	0.52	0.53	0.43	0.35	10	14	39	17	22	6
MSp	1.91	2.57	4.36	2.93	5.46	5.36	170%	**	186%	*	209%	**	0.40	0.33	0.59	0.45	0.51	0.58	10	14	39	17	22	6
Ea	3.46	3.29	4.99	3.84	5.73	4.41	152%	*	149%		134%	*	0.34	0.42	0.67	0.61	0.66	0.55	10	14	36	14	22	6
Ep	2.99	2.75	4.29	4.05	4.44	3.97	156%	*	110%		144%	*	0.46	0.39	0.58	0[.47	0.64	0.67	10	14	36	14	22	6
Ca	2.31	2.32	4.23	4.09	4.33	5.61	182%	**	106%		242%	**	0.43	0.54	0.38	0.34	0.40	0.96	10	14	36	14	22	6
Cp	2.25	2.83	3.84	3.82	3.86	5.14	136%		101%		181%		0.43	0.45	0.52	0.31	0.63	0.56	10	14	36	14	22	6
D	4.06	4.30	3.98	3.02	4.59	7.33	93%		152%		171%		0.38	0.54	0.72	0.55	0.72	0.64	10	14	36	14	22	6
P4	5.98	4.75	5.68	5.28	5.94	7.37	119%		112%		155%		0.26	0.51	0.43	0.44	0.43	0.24	10	12	36	14	22	5

Average deviation represents the Euclidian distance of a given cell nucleus prior to its division from the corresponding mean position in the control group (unequal *lin-5,* labeled as C in the table). EQ = equalized embryos (alive and dead together), EA = Equalized alive, ED = Equalized dead. Groups were statistically compared using Welsh's two sample *t*-test with Bonferroni-Hochberg correction. There were no cells among ED embryos that would have significantly lower positional divergence compared to EA embryos. N for each cell might differ depending how many embryos were lineaged up to a given stage.

As expected, embryos with the early EMS skew were by far the most affected and showed very high cumulative positional divergence (**Figure 30B**). To understand the relative contribution of this phenotype towards overall divergence, we plotted ED embryos excluding those with such EMS spindle skew (**Figure 30A, B**, magenta line). We found that in this case deviation in ED embryos started rising sharply with the 8 to 15-cell stage transition, suggesting the existence of a new defect causing mispositioning from the 15- cell stage onwards (since cell divisions in *C. elegans* embryos are highly asynchronous, stages with an odd number of cells occur).

We were surprised to find substantial differences in overall positional divergence between wild-type and *lin-5(ev571)* controls, as evidenced in particular in the initial and final parts of the dark blue curve in comparison to the light blue one in **Figure 30A**. This might be caused, among other factors, by the smaller overall size and increased aspect ratio of wild-type embryos in our dataset (**Figure 17**).

Despite normalizing for the dimensions of each embryo, the overall shape of the eggshell might impact cell positions. Furthermore, a combination of smaller size with a relatively low compression in wild-type embryos (**Figure 17**) might allow cells to move more freely.

Normally, under compression below ~20 µm (e.g., when mounting embryos on an agarose pad under the coverslip), embryo remain stably oriented throughout development until active movement begin. Typically, nuclei at the four-cell stage are in a plane parallel to the coverslip, and the DV axis is perpendicular to the coverslip in later stages. However, less compressed, smaller wild-type embryos can rotate away from their typical orientation, which would increase the measured deviation as time gets further away from the MS division that was used to rotationally align embryos. The notion of increased flexibility and differential cell movements is in line with the known effects of compression on *C. elegans* embryogenesis (Giurumescu et al., 2012; Hench et al., 2009; Jelier et al., 2016).

The question remains as to why the wild-type embryos in our dataset were smaller in the first place. Worms maintained at lower temperature were shown to produce larger embryos (Neves et al., 2015). In agreement with these results, our wild-type worms maintained at 20°C produced smaller embryos than the temperature sensitive strain kept at 16°C.

2.12.1   Increased variability of cell positions in equalized embryos

We were wondering whether phenotypes in equalized embryos are stereotyped or rather more stochastic. If equalized embryos were to display a stereotyped phenotype, we would expect relatively low variability within a group, despite increasing deviation during embryogenesis when compared to controls. In other words, this analysis should reveal whether embryos within the same group develop similarly, as expected for normal stereotypic *C. elegans* embryogenesis or generate variable phenotypes.

Similar to our previous analysis of cell cycle timing (**Figure 21**), we calculated the coefficient of variation (CV) for the position of every cell along three principal embryonic axes (AP, DV, LR) in WT, Ctrl, EA, ED, and INV embryos. Considering all 170 analyzed cells together, CV along the AP axis was not different between Ctrl and EA embryos (9.8%, and 11.1%, P=0.054), but cell positions were more variable along the AP axis in ED and INV embryos when compared to EA embryos (CV of 25%, and 20%, respectively, P<0.001 in both cases). Similarly, CV along the LR axis was significantly larger in ED compared to EA embryos (20% vs 25%, P<0.001), but surprisingly not in INV embryos, perhaps due to a much smaller number of inverted embryos in the analysis. Cells positions were most variable along the DV axis in all five groups of embryos. While there was a clear increase in CV comparing Ctrl with equalized embryos (13.7% vs 26%, p<0.001), alive and dead embryos did not differ (25.4% vs 26.8%, p=0.43).
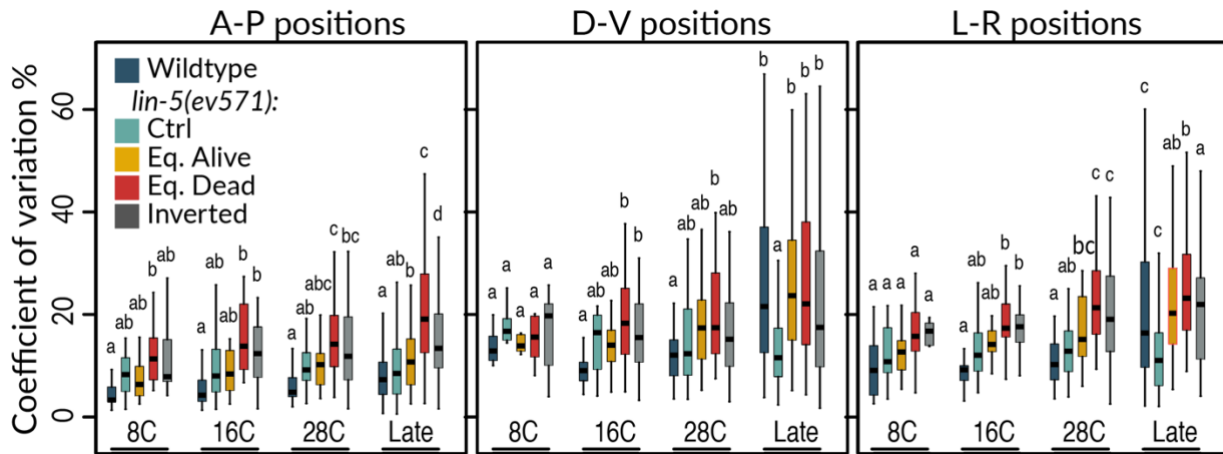
Figure 31 - Variation in cell positions during embryogenesis

Coefficient of variation for cell positions along the three principal embryonic axes for five indicated groups of embryos at the 8 cells stage (8C), 16 cells stage (16C), 28 cells stage (28C), and thereafter – comprising all subsequent stages up to the ~120 cell stage. Every data point used to construct a boxplot represents the coefficient of variation for a single cell (from at least 10 embryos within each group). Therefore, boxplots at the 8-cell stage contain 8 data points (cells), at the 16-cell stage 16 data points, etc. Late-stage contains cells beyond 28C until ~120C stage. Embryos with skewed EMS division were removed from analysis. WT embryos have high variability along LR and DV axes in late stages, suggesting that they were able to rotate along AP axis at late development (See the main text above). Comparisons between groups were performed using Anova and Tuckey honest significant difference (HSD) post-hoc test. Two boxplots that do not share the same letter are significantly different from each other with p < 0.05.

In addition, we compared CV at different stages of development between groups of embryos (**Figure 31**). We observed increased variation among embryos that died (INV, and ED) compared to the wildtype and unequal *lin-5(ev571)* controls, similarly to the previous results of timing variation, yet this increase was not significantly different at all stages. This trend was progressively more obvious with time, especially along the AP, and LR axes. This further supports the notion of stochastic aberration occurring in embryos that die, instead of exhibiting a stereotyped phenotype (see **Table 5** overall mispositioning of individual cell).

Altered cell cycle timing in equalized embryos definitely contributes to diverging cell positioning and increased variability within groups. This is because we compared cell positions at metaphase. If a given cell divided several minutes earlier or later than normally, this alone may result in a significant deviation because such a cell might not be in its normal position, as it might be migrating or moving passively with surrounding cells. This is similar to the phenotype of E2 cells that divide precociously before full ingression on the embryo periphery, and are, therefore, at different positions than in unequal controls (**Table 5, Figure 25E**, and **Figure 33**)

2.12.2 Cells with significantly different positions in equalized embryos that die

In spite of the apparent global mispositioning and increasing variability among equalized embryos over time, we sought to uncover some systematic differences among equalized embryos that could explain some of the remaining lethality. To this end, we excluded embryos with skewed EMS division from further analysis, because they likely represent their own class of early phenotypes, and we wanted to uncover new phenotypes that could by masked by the extreme aberrations of embryos with the EMS skew. Using this purged dataset, we compared the positions of individual cells along the AP, DV, and LR axes between unequal embryos and Ctrl, as well as between EA and ED embryos. In addition, we focused on the Euclidian distance of overall mispositioning of individual cells and their displacement through their cell cycle (**Figure 33**).

First, we found that 76/170 of the measured cells had a significant deviation from their normal cell position in equalized embryos as compared to unequal controls. Among those cells, MSa, MSp, and their descendants were among the most displaced in equalized embryos with respect to controls with about 1.4-3.5 times larger overall deviation (**Figure 32B, Figure 33, Table 5**).

Comparing EA and ED embryos, we again detected MSa/MSp cells to be among the most mispositioned, together with several cells from the ABara lineage (**Figure 32B, Figure 33, Table 5**). This was quite intriguing since MS and ABara are in direct contact and engage in an important interaction required for pharynx induction (see **Chapter 2.11.3**). The overall mispositioning of ABara clearly stems from its more dorsal position in ED embryos (**Figure 32B, Figure 33, Table 5**). Importantly, MS cells form mesodermal tissues, and as such, are among the first cells to ingress inside the embryo during gastrulation. These cells move to specific positions within the embryo to form the posterior pharynx and body wall muscles, among others. Hence, we speculate that mispositioning of MS cells might affect interactions with other cells and possibly even gastrulation movements.

There were several more cells with significantly different positions along at least one of the three embryonic axes when comparing EA and ED embryos, especially in later stages of development (**Figure 32, Figure 33**). In conclusion, we see many cells at significantly different positions following equalization of the first division, especially when comparing EQ to Ctrl embryos but also EA and ED embryos. However, it remains unclear which of these movements could be causally linked to embryonic lethality, as well as which of them occurs first since the embryo is a closed system where cells directly or indirectly interact.

Figure 32 - Comparison of cell positions at the 8- and 16-cell stage in equalized embryos

Shown are dorsal (XY) and lateral (XZ) views at the 8- (**A**) and 16- cell stage (**B**). Ellipses indicate distribution of cell positions in the EA (grey) and ED (colored) embryos. Arrows show direction of change between mean cell positions in EA and ED. Bold arrows indicate significant difference in at least one direction (see Figure 33, and Table 5 for statistics and data distribution).

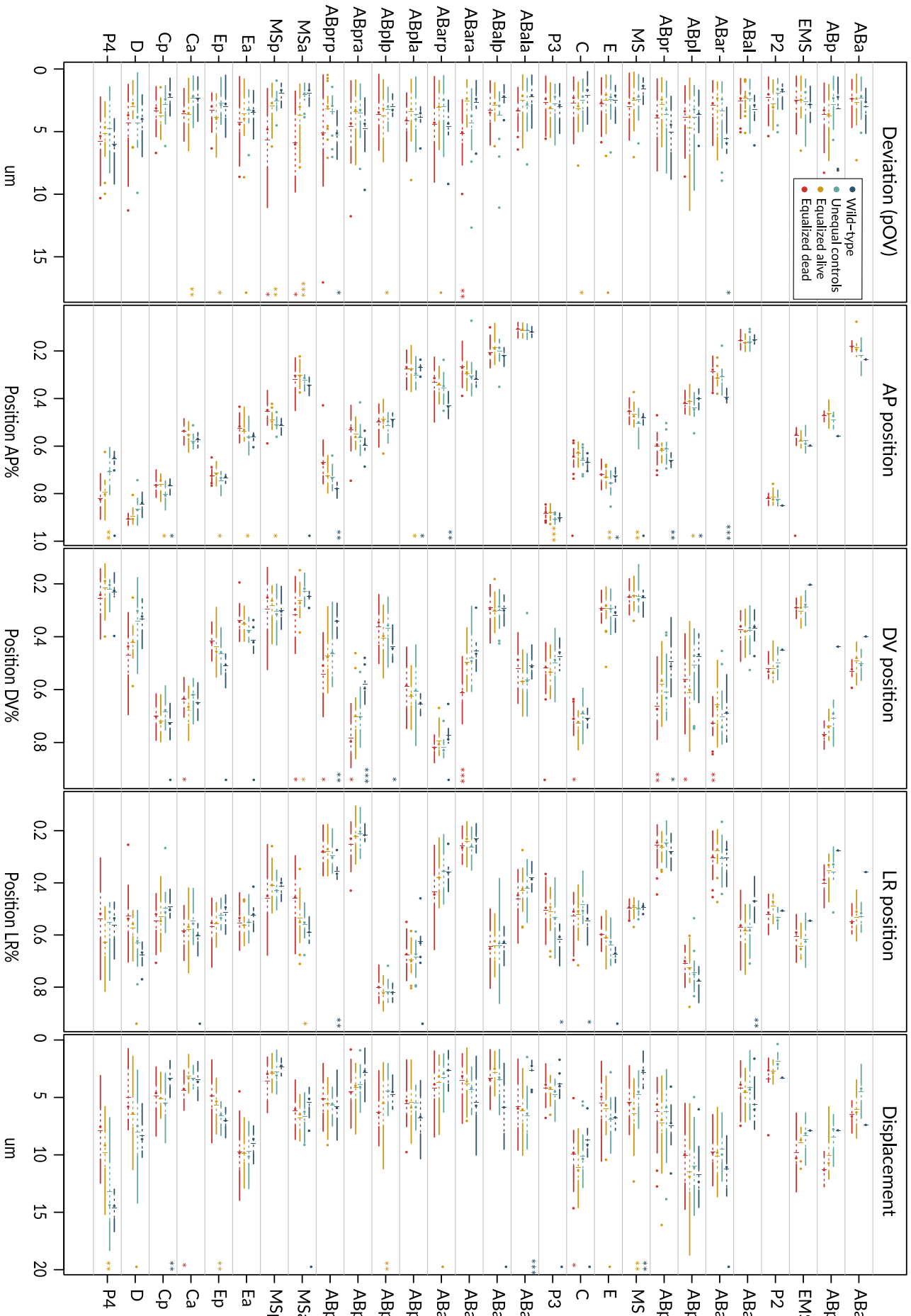A **8-cell stage**

B **16-cell stage**

X – embryo length [microns]

60
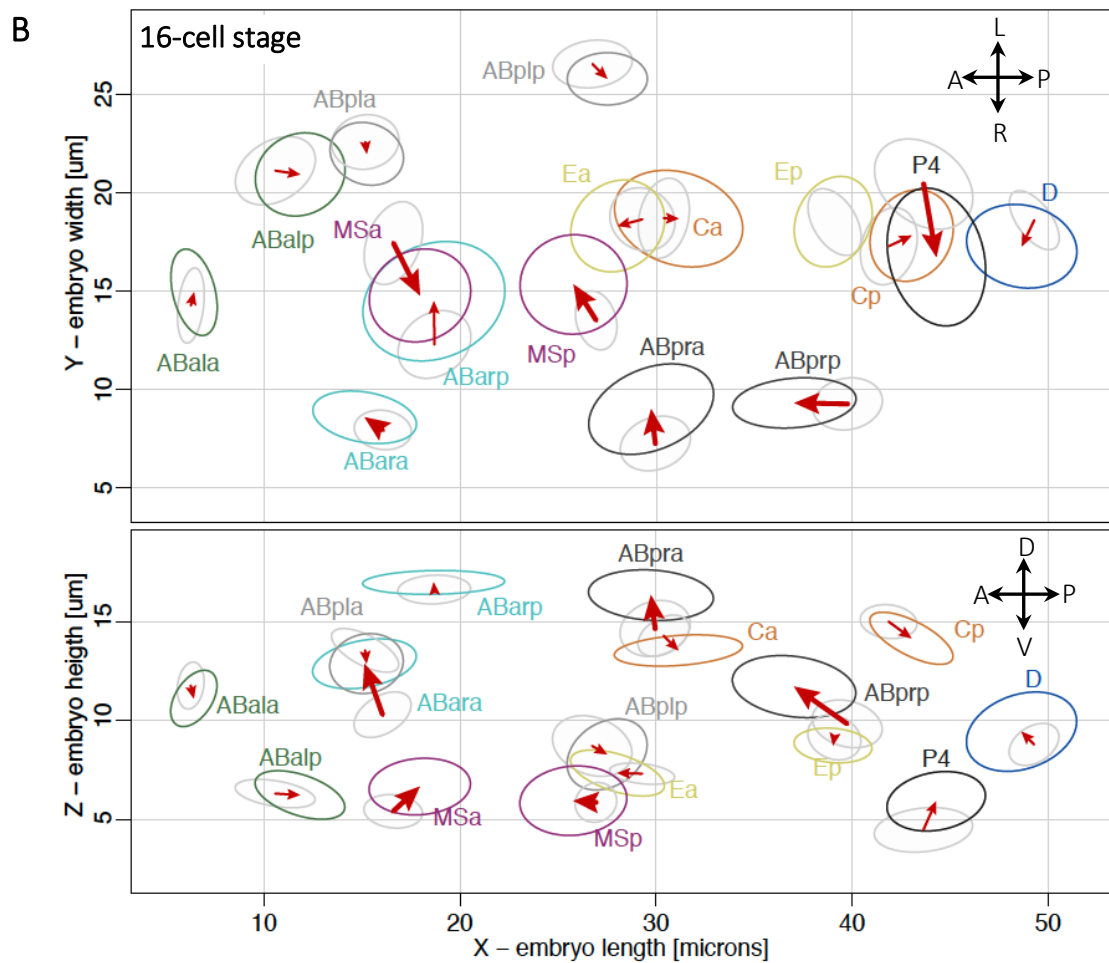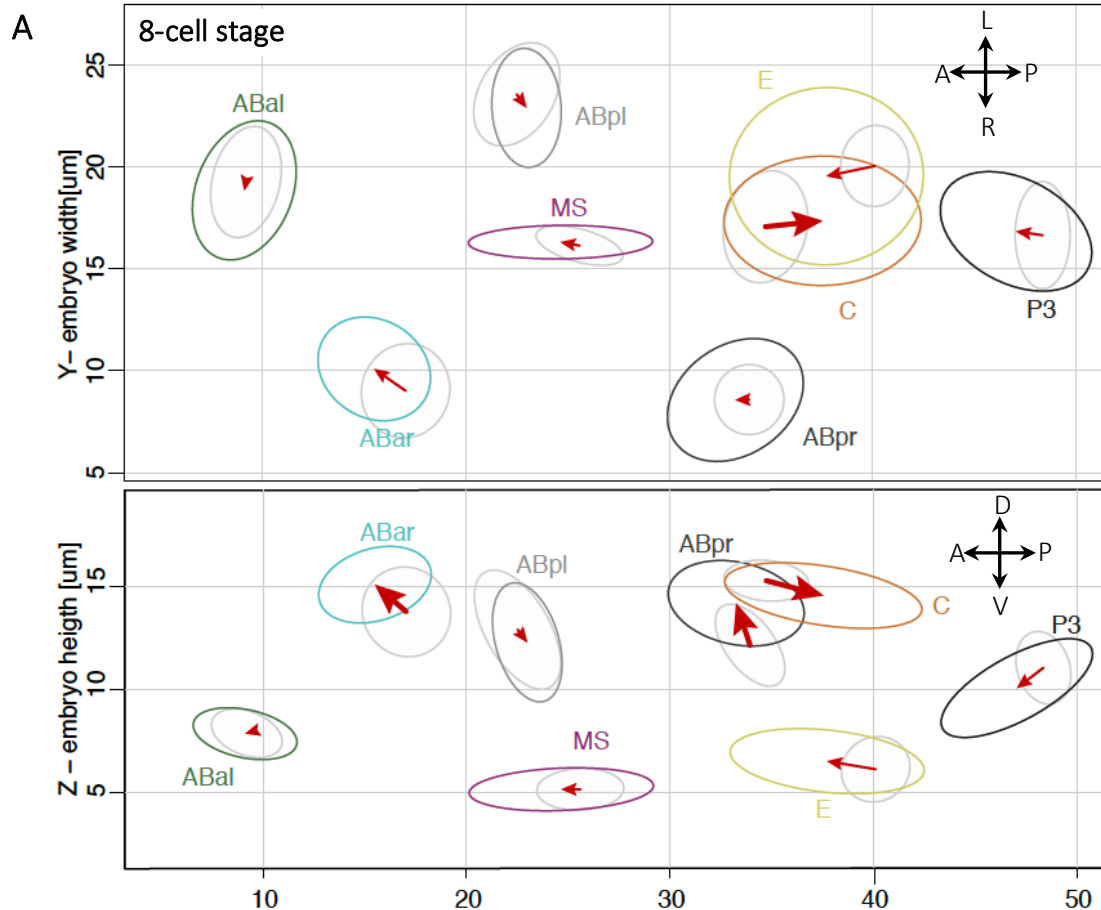
Cell positions and movement (displacement) of cells up to 16-cell stage. Asterisks indicate statistical significance of the Welsh two sample t-test after BH correction for comparison between groups as follows: blue = WT vs Ctrl, yellow = Ctrl vs all EQ, red EA vs ED; dot P < 0.1, * P <0.05, ** P < 0.01, *** P < 0.001. Embryos with skewed EMS division were excluded from this analysis. Lines of the graph are essentially condensed boxplots in which solid lines span ± 1.5 x interquartile range (IQR - 50% of all data points) indicated by the dotted line segment. If the distribution is tighter than 1.5x IQR, the line stops at the minimal and maximal value, respectively. Points outside of the range are outliers.

2.13 Developmental outcome can be predicted already at 16C stage

Lineage tracing provides detailed multivariate information about the behavior of all cells in the embryo, including time and positional information. In total, we collected datapoints for ~170 cells that appear during embryogenesis before the ~120 cell stage. For each cell we measured 13 primary variables, including cell cycle timing, cell position along the three embryonic axes, division angles, as well as angular and positional deviation, resulting in more than 2200 data points for every embryo. This complex data, however, posed a challenge due to the frequent correlation between variables and individual cells.

We employed several statistical methods in order to disentangle this complexity and to uncover patterns within this lineaging data set. More specifically, we were interested in global differences between EA and ED embryos that set them apart.

First, using principal component analysis (PCA), we observed a relatively visible, albeit not perfect, separation of unequal and equalized embryos along the first component (PC), starting already at the 15-cell stage (**Figure 34B**), in contrast to the 8-cell stage, when groups appeared more mixed (**Figure 34A**). This trend was more apparent when we plotted the first component against the relative
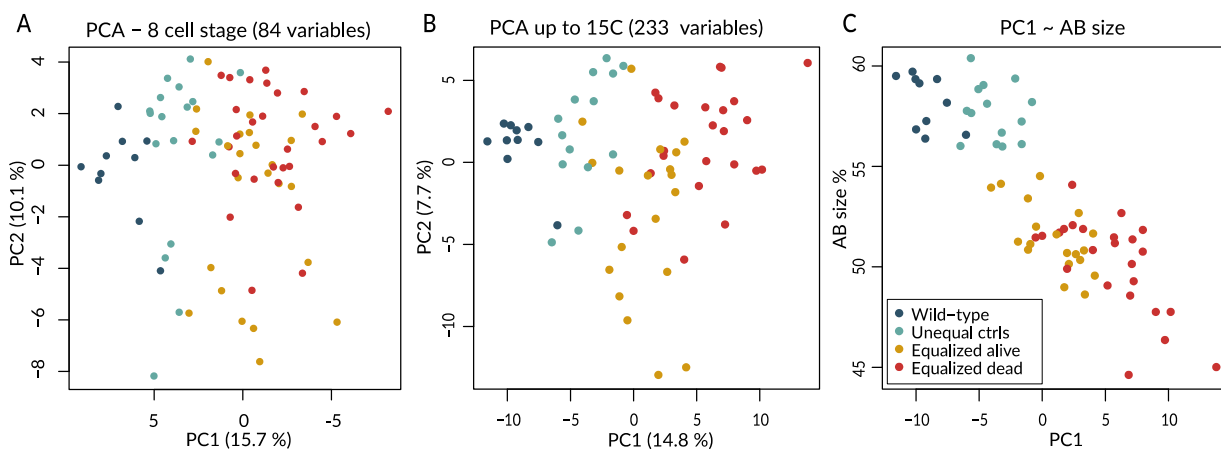
Figure 34 - Principal component analysis of lineaged embryos at 8- and up to the 15-cell stages

(**A**) Principal component analysis using all variables (cell timing, positions, division angles, deviations) at the 8-cell stage and (**B**) up to the 15-cell stage. (**C**) The first principal component PC1 from panel B correlates with initial asymmetry at the two-cell stage (AB size was not included in the initial PCA calculation). Variables with smaller than 5% variation among all embryos were excluded (30 variables).

AB size of each embryo, an independent variable that was not used for the PCA (**Figure 34C**).

We decided to explore the 15-cell stage in a greater detail. We compared all cells between EA and ED embryos to reveal possible key factors leading to embryonic lethality. We filtered variables by an absolute effect size of at least 10% and with $p < 0.002$, calculated for a false discovery rate < 10% (see Methods 4.5.5). We obtained 10 variables that met these criteria (**Figure 35A-B, Table 6**). We observed that the PC1 calculated with these variables separates EA and ED embryos almost perfectly (**Figure 35C**).

Surprisingly, only 2/10 variables pertained to the posterior linages that we expected to be more affected given previous observations. Closer examination revealed that these ten variables clustered in two anticorrelated groups (**Figure 35E**), suggesting that changes to one part of the embryo in turn influence many other cells. This is not surprising considering that the embryos develop tightly packed within the eggshell.

Interestingly, we found that some of filtered variables were related to phenotypes discussed previously in Chapter 2.11.2. Firstly, the MS division angle deviation (MS.aMean) had the largest relative change among all variables at the 15-cell stage comparing EA and ED embryos (**Figure 35A**). Although the MS division orientation along the AP axis and the deviation of the MSa and MSp positions were not selected due to our stringent cut-off, they are nonetheless within top 30 hits according to non-adjusted p-value (**Table 6**). All these three MS related variables point to the phenotype described in (**Figure 28**). Two other significantly different variables (ABara.pOV – overall positional deviation, ABara.pDV – dorso-ventral position) clearly show that ABara moved more dorsally in ED embryos (**Figure 32**, **Figure 35A**). As mentioned previously, ABar and MS are in direct contact, and MS induces pharynx in the ABara lineage (reviewed in Mango, 2007). This raises the possibility that there is a direct link between the ectopic induction of pharynx in dying embryos and ABara position. However, pharynx induction was typically not affected in ABara, apart from a single embryo out of 20 EQ embryos scored. The most frequent pattern was ectopic induction in ABala, suggesting that repositioning of ABara more dorsally might expose ABala or one of its daughters to an abnormal interaction with MS/MSa. This hypothesis remains to be tested in the future using our 3D segmentation data.

In addition, we found that Ca moves over 1.4-times longer distances in ED embryos (Ca.netdis, **Figure 35B**), despite having the same cell cycle duration in both EA and ED embryos (**Supplementary Figure** 1). Therefore, increased Ca migration is not linked to its cell cycle duration, unlike the situation for other cells that migrate less in ED embryos such as, Ea, P4 and D. Ca movement might reflect overall repositioning of other cells within the embryo. In support of this interpretation, the mother of Ca, C is positioned more posteriorly in ED embryos and moves less over its cell cycle (**Figure 32, Figure 33**).

Figure 35 - Selection of significant variables distinguishing equalized dead/alive embryos

(A) Volcano plot illustrates the selection of variables from embryos up to the 15-cell stage. The following cut-offs were chosen: p-value < 0.002 (Welsh's *t*-test. alpha value was obtained for 10% false discovery rate) and minimal effect change (dead-alive/alive) of ±10%. Variables are encoded as combination of Cell name and measured variable in the following way: Cell.**variable;** netdis = net displacement from birth to the next cell division, **a**XX and **p**XX – indicating division angle and positional deviation, respectively, where XX indicates respective direction of measure: AP = anterio-posterior, DV = dorso-ventral, LR = left-right LR, or overall spatial (pOV) or angular (aMean) deviation. **(B)** Pairwise comparison of filtered variables between EA and ED embryos. Angles are express in degrees from given axis, displacement and positional deviation are in μm. Positions are indicated relative to the AP, DV, and LR length of embryo. **(C)** PCA of equalized embryos using the 10 filtered variables shows relatively good separation of alive/dead along PC1, which is not correlated with relative AB-size **(D)** in contrast to using all variables (Figure 34) **(E)** Correlogram showing Pearson correlation coefficient and relationship between variables based on similarity.

Table 6 – Comparison between alive and dead embryos up to 15-cell stage			
	Fold Change ED/EA	*t*-test P value	P adjusted (BH)
ABara.pDV *	1.27	0.0000	0.001
ABara.pOV *	2.10	0.0000	0.006
Ca.netdis *	1.41	0.0002	0.014
ABpr.aDV	0.75	0.0002	0.014
ABpr.aLR	0.89	0.0004	0.020
ABpr.pDV	1.18	0.0006	0.023
ABar.pDV	1.16	0.0007	0.023
ABala.pOV	1.56	0.0008	0.023
ABpl.aMean	0.60	0.0011	0.028
MS.aMean	2.93	0.0012	0.028
ABprp.aAP	0.63	0.0020	0.040
ABpra.pDV	1.12	0.0021	0.040
ABpl.aDV	0.84	0.0026	0.040
ABpra.aDV	0.91	0.0026	0.040
ABplp.pDV	0.80	0.0026	0.040
ABpl.pDV	0.81	0.0029	0.040
ABarp.aAP	0.54	0.0029	0.040
ABprp.aDV	0.91	0.0046	0.059
Ca.pDV	0.90	0.0052	0.064
MSp.pOV	1.82	0.0056	0.065
MS.aAP	2.62	0.0063	0.069
ABpra.aAP	0.71	0.0082	0.085
Ca.aLR	0.92	0.0084	0.085
ABarp.aLR	0.92	0.0090	0.087
MSp.pAP	0.93	0.0093	0.087
ABar.pLR	1.17	0.0106	0.095
ABar.aDV	0.94	0.0125	0.108
ABpla.pDV	0.88	0.0134	0.111
MSa.pOV	1.58	0.0180	0.141
ABpl.aLR	0.92	0.0181	0.141
ABar.aLR	1.11	0.0201	0.151
ABprp.pAP	0.95	0.0244	0.178
Ea.aAP	0.77	0.0253	0.179
ABarp.aDV	0.92	0.0296	0.203
ABprp.aMean	1.32	0.0305	0.203
ABpr.netdis	0.74	0.0346	0.215
ABpl.pOV	0.65	0.0350	0.215
ABarp.pLR	1.15	0.0351	0.215
ABprp.pDV	1.13	0.0370	0.221
ABalp.aDV	0.90	0.0389	0.227
ABplp.aDV	0.95	0.0429	0.244
ABplp.aAP	0.77	0.0481	0.267
Cp.pOV	0.79	0.0507	0.275

Statistical comparisons of cells between EA and ED embryos (Wesh t-test) used to generate the volcano plot in Figure 35A. Only the first 43 variables out of 233 compared are shown. See legend of Figure 35 for more details. BH corrected P-values are shown, but were not considered in the selection of significant hits. Instead, an alpha threshold value was empirically determined for a 10% false-discovery rate by repeated calculation of Welsh t-test on experimental data with scrambled group labels (see Methods). Variables labeled with * are the best predictors of outcome.
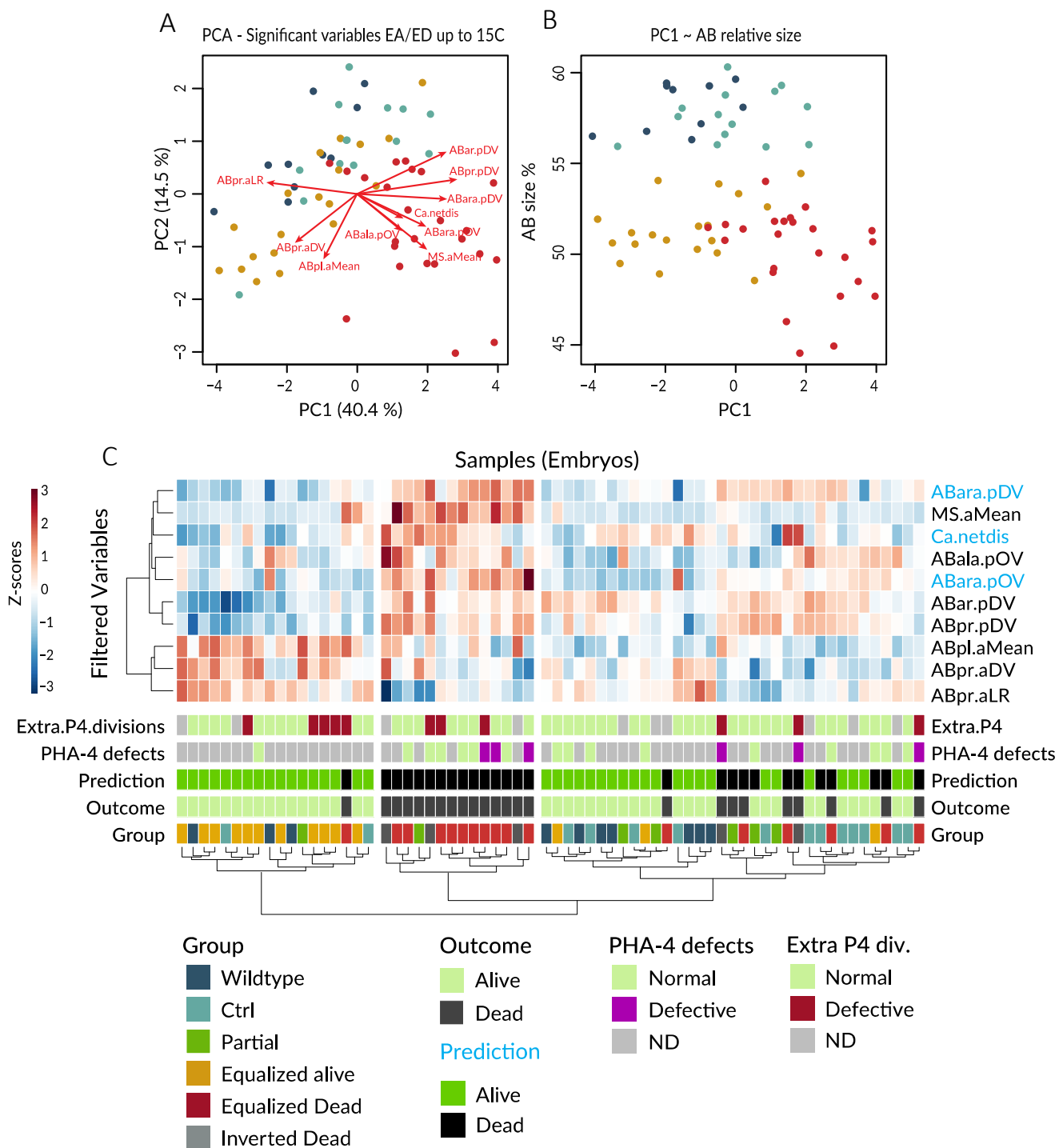
Figure 36 - *Comprehensive analysis of lineaged embryos allows outcome prediction*

(A) PCA using only the filtered variables from Figure 35 applied to all embryos except those with highly skewed EMS division. **(B)** PC1 from panel A plotted against relative size of AB shows limited correlation (compare with Figure 34). **(C)** Clustering of lineaged embryos based on filtered variables and prediction of the logistic regression model. Rows below the heatmap indicate presence of extra P4 divisions (Figure 22), PHA-4 defects (Figure 29), and the prediction of developmental outcome based on the three variables highlighted in blue. The model was trained on equalized embryos only (groups Alive and Dead with AB in 48-52.5% range) and then applied on all remaining embryos. Total accuracy was 95.5% (100% sensitivity, 93% specificity), 96% on unequal controls not used for training, and 97% on training data. In total 64 embryos were analyzed.

Furthermore, the more posterior position of C and the more dorsal position of ABara in ED embryos could be linked. Indeed, spindle orientation in ABar is under the control of Wnt signaling originating from C (Thorpe et al., 1997), which moves between the two ABp cells to form a close contact with ABar during the early 8-cell stage. Thus, if C had only limited or no contact with ABar, its spindle would not be correctly oriented and, therefore, its daughters ABara/p could be mispositioned.

Next, we performed clustering using these 10 filtered variables and observed that dying embryos mostly fall into a single cluster comprised of equalized and inverted embryos, whereas most unequal controls (wildtype and *lin-5(ev571)*), nearly equal, and equalized alive embryos group together in two remaining clusters (**Figure 36**).

We attempted to find a combination of variables that could be used to predict the outcome of development already at the 15-cell stage in EQ embryos. To this end, we used an iterative process to find a logistic regression model having the smallest Akaike Information Criterion (AIC) value (see Methods). We found that the resulting model trained only on equalized embryos (again applying a definition of AB size in the range between 48-52.5%) contained just three variables (Ca.netdis, ABara.pDV, ABara.pOV – labeled in blue in **Figure 36C**). The resulting model applied on all remaining embryos (inverted, nearly equal, and unequal controls) had a high accuracy of 95.5% (See Table below), suggesting that we were able to find features that truly distinguish dying embryos from alive ones, be it equalized or unequal.

We then tried to repeat the same process at the 8-cell stage. The resulting model contained three variables (MS.aMean, ABpr.aDV, ABar.pDV), and predicted the outcome with 87.1% accuracy in EQ embryos, but mostly failed when applied to all embryos with accuracy of only 67.5%. Nonetheless, MS.aMean refers to the MS division angle deviation discussed above and in **Chapter 2.11.2**, suggesting that MS spindle orientation is indeed an important factor affecting the outcome of development.

Our analysis, however, has several shortcomings. First, even if we assume that the identified features are the best predictors, we do not fully understand the underlying mechanisms. Second, our methodological approach has its limitations, since we trained the model and evaluated it on the same data of equalized embryos, potentially risking overfitting.

Therefore, we investigated an alternative approach employing the LASSO regression with repeated 10-fold cross-validation to obtain a predictive outcome in equalized embryos. This approach allowed us to perform an unbiased selection of the best predictors from all 233 variables in embryos from 8- to 15-cell stage without any prefiltering.

The LASSO regression is a type of linear regression that uses machine learning to select a few uncorrelated features with highest predictive power for a given response variable (Tibshirani, 1996). The LASSO regression differs from the classical logistic regression by including the so-called shrinkage coefficient lambda, which eliminates variables that contribute only a little to the fit. The machine learning aspect of the LASSO regression iteratively searches for an optimal lambda value, generating a model with minimal fitting error across individual test subsets (folds) during the cross-validation process. In addition, to obtain a more robust final model, we repeated the described cross-validation process 100-times and used the mean value of lambda.

Interestingly, the model selection converged on the combination of 5 variables, including all three selected by our initial approach and identifying two additional predictors: ABala.pOV and ABpr.aDV. The fact that this method identified the same three predictors as our initial approach validates our conclusions. Moreover, the model generated by LASSO had a prediction accuracy of 97% on the training data, but of only 75% when applied on unequal controls, and 88% on all the data together, which is quite similar to the original model. The lower performance of the LASSO model when applied to all embryos might be due to the training cross-validation, which favors a model performing robustly on equalized embryos while it is never exposed to unequal controls.

We conclude that as little as three features in early development can be used to almost invariably successfully predict the outcome of development in equalized embryos. The variables identified by our two methods indicate that ABara and ABala cells in ED embryos are substantially deviated from their normal positions in comparison to EA embryos, and that this is accompanied by increased Ca movement.

3   Discussion

Asymmetric cell division (ACD) plays an essential role in generating cell fate diversity during development and for stem cell maintenance and tissue homeostasis (reviewed in Ajduk and Zernicka-Goetz, 2016; Vertii et al., 2018; Yassin and Russell, 2016). Daughter cells arising from an ACD are frequently unequal in size in addition to having different fates, such as the differentially sized micro- and macromeres of early sea urchin embryo (Boveri, 1902; Ransick and Davidson, 1993), the constituent cells of the developing *Drosophila* bristle (Rhyu et al., 1994; Uemura et al., 1989), or many neuroblasts in *C. elegans* and *Drosophila,* where smaller daughter cells typically enter the apoptotic program (Cai et al., 2003; Ou et al., 2010; Teuliere et al., 2014). The importance of unequal volumes for fate decisions was demonstrated only for some of these examples (see Introduction section), but this question remains poorly understood and deserves more attention.

In this thesis, we focused on the first division of *C. elegans* that is characterized by the highly conserved and very precise asymmetry between the larger anterior AB and the smaller posterior P1 cell. Prior to this work, it was challenging to study the importance of solely the unequal cell size due to the lack of available tools. Polarity-defective *par* mutant embryos divide equally in the first division but die without exception due to the lack of proper AP patterning (Kemphues et al., 1988). Even mutations that do not affect polarity, but instead affect spindle positioning resulting in equal cleavage of the zygote, such as embryos without functional GPR-1/2 or LIN-5, were of little use because they impair other divisions during embryogenesis and are likewise lethal (Srinivasan et al., 2003). Evolutionary considerations suggest that the unequal first division might be critical for nematode development, as this trait is shared amongst many related nematode species in the *Rhabditidae* genus (Brauchle et al., 2009).

In summary, we presented experimental evidence for the critical importance of the size-asymmetry of the first cleavage of the *C. elegans* zygote for successful embryogenesis. We demonstrated that embryonic lethality increases with decreasing size-asymmetry. Furthermore, we showed that embryos with inverted cell-size asymmetry with AB smaller than P1 always died. Therefore, a simple physical alteration of cell size has profound effects on embryonic development, causing cell positioning, cell cycle timing, and differentiation defects.

3.1 Polarity in equalized embryos

It is unclear, however, what may be the advantage of having unequally sized cells. Theoretically, fate determinants could be segregated asymmetrically in equally sized daughter cells, and this is indeed often the case during development. Possibly, such unequal cell sizes may have evolved to make the first asymmetric division more robust, ensuring that fate determinants get segregated appropriately. Coupling of spindle positioning to the polarity network might have evolved to fit the shape of gradients of cytoplasmic fate determinants so that they get robustly allocated to the respective daughter cell. Why would evolution foster a system in which cell fates are regulated through unequal cell division, a considerable feat that requires many elements to work in unison, as opposed to tuning the polarity network or cytoplasmic gradients through a slight change in their kinetics and diving cells equally? The answer to this question awaits further investigation, including in other species. It is also entirely possible that an unrelated reason lies behind the unequal division of *C. elegans* zygote, such as the allocation of material/building blocks towards relevant tissues that develop from each cell, so that developing organs are in optimal proportions.

Interestingly, we observed a slight enrichment of MEX-5::mCherry in P1 of equalized embryos (about 8% more than in the control), indicating that the position of the cytokinetic furrow, dictated by the position of the spindle midplane, indeed can determine the resulting concentration of at least one cytoplasmic polarity mediator (Figure 11). It remains unclear whether this small increase in MEX-5 concentration in P1 correlates with incomplete fate acquisition in some posterior lineages later in embryogenesis and with lethality. It might come across as initially surprising that the total GFP::PAR-2 signal was indistinguishable in P1 between unequal controls and equalized embryos. However, the fact that PAR-2 localizes to a smaller cortical domain at the posterior could explain why we did not detect any difference since the cytokinetic furrow moved further away towards anterior in equalized embryos. A more detailed analysis of PAR-2 cortical distribution and temporal dynamics could reveal some differences between unequal and equalized embryos. It would be interesting also to investigate the distribution of anterior PAR proteins such as PAR-3/6. We would expect to see similar differences at the two-cell stage as with MEX-5. Moreover, the distribution of PAR-2/PAR-6 could be assessed during later development, i.e., before and during gastrulation as cells polarize along apicobasal axes (Nance et al., 2003).

3.2 Defects in cell cycle timing

The interplay between cell division timing, asynchrony, and gene expression has been recognized as crucial for normal development of *C. elegans* and attracted extensive attention (Encalada et al., 2000; Hashimshony et al., 2015; Ho et al., 2015; Lu et al., 2009; Nair et al., 2013; Wong et al., 2016).

Unequal cell volumes of two-cell stage embryos contribute to the asynchrony of the following division, probably because of lower amounts of some limiting replication factor in P1, leading to increased sensitivity of the replication checkpoint in this cell (Brauchle et al., 2003). We showed that some embryos with an equalized cell size assume an aberrant T-shape configuration at the 4-cell stage, most likely due to a combination of factors, including decreased asynchrony between AB and P1 divisions. However, a more careful analysis of asynchrony in these rare cases is required to assess this interpretation. It seems quite apparent from our recordings of such embryos that forces generated by the extending mitotic spindles in AB and P1, which normally lead to the sliding of AB along the eggshell towards a correct oblique configuration, balance each other out in this case, as both cells divide much closer in time. Since embryos with the T-arrangement represent only a small fraction of phenotypes occurring in equalized embryos, which have generally reduced division asynchrony between AB and P1, probably other factors are at play, such as the shape of the embryo and perhaps its absolute size. This simple phenotype would likely be amenable to physical modeling that could disentangle individual contributions of cell size, division asynchrony, and embryo shape.

Indeed, the effect of the embryo shape on the four-cell stage geometry was demonstrated in the *lon-1* mutant, which produces elongated embryos. The authors observed that some *lon-1* embryos (dividing unequally) with aspect ratio above 2 assume the T-configuration of blastomeres at the four-cell stage (Yamamoto and Kimura, 2017). Furthermore, they demonstrated that asymmetric attraction between blastomeres, mediated by E-cadherin and β-catenin, is vital for the stability and robustness of the typical four-cell stage blastomere geometry.

Interestingly, we observed cell cycle acceleration in the majority of P1 lineage cells, suggesting that equalization of cell size at the first division has long-lasting effects on the embryo. However, if cell cycle pace were determined merely by cell size, we would expect to observe a slowdown of AB lineage cells in equalized embryos, as they have smaller than usual volumes. However, we did not observe any such slowdown in equalized embryos, suggesting that AB lineage cells are less sensitive to volume changes than P1 lineage cells. The Polo-like kinase mitotic activator PLK-1 is normally enriched in AB, even upon depletion of ternary complex components leading to the equalized first division (Budirahardja and Gönczy, 2008). Therefore, it is likely that AB lineage cells in our equalized embryos retain enough of this kinase, or some other limiting factors, and therefore do not exhibit any slowdown of cell cycle progression despite their smaller size.

We found that cells in the P1 lineage are accelerated at most by 15% for P4, but typically less, between 5-12% for the E, C, MS and D lineages. Importantly, we showed that the acceleration of cell cycles of P1 descendants accumulates over time, causing several cells, including Ea/Ep, D and P4 to divide substantially earlier than usual, ultimately changing the temporal order of division compared to the unchanged AB lineage division timing.

Accelerated cell cycle timing might have repercussions for fate acquisition, which was, in several cases, shown to rely on the timely expression of select transcription factors (TFs). The expression of TFs is frequently aligned with cell cycle progression (Murray et al., 2012; Nair et al., 2013; Sarov et al., 2012). A certain minimal cell cycle duration might be required for complete TF activation within the appropriate cell cycle. Also, if the cell is supposed to engage in a signaling interaction with its neighbors at a specific time window during embryogenesis, timely expression of signaling molecules would be essential. Hence, shorter cell cycles in the P1 lineage might interfere with the proper induction of transcriptional programs either directly or indirectly via aberrant signaling.

A prime example of cell cycle duration linked to TF expression is our observation of END-3 expression in E2 cells of equalized embryos. END-3::GFP never reached the same levels as in unequal embryos, possibly because of the much shorter cell cycle of E2 cells. In another set of equalized embryos expressing a GFP fusion with the downstream GATA TF ELT-2, we observed a randomized expression pattern in eight intestinal progenitors at the ~100-cell stage, likely due to insufficient induction in prior stages by END-1/3, which never reached the required threshold levels for activation of downstream specification cascade. We assume that there is a direct link between lower END-3 expression and incomplete specification of intestinal cells; however, we did not test this hypothesis directly. In line with this conclusion, an intriguing study probing the robustness of intestinal specification demonstrated that END-1/3 must reach a critical threshold expression level for complete activation of ELT-2 and, hence, for the faithful acquisition of intestinal fate in all endodermal cells (Maduro, 2015).

Despite the frequent abnormal pattern of ELT-2 in equalized embryos, this alone cannot explain embryonic lethality. Indeed, embryos with only half of the intestinal progenitors acquiring a correct fate were reportedly developing into superficially normal larvae (Choi et al., 2017). Besides, at least some *end-1 end-3* double mutant embryos completely missing endoderm can undergo normal morphogenesis, elongate, and hatch (Owraghi et al., 2010).

Similar defects of stochastic and incomplete fate specification could occur in other lineages that we did not investigate specifically. For instance, it would be interesting to investigate muscles and hypodermal (skin) fates since they arise from several lineages derived both from AB and P1. Such an experiment would enable resolving effects of the equalized first division on both lineages simultaneously, similar to

what we did using the PHA-4::GFP reporter, which is expressed in the ABa as well as in the P1-derived MS lineages.

An additional difficulty for the interpretation of changed cell cycle timing in equalized embryos stems from the fact that not only different cell volume, but also different cell fates contribute to cell cycle timing. For example, the AB cell cycle is faster compared to that of P1, due to a higher concentration of cell cycle regulators, including the kinase PLK-1 that promotes mitotic entry in AB, and due to less active replication and spindle assembly checkpoints in comparison to P1 (Brauchle et al., 2003; Budirahardja and Gönczy, 2008; Gerhold et al., 2018). Another example of fate-related cell cycle timing are E2 cells, which require active transcription from the zygotic genome to massively lengthen their cell cycle in comparison to their cousins (Encalada et al., 2000), and to many other cells (Ho et al., 2015).

3.3   Abnormal cell positions

A change in the sequence of cell divisions can likely lead to abnormal cell-cell contacts and alterations in mechanical interactions between cells. In this context, spindle orientation within dividing cells is critically important because it dictates the future position of daughter cells within the embryo and can also affect the positions of adjacent cells by pushing them away.

Tightly controlled spindle orientation is crucial during *C. elegans* embryogenesis, as most cells do not undergo directional migration but instead rely on division orientation and forces produced by apical constriction in gastrulating cells for proper positioning (reviewed in Goldstein and Nance, 2020). Therefore, possibilities for cell position corrections are likely limited in worm embryos, in contrast to many other metazoan systems, which employ extensive cell migration and spatial gradients of morphogens that dynamically instruct cell fates.

3.4   Effects of changed cell volumes

Altered cell volumes in equalized *C. elegans* embryos might impact spindle positioning through several mechanisms. First, the division orientation is often regulated by cell polarity and cell-cell signaling, for instance through Wnt signaling, such as in EMS, which receives Wnt/Src signal from P2 (Goldstein, 1995; Liro and Rose, 2016; Zhang et al., 2008). Such spindle-orienting mechanisms can function properly only if both receiving and signaling cells express corresponding receptors and ligands, the expression of which might be directly linked to cell fates. Accordingly, Wnt signaling mutants have been shown to misorient division axes in multiple cells, including EMS and ABar (Bei et al., 2002). Second, altered blastomere volumes very likely affect the shapes of individual cells, which in turn might influence spindle positioning. It has been recently shown in the early mouse embryo that the interplay between cell shape and apicobasal cell polarity impacts resulting division orientation (Niwayama 2019).

These observations provided evidence for a tug-of-war mechanism for spindle positioning between cell polarity and the so-called Hertwig's rule, which states that cell divisions occur along the longest cell embryonic axis (Hertwig, 1884). Our 3D segmented data should allow us to test whether spindle orientation in equalized *C. elegans* embryos, especially in the frequently aberrant MS division, is affected by cell shape according to Hertwig's rule. Since blastomeres in equalized embryos have different volumes (**Table 3**), their shape is likely also affected. It would be, therefore, interesting to correlate spindle orientation with the longest cellular axis, which might differ in EQ embryos in comparison to controls.

We very likely detected the consequences of abnormal cell positioning and spurious cell-cell contact in the observed ectopic induction of the pharynx-specific transcription factor PHA-4 in the ABala lineage of equalized embryos. It seems likely that MS or its daughters, which normally induce anterior pharynx only in ABara and ABalp, but not in the inaccessible anterior-most ABala cell, made an abnormal contact with ABala in equalized embryos, leading to Delta/Notch-mediated transformation towards pharyngeal fate. These inductive events could be directly monitored by following the localization of LIN-12/Notch, which moves to the nucleus following induction by Delta ligand (Sarov et al., 2012).

It is worth noting that there was not a single embryo with abnormal PHA-4::GFP expression pattern that would eventually develop (n=7), suggesting that defective pharynx differentiation correlates perfectly with the lethal outcome. However, 8/15 equalized embryos with normal PHA-4::GFP expression pattern died, implying that other issues preclude normal development. If we were to assay more lineage markers, we would most likely find other abnormal cell-cell interactions and fate transformations.

Cell size might influence the switch from asymmetric to symmetric division mode in the P lineage, according to a recent report. In the wild-type, whereas P1, P2, and P3 divide unequally, P4 divides equally because it reaches critically small dimensions that do not allow the formation of the reciprocal PAR protein gradient due to the inherent reaction-diffusion limits of the PAR system (Hubatsch et al., 2019). The P4 daughters Z2 and Z3 then stay quiescent until hatching, after which they give rise to the whole germline (Sulston et al., 1983). We detected ectopic divisions in the P4 lineage of equalized embryos that produce new cells that would never exist in the wild-type. This observation raises the possibility that cell volume reduction at this stage might be required not only to switch to a symmetric division mode but also for the fate of germline progenitors and to maintain them quiescent until hatching.

It is worth noting in this context that even twice larger embryos created by the laser-induced fusion of two oocytes develop into unequal and asynchronously dividing two-cell stage, which divides to form normally arranged four-cell stage, and in some cases, provided a favorable ploidy, develops into a giant worm (Irle and Schierenberg, 2002). Such giant worms were, however, often sterile or produced much

less progeny. Interestingly, sterility and reduced brood size occur also in *lin-5(ev571)* even at the permissive temperature with lower frequency (Lorson et al., 2000), and seemed exacerbated in equalized survivors (data not shown, due to low numbers of observations).

The increased cell volumes of P1 descendants in equalized embryos could lead to a dilution of maternal factors segregated through asymmetric cell divisions and a lower concentration of newly synthesized fate determinants. Besides, nuclear diameter scales with cell volume in *C. elegans* (Uppaluri et al., 2016), as it does in many other systems (Reber and Goehring, 2015), affecting the final concentration of molecules such as TFs in the nucleus. Even if the same absolute number of TF molecules were synthesized and imported into the nucleus of a larger cell compared to a normal embryo, the final concentration of TF would be lower. This reasoning, however, omits possible compensatory feedback mechanisms that could adjust transcriptional output accordingly to actual cell volume. Nonetheless, our data suggest that decreased concentration of TFs could explain the incomplete fate acquisition and weaker induction that we observed, for instance, for END-3::GFP and ELT-2::GFP.

Finally, the inverse manipulation of the first division size-asymmetry, i.e., making AB larger than usual and P1 smaller, awaits experimental realization. This experiment could provide a complementary picture to the results presented in this thesis. However, this experiment was technically not possible until very recently. Optogenetically-mediated cortical force manipulation (Fielmich et al., 2018), equivalent to the one we performed to equalize the first division, could be now used to enhance size asymmetry. Similar questions that we asked in this thesis regarding division timing, fate induction by cell-cell contacts, and overall cell positioning could be addressed. Also, the fundamental size limits of P1 that are incompatible with normal development could be revealed. Since founder blastomeres contribute to precisely defined tissues and organs through the invariant division patterns, we predict that some organs would not be able to assemble correctly during gastrulation. These open questions deserve further research.

3.5 Developmental robustness

The feature that enables embryos to produce a stable phenotypic outcome in spite of environmental and transcriptional noise has been referred to as developmental robustness (Keller, 2002). We found that equalized *C. elegans* developed less robustly overall, as manifested not only by the lethality incurred by ~65% of embryos, but also by the higher variability in cell cycle timing, division orientation, cell positioning, and stochastic fate acquisition in the intestine, even amongst survivors.

Interestingly, we observed that equalized embryos that died were on average compressed by ~2 microns more than equalized embryos that lived. However, this level of extra compression was perfectly compatible with development of unequal control embryos, strongly suggesting that equalized embryos somehow lost an inherent resilient feature against mechanical stress. We measured

compression of embryos inside adult hermaphrodites at different stages carrying variable amounts of embryos (data not shown) but found that even the most compressed embryos in vivo were less compressed than in a typical experimental setting (24.7±2.5 µm in vivo vs. 21±2.4 µm for lineaged embryos mounted with beads, N=125, and 91, respectively), indicating that we are typically exposing embryos to more challenging compressive conditions than they likely experience in the mother. It is, however, not known what forces and deformations embryos might experience in the wild, where worms live in decomposing plant matter or the soil.

Active compensatory movements are known to occur in compressed wild-type embryos during mid-gastrulation to align distorted embryonic axes to their normal position (Jelier et al., 2016). It remains to be investigated whether equalized embryos perform these active movements in the same manner and whether there are any differences between embryos that die and live. Our current lineaging data set does not contain many embryos lineaged up to the stage when these compensatory movements occur.

3.6 Predictions of developmental outcomes

We cannot pinpoint a single factor that could predict which equalized embryo will die and which will live. Instead, a small change in the initial concentration of inherited fate determinants in P1 might trigger a cascade of events that brings the developmental program to the point of no return, whereby the course of fate specification cannot get back on track. The equalized first division likely tips the balance from a robust stereotypic program towards a sensitized state, in which stochastic environmental and transcriptional effects prevail, leading to embryogenesis failure. Our hypothesis is in line with the famous butterfly effect, where a minute change in initial conditions can have dramatic effects on the final state.

Nonetheless, we attempted to find a pattern in the chaos that would predict the developmental outcome at early stages. We discovered that a combination of just three features at the 15-cell stage allows predicting outcome in EQ embryos with 97% accuracy, indicating that despite high variability at later development, early timepoints carry a significant signature of what is to come later. Unfortunately, even if we assume that the identified features are the best predictors, we do not fully understand the underlying mechanisms, which will require further study.

In conclusion, we demonstrated that unequal cell volumes in the two-cell stage *C. elegans* embryo play a crucial role in ensuring robust developmental outcomes by setting up asynchronous timing between AB and P1 lineages, correct cell positioning, and reliable fate acquisition during later embryogenesis.

4 Methods

4.1 *C. elegans* strains and culture

C. elegans strains used in this study are listed in the Appendix Table 7. Strains were maintained on standard NGM plates and fed with OP50 Escherichia coli. Temperature sensitive strains were kept at 16°C, other strains at 20°C. Crosses of *lin-5(ev571)* with fluorescent marker strains were performed as described previously and the homozygous progeny was selected based on temperature sensitivity and fluorescent marker expression (Fay, 2013). Worms were well fed and maintained for at least one generation after establishment of a given strain prior to dissection and embryo imaging. *lin-5(ev571)* 1-2 day old adult hermaphrodites were dissected in M9 buffer that had been pre-chilled at 15°C, and one-cell stage embryos with visible pronuclei collected using a mouth pipet and mounted either on 2% agarose pads for DIC imaging with oil immersion objectives, or else into a bead slurry containing 20 μm polystyrene beads (Polysciences - #18329-5) either in M9 + 0.5% (w/v) methylcellulose for water immersion objectives or in 20% iodixanol (Optiprep, Sigma Aldrich) for imaging with glycerol objectives.

4.2 Temperature shift

Rapid temperature shifts were performed with the CherryTemp fluidic temperature controller (Cherry Biotech, France). The CherryTemp device is equipped with two thermalization chambers that were set to 17°C and 27°C. By changing the chamber through which the thermalization solution flowed, the sample was rapidly (~15 s) shifted to the desired temperature. To generate equally dividing *lin-5(ev571)* one-cell stage embryos, we performed the upshift right after NEBD or at metaphase for embryos expressing fluorescently labeled histone, and kept them at the restrictive temperature (27°C) until completion of cytokinesis (~5 min), after which the sample was shifted back to the permissive temperature (17°C) for the rest of embryogenesis. Embryos imaged only for a fraction of embryogenesis (e.g. until the 4-cell stage) were moved to an incubator set to 17°C and the outcome of embryonic development scored the next day. Control experiments were performed by upshifting the wild-type one-cell stage embryos in the same manner as for *lin-5(ev571)*, as well as by upshifting *lin-5(ev571)* embryos at the two-cell stage for 5 minutes to account for possible defects due to impaired *lin-5(ev571)* function unrelated to equalization. In all experiments, we scored as "alive" embryos that reached a normal looking, motile, 3-fold pre-larval stage, or that hatched, and as "dead" embryos with an abnormal morphology and therefore unable to hatch (we never observed any unhatched elongated embryo in our experiments in >250 upshifted embryos).

4.3 Time-lapse microcopy

DIC time-lapse microscopy (Figure 7) was performed on a Zeiss Axioscop 2 equipped with DIC optics and a 100x (1.25 NA Achrostigmat) objective, and recorded on a USB3.0 1.3MP monochrome CMOS camera (Ximea - model MQ013MG-E2, Slovakia) controlled by the open-source µManager software (Edelstein et al., 2014).

Combined DIC and epifluorescence time-lapse microscopy (Figure 11, Figure 26) was performed on a motorized Zeiss Axio Observer D1 using a 63x water-immersion objective (1.2 NA C-Apochromat), equipped with an Andor Zyla 4.2 sCMOS camera, a piezo controlled Z-stage (Ludl Electronic Products), and an LED light source (Lumencor SOLA II), using also the CherryTemp device to maintain the temperature at 17°C throughout embryogenesis. The setup was controlled by µManager.

4.3.1 Time-lapse microscopy for lineage tracing

Embryos for the lineaging dataset were acquired on a Leica SP8 laser scanning confocal microscope equipped with a 60x HC PL APO 1.3 NA glycerol immersion objective, HyD detectors (set to 100% sensitivity), and a tunable Chameleon laser (Coherent). Time-lapse recordings were acquired at 2.5 min intervals, capturing 35 slices at 0.75 µ spacing, and this for 100 frames. The microscope was set to 8kHz resonance scanning mode to reduce phototoxicity (Richards et al., 2013), 4 x line averaging plus 2 x frame accumulation, with a pixel size of 140 nm, a pixel dwell time of 50-70 ns, and the pinhole set to 1.2 Airy units. To compensate for the signal loss deeper in the sample, the excitation light was ramped from $2 \rightarrow 15\%$ for the 488 nm laser line and from $2 \rightarrow 18\%$ for the 585 nm laser line. Embryos were mounted in M9-20% iodixanol (Optiprep – Sigma Aldrich) to match the sample's refractive index and mounted in a sandwich between two #1.5 coverslips (40x22 mm and 18x18 mm) separated by 20 µm polystyrene beads and sealed with melted VALAP sealant (vaseline, lanolin, paraffin). Sample temperature was maintained at 17°C using the CherryTemp temperature controller. The coverslip sample sandwich was attached to the CherryTemp thermalization chip glass surface through adhesion by a thin layer of water.

4.3.2 Optogenetic-mediated division equalization

Worms expressing LIN-5::EPDZ::mCherry; PH::EGFP::LOV; GFP::TBB2 in embryos (strain SV2121, kind gift from the Sander van Heuvel lab) were dissected in a dark room under a red light to prevent premature activation of PH::LOV and mounted for imaging on 2% agarose pads (Fielmich et al., 2018). Imaging was performed on a Leica SP8 in the Live Data Mode control setting in the LAS X software, allowing to toggle laser lines on/off during acquisition. The microscope settings were the same as above with the following modifications: no Z-compensation of exposure, time-lapse acquired at 10s interval, 80-100 frames collected (from one to four-cell stage), with 11 slices at 1.25 µm spacing; moreover, the temperature was maintained at 22°C. LIN-5::EPDZ::mCherry distribution was monitored with a 585 nm

laser, and transmitted light (585 nm) images collected on an additional PMT detector to follow NEBD for analysis of AB/P1 mitotic asynchrony. Interaction of LIN-5::LOV with PH::EPDZ was induced in a small rectangular region (~10x5 μm) positioned at the anterior cortex from NEBD until completion of cytokinesis by activating a blue 488 nm laser (3-5% intensity). This laser was active solely during frame acquisition.

4.3.3 Cell cycle retardation with 405 nm laser

In order to enhance the asynchrony between AB and P1 at the second cell cycle, we continuously scanned a pulsed 405 nm diode laser (at 70% output, 700 miliwatts/cm^2 at 100%) over the entire P1 nucleus at 8 kHz (70 ns dwell time on the SP8 confocal setup described above) early in the two-cell stage. This induces photodamage, likely in the form of thymidine dimers in DNA, plausibly causing replication fork stalling in the targeted cell and activation of replication checkpoint. However, we have no experimental evidence to support this. Typically, UV lasers with shorter wavelength were used to delay cell cycle or to kill individual blastomeres in *C. elegans.* Using otherwise wild-type embryos expressing mCherry::H2B, we determined experimentally an optimal non-lethal duration of continuous laser scanning required to obtain an additional ~100 seconds of delay between AB and P1 mitoses, to enhance asynchrony from the normal 3.5 minutes to ~5 minutes. We then applied the same treatment to *lin-5(ev571)* equalized embryos to slow down P1 and restore asynchrony of the second division closer to the wild-type situation.

4.4 Image processing and analysis

All images were rotated, Z-projected and adjusted in Fiji (ImageJ) for display (Schindelin et al., 2012).

4.4.1 AB size measurement in 2D

The 2D surface of the AB and P1 cells was manually determined from DIC images or from the GFP::PH plasma membrane signal in strains expressing this marker by tracing cell outlines with a Fiji polygon tool at the mid-plane, with both nuclei in focus, when the interface between AB and P1 was perfectly straight, ~5 minutes after cytokinesis of the one-cell stage embryo (**Figure 7A**). The size of AB was then expressed relative to the embryo cross-sectional area, corresponding to the sum of P1 and AB areas.

4.4.2 Assessing accuracy of the cell size measurement

To assess how well 2D cell-area measurements at the mid-plane correspond to actual 3D cell volumes, we performed the temperature upshift experiments in embryos expressing GFP fused to the PH domain from the mammalian PKC kinase that binds to the phosphoinositide PIP2 and thus labels the plasma membrane. This allowed us to segment the full 3D volumes of AB and P1 (**Figure 37A**) using a watershed-based segmentation (MorphoLibJ plugin in Fiji, see Chapter 4.4.5 for more details). We measured the correlation between 2D size estimation and actual 3D volume (**Figure 37C**). The two methods correlate extremely well (r=0.98, p < 0.001). The measured deviation between these two
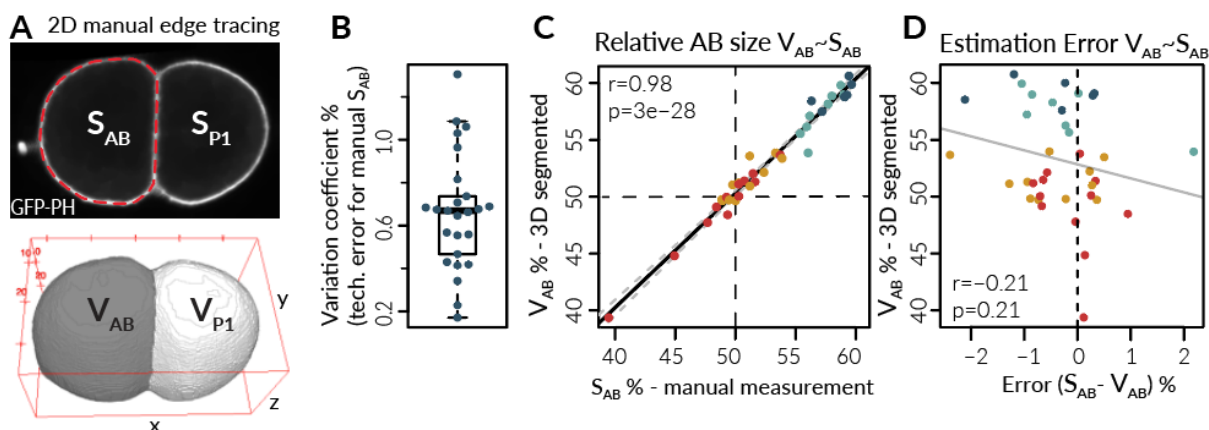
Figure 37 - Cell size measurement methodology and precision

(A - top) Cell size was measured from the mid-plane image with the largest embryo cross-sectional area. Cell boundaries were manually traced with the polygon Fiji tool either based on GFP-PH or in other experiments on the DIC images to measure the 2D area. (A - bottom) We then segmented cell volumes from pre-filtered data using the Interactive Morphological 3D reconstruction Fiji plugin. **(B)** Mean variation coefficient of repeated manual area measurements, i.e. technical error, is 0.66%; each embryo was measured 3-5 times. **(C)** Relative AB size calculated based on the 2D surface correlates extremely well with the relative AB volume. **(D)** Mean estimation error percentage for relative AB size based on difference between surface and volume was -0.42%, p<0.001 for H_0 that difference = 0. There is no significant correlation between estimation error and relative asymmetry. indicating that the 2D estimation is not biased.

methods is within the technical error of repeated manual 2D surface measurements (mean error between 2D and 3D for AB size was -0.4 ± 0.81%, in comparison to 0.6% variation in repeated manual area measurements).

4.4.3   Analysis of marker gene expression

PAR-2::GFP and mCherry::MEX-5 are both endogenously tagged with CRISPR-CAS-9 genome editing and obtained from the CGC (See Table 4 in Appendix for detailed genotype and source). These strains were imaged on a wide-field Zeiss Axio-Observer microscope as described in Chapter 4.3. Images were taken every 30 seconds until the four-cell stage, capturing 11 planes at 1.5 μm spacing. To quantify the signal, we measured the mean intensity in the mid plane at the two-cell stage, including the area of the nucleus and the entire cortex. MEX-5 intensity was normalized to the mean AB intensity in control embryos from the corresponding day because MEX-5 intensity differed significantly between experiments, even in the otherwise wild-type background.

For the analysis of endodermal differentiation, we imaged transgenic embryos expressing END-3::GFP or ELT-2::GFP in an otherwise wild-type or a *lin-5(ev571)* background using combined DIC and epifluorescence time-lapse microscopy as described above, in two-minute intervals, with 1 μm optical slicing, capturing a 25 μm stack following the same temperature shift experiment during the first division as described above. 3D gastrulation movements of the Ea/Ep cells were tracked with the TrackMate Fiji plugin (Tinevez et al., 2017) utilizing the nuclear END-3::GFP signal expressed from the

beginning of the E2 cell cycle. We then quantified the peak GFP intensity, i.e. the mean voxel intensity in the nuclear volume obtained from the TrackMate sphere detection, during the E2 cell cycle. The ELT-2::GFP expression pattern was scored visually for the number of GFP positive endodermal cells at the E8 stage. Analysis of pharyngeal differentiation was based on the PHA-4::GFP expression pattern (strain RW10425 crossed to the *lin-5(ev571)* background). We imaged these embryos with the SP8 confocal microscope as described above and then extracted the cell lineage based on the pan nuclear mCherry::H2B marker, identifying GFP positive cells at ~100-cell stage.

4.4.4   Lineage tracing

Time-lapse 3D recordings of embryos expressing mCherry**::**H2B in an otherwise wild-type or *lin-5(ev571)* background were first pre-processed to enhance the nuclear signal and remove noise with the Noise2Void/CARE machine learning python pipeline (Krull et al., 2019). After that, a custom Fiji macro was used to rotate images to the canonical orientation (anterior side on the left), and to correct the drift using the first polar body as a fiducial marker, which was fitted with a 3D Gaussian function at each time-point.

Sub-pixel polar body coordinates were used to calculate the drift, which was then corrected by translating the image stack in 3D. The lineage was then traced using a level-set based model-evolution based cell tracking program implemented in MATLAB (MathWorks, USA)(Dzyubachyk et al., 2010; Krüger et al., 2015) and corrected in the WormDeLux Java-based lineage editor (Jelier et al., 2016). Results were exported in the StarryNite format (Bao and Murray, 2011). Cells were then automatically named in the lineage editor according to the canonical Sulston lineage (Sulston et al., 1983) and carefully checked afterward for possible errors, especially in mutant embryos that often substantially deviated in division orientation and cell positioning from the wild-type model used for naming.

4.4.5   Cell segmentation and volumetric analysis

Time-lapse movies of embryos expressing the plasma membrane marker GFP**::**PH and the nuclear marker mCherry**::**H2B either in an otherwise wild-type or *lin-5(ev571)* background were acquired on a Leica SP8 as described above for the lineaging dataset, but capturing a frame every 120s from the two-cell stage until the division of MSa/MSp cells. GFP was detected with a 488 nm laser ramped from 2 → 15% intensity to compensate for signal loss in depth. Individual channels were then processed with Noise2Void/CARE (Krull et al., 2019) to reduce noise and improve continuity of the membrane signal. Subsequent analysis was performed in Fiji. First, the membrane channel was downscaled 2x in XY and resampled 3x in Z to obtain a nearly isotropic voxel size (0.28x0.28x0.25 µm). Next, for every time point, a binary mask of the outer embryo margins, based on the plasma membrane GFP signal, was determined by Mean auto thresholding followed by fitting a 2D convex hull around non-zero pixels in the XZ resliced stack. 3D contours of embryos were obtained by merging smoothed XZ planes and

reslicing them back to the original XYZ coordinate system. The resulting 3D binary mask restricted the region for the watershed-based segmentation (MorphoLibJ v1.4.1 FIJI plugin) of individual cells (Legland et al., 2016). This plugin allowed us to determine the segmentation threshold appropriate for every time point, and enabled correction of over-segmentation errors.

Volume, positional coordinates, and shape statistics were then exported from Fiji as .csv files using the 3D manager plugin. The cell lineage was traced from the mCherry::H2B nuclear channel. Cells were automatically named according to the Sulston convention as described above, and nuclear coordinates imported into R were then used to match and name segmented cell volumes. R was used for downstream statistical analysis and plotting of results. The volumes of individual cells were averaged from at least three time points to compensate for possible segmentation variations (total segmentation SEM for all cells was only 0.14%). The total cellular volume of any given embryo was determined by summing all cell volumes at each time point and used to determine relative volumes of individual cells. Sister cell asymmetry was computed as a volume ratio of averaged sister cell volumes for every embryo. We did not observe any systematic volumetric change of individual cells, suggesting a lack of compensation by material exchange between cells during early development. Likewise, total embryo volume stayed constant over time in all embryos (data not shown), as expected given that *C. elegans* embryos develop in an impermeable eggshell). Relevant pairwise comparisons were performed using Wilcoxon rank sum test and p-values corrected with Bonferroni-Hochberg method in case of multiple comparisons, as indicated explicitly in each case.

4.5   Statistics and data analysis

4.5.1   Lineage analysis

Lineages in the StarryNite format were imported into R version 3.6.1 (R Core Team, 2014). Then, the growth curves of all embryos were aligned to match the mean wild-type development pace at 17°C based on the maximum correlation after rescaling its timing by a linear coefficient in the range of 0.85-1.14. Differential developmental speed could be caused by slight variations in temperature and by inherent embryo variability (e.g. embryo size, the energy content in the form of lipids and proteins, and perhaps the state of the parent hermaphrodite). We then set ABa division time as time 0 because time-lapse recording for the lineaging experiments typically started at the four-cell stage, after the temperature upshift was performed. From normalized timing, we computed cell cycle duration (variable name (v): LifeTime), as well as recorded the time of division (v: EndTime) and of cell birth (v: StartTime)

Embryos were then aligned in space with respect to inferred anterior-posterior (AP) and dorsoventral (DV) axes using a custom Java-based script provided by our collaborator Rob Jelier as described previously (Jelier et al., 2016). Briefly, the alignment method first determined the AP axis coinciding

with the first principal component of the PCA calculated from all nuclear positions within first 100 frames of development. The DV axis is orthogonal to the AP axis and proceeds through the ventral surface of the embryo defined as the average position of the MS lineage cells. Finally, the left-right (LR) axis is orthogonal to both AP and DV axes. The angular deviation from the MS cell position in the average reference embryo was calculated using unequal *lin-5(ev571)* embryos as reference, and the cell position matrix transformed accordingly. However, the ventral side cannot be reliably determined in mutant embryos with deviating early divisions (e.g. EMS division angle). Thus, this MS-alignment method would lead to considerably higher positional deviation of most cells in such embryos. Division angles (v: aAP, aLR, aDV) were then computed with respect to the inferred embryonic axes, and overall angular deviation (v: aMean) computed as an angle between the reference division vector and the observed spindle orientation vector in a given embryo. Nuclear positions were then normalized to embryo dimensions along each inferred axis (Jelier et al., 2016).

4.5.2 Trajectory and Displacement

We calculated the total trajectory length (totdis) and the net displacement (netdis) of each cell as the Euclidian distance between 3D cellular coordinates at birth and at anaphase, right before the next division.

4.5.3 Division angles

For every cell, we calculated the division angles (AP, LR, DV) with respect to inferred embryonic axes, and the overall angular deviation (aMean) as the mean angle between reference division vector and spindle orientation vector of a given embryo in 3D.

4.5.4 Positional divergence

Positional divergence (**Figure 30**) was calculated as the Euclidean distance between each nucleus at the last time point before its division and its position given by the center XYZ coordinates of the nucleus in the average reference embryo; unequal *lin-5(ev571)* embryos were used as reference. The cumulative sum of cellular divergence over time was divided by the number of cells at each time point to capture the time dependence of overall positional errors in each embryo.

4.5.5 Principle component analysis (PCA) and variable filtering

Numerous parameters were determined for all embryonic cells in each embryo: time of birth (StartTime), time of division (EndTime), cell cycle duration (LifeTime), net displacement (netdis), trajectory length (totdis), 3D position right before its division (pAP, pDV, pLR), division angles with respect to the three embryonic axes (aAP, aDV, aLR), computed positional overall divergence (pOV) and angular divergence of mitotic spindle orientation (aMean). In addition, we calculated sister cell asynchrony expressed as a cell cycle ratio of the two cells. Data were normalized and centered before principal component analysis was performed in R.

Next, we filtered variables according to the effect size and statistical significance comparing dead and hatched *lin-5(ev571)* embryos at the 15-cell stage. The effect size was calculated as (Dead-Alive)/Alive. We chose an arbitrary threshold of 15% and calculated Welch's unequal variances t-test for each variable. The p-value cut-off alpha = 0.005 was determined for the 10% false discovery rate. False Discovery Rate (FDR) simulation was performed by repeated random shuffling of group labels among individual samples and calculating Welch's t-test for all variables at every iteration. Thereafter, the number of false positive results was counted at varying alpha levels, and the largest alpha value for which less than 10% of simulated test results were positive (false positives) was selected as the final cut-off. We then plotted the effect size versus p-value for the original data as a volcano plot.

4.5.6 Predictive models of the developmental outcome

Using these filtered variables, we searched the parameter space for the generalized linear model with the lowest Akaike Information Criterion (AIC, using the bestglm R package) that would predict the outcome of development in equalized embryos (AB size between 48-52.5%). A slightly uneven range was chosen in order not to reject several lineages that fell just above 52%. The average AB size was not significantly different between dead and alive equalized embryos within this range. Next, we used only equalized embryos to train the model, but did not split the data into test/train subset due to the small number of samples. Instead, we applied the best model, i.e. with the lowest AIC, on all lineaged embryos including inverted, near-normal, and unequal *lin-5(ev571)*, as well as wild-type embryos to evaluate model performance, and reported accuracy of resulting model for those subsets of embryos.

Alternatively, penalized LASSO regression with 10x repeated 10-fold cross-validation was employed to obtain the classifier model as above. However, many variables in the *C. elegans* embryo are correlated and, therefore, many models with a similar performance were obtained. None of these models performed better on the unseen inverted and control data than the model obtained by the simpler approach described above. However, it is important to mention that an ideal model should predict accurately the outcome in equalized embryos, but not necessarily in wild-type or inverted embryos, since it was not trained to that end.

5   Supplementary movies

Movie S1 - The first asymmetric cell division in wild-type *C. elegans* embryos. Note the rocking of the spindle as it moves towards the posterior pole during anaphase. The resulting two-cell stage embryo had AB size of 61.6% of total mid-plane surface. Time is indicated in minutes::seconds in this and all other movies. The embryos is ~50 μm-long.

Movie S2 - The first asymmetric cell division in the *lin-5(ev571)* mutant at the permissive temperature. In spite of dampened spindle rocking indicating reduced cortical pulling forces, the first division still produces unequally sized AB and P1 cells (AB size 57.7%).

Movie S3 - Transient upshift of *lin-5(ev571)* embryo to 27°C from metaphase until the completion of division results in equalized or even inverted cell division (this embryo), where AB is substantially smaller than P1 (AB size 47.1%).

Movie S4 - Optogenetic recruitment of LIN-5 to the anterior cortex during mitosis balances posterior forces and results in equalized division (AB size 48.7%). LIN-5::EPDZ::mCherry was recruited to membrane-bound PH::EGFP::LOV by exposing a small rectangular region at the anterior cortex with 488 nm laser during mitosis.

Movie S5 - Equal cell size of AB and P1 leads to decreased asynchrony between AB and P1 and, in about 5% of embryos, to aberrant the T-shape four-cell stage conformation shown here (AB size 50%).

Movie S6 - Transformation of MS to an endodermal fate in equalized embryo (AB size 49.6%) with T-conformation at the four-cell stage. Embryo is expressing the endodermal marker END-3::GFP that is first present in Ea and Ep cells. In this embryo, by contrast, MSa and MSp cells express END-3::GFP, indicating fate transformation to the endodermal program of the E lineage.

Movie S7 - Expression of the endodermal marker END-3::GFP in unequal (left) and equalized (right) *lin-5(ev571)* embryos. Ea and Ep cells express less END-3::GFP than they normally do and divide prematurely before complete ingression to the blastocoel in equalized embryos.

Movie S8 - Ventral closure of epidermis in control unequal *lin-5(ev571)* embryo. Ventral closure marks the end gastrulation. Lateral cells migrate over ventral neuroblasts to enclose the embryo by in a continuous epidermal layer (hypodermis). Subsequently, differentiating muscles start to contract, and the embryo gradually elongates into a tubular body shape.

Movie S9 - Equalized embryos fail to undergo ventral epidermis closure, resulting in extrusion of internal tissues from the body cavity as muscles start contracting. Embryo shown here had AB size of 53% at the two-cell stage.

6 References

Ajduk A, Zernicka-Goetz M. 2016. Polarity and cell division orientation in the cleavage embryo: from worm to human. *MHR Basic Sci Reprod Med* **22**:691–703. doi:10.1093/molehr/gav068

Bajaj J, Zimdahl B, Reya T. 2015. Fearful Symmetry: Subversion of Asymmetric Division in Cancer Development and Progression. *Cancer Res* **75**:792–797. doi:10.1158/0008-5472.CAN-14-2750

Bao Z, Murray JI. 2011. Mounting Caenorhabditis elegans Embryos for Live Imaging of Embryogenesis. *Cold Spring Harb Protoc* **2011**:pdb.prot065599. doi:10.1101/pdb.prot065599

Bao Z, Murray JI, Boyle T, Ooi SL, Sandel MJ, Waterston RH. 2006. Automated cell lineage tracing in Caenorhabditis elegans. *Proc Natl Acad Sci U S A* **103**:2707–2712. doi:10.1073/pnas.0511111103

Bao Z, Zhao Z, Boyle TJ, Murray JI, Waterston RH. 2008. Control of Cell Cycle Timing during C. elegans Embryogenesis. *Dev Biol* **318**:65–72. doi:10.1016/j.ydbio.2008.02.054

Baugh LR, Hill AA, Slonim DK, Brown EL, Hunter CP. 2003. Composition and dynamics of the Caenorhabditis elegans early embryonic transcriptome. *Dev Camb Engl* **130**:889–900. doi:10.1242/dev.00302

Begasse ML, Leaver M, Vazquez F, Grill SW, Hyman AA. 2015. Temperature Dependence of Cell Division Timing Accounts for a Shift in the Thermal Limits of C. elegans and C. briggsae. *Cell Rep* **10**:647–653. doi:10.1016/j.celrep.2015.01.006

Bei Y, Hogan J, Berkowitz LA, Soto M, Rocheleau CE, Pang KM, Collins J, Mello CC. 2002. SRC-1 and Wnt Signaling Act Together to Specify Endoderm and to Control Cleavage Orientation in Early C. elegans Embryos. *Dev Cell* **3**:113–125. doi:10.1016/S1534-5807(02)00185-5

Berkowitz LA, Strome S. 2000. MES-1, a protein required for unequal divisions of the germline in early C. elegans embryos, resembles receptor tyrosine kinases and is localized to the boundary between the germline and gut cells. *Development* **127**:4419–4431.

Bienkowska D, Cowan CR. 2012. Centrosomes Can Initiate a Polarity Axis from Any Position within One-Cell C. elegans Embryos. *Curr Biol* **22**:583–589. doi:10.1016/j.cub.2012.01.064

Boveri T. 1902. Über die Polarität des Seeigel-Eies: mit Tafel I. Stuber.

Bowerman B, Eaton BA, Priess JR. 1992. skn-1, a maternally expressed gene required to specify the fate of ventral blastomeres in the early C. elegans embryo. *Cell* **68**:1061–1075. doi:10.1016/0092-8674(92)90078-Q

Brauchle M, Baumer K, Gönczy P. 2003. Differential Activation of the DNA Replication Checkpoint Contributes to Asynchrony of Cell Division in C. elegans Embryos. *Curr Biol* **13**:819–827. doi:10.1016/S0960-9822(03)00295-1

Brauchle M, Kiontke K, MacMenamin P, Fitch DHA, Piano F. 2009. Evolution of early embryogenesis in rhabditid nematodes. *Dev Biol* **335**:253–262. doi:10.1016/j.ydbio.2009.07.033

Brenner S. 1974. The genetics of Caenorhabditis elegans. *Genetics* **77**:71–94.

Bringmann H, Hyman AA. 2005. A cytokinesis furrow is positioned by two consecutive signals. *Nature* **436**:731–734. doi:10.1038/nature03823

Budirahardja Y, Gönczy P. 2009. Coupling the cell cycle to development. *Development* **136**:2861–2872. doi:10.1242/dev.021931

Budirahardja Y, Gönczy P. 2008. PLK-1 asymmetry contributes to asynchronous cell division of C. elegans embryos. *Development* **135**:1303–1313. doi:10.1242/dev.019075

Cai Y, Yu F, Lin S, Chia W, Yang X. 2003. Apical Complex Genes Control Mitotic Spindle Geometry and Relative Size of Daughter Cells in Drosophila Neuroblast and pI Asymmetric Divisions. *Cell* **112**:51–62. doi:10.1016/S0092-8674(02)01170-4

Chin-Sang ID, George SE, Ding M, Moseley SL, Lynch AS, Chisholm AD. 1999. The Ephrin VAB-2/EFN-1 Functions in Neuronal Signaling to Regulate Epidermal Morphogenesis in C. elegans. *Cell* **99**:781–790. doi:10.1016/S0092-8674(00)81675-X

Chisholm AD. 2006. Gastrulation: Wnts Signal Constriction. *Curr Biol* **16**:R874–R876. doi:10.1016/j.cub.2006.09.028

Choi H, Broitman-Maduro G, Maduro MF. 2017. Partially compromised specification causes stochastic effects on gut development in C. elegans. *Dev Biol* **427**:49–60. doi:10.1016/j.ydbio.2017.05.007

Choi J, Zhou H, Landig R, Wu H-Y, Yu X, Stetina SEV, Kucsko G, Mango SE, Needleman DJ, Samuel ADT, Maurer PC, Park H, Lukin MD. 2020. Probing and manipulating embryogenesis via nanoscale thermometry and temperature control. *Proc Natl Acad Sci*. doi:10.1073/pnas.1922730117

Colombo K, Grill SW, Kimple RJ, Willard FS, Siderovski DP, Gönczy P. 2003. Translation of Polarity Cues into Asymmetric Spindle Positioning in Caenorhabditis elegans Embryos. *Science* **300**:1957–1961. doi:10.1126/science.1084146

Cowan CR, Hyman AA. 2004. Centrosomes direct cell polarity independently of microtubule assembly in C. elegans embryos. *Nature* **431**:92–96. doi:10.1038/nature02825

Dan K. 1979. Studies on Unequal Cleavage in Sea Urchins I. Migration of the Nuclei to the Vegetal Pole. *Dev Growth Differ* **21**:527–535. doi:10.1111/j.1440-169X.1979.00527.x

DeRenzo C, Reese KJ, Seydoux G. 2003. Exclusion of germ plasm proteins from somatic lineages by cullin-dependent degradation. *Nature* **424**:685–689. doi:10.1038/nature01887

Dewey EB, Taylor DT, Johnston CA. 2015. Cell Fate Decision Making through Oriented Cell Division. *J Dev Biol* **3**:129–157. doi:10.3390/jdb3040129

Draper BW, Mello CC, Bowerman B, Hardin J, Priess JR. 1996. MEX-3 Is a KH Domain Protein That Regulates Blastomere Identity in Early C. elegans Embryos. *Cell* **87**:205–216. doi:10.1016/S0092-8674(00)81339-2

Dzyubachyk O, van Cappellen WA, Essers J, Niessen WJ, Meijering E. 2010. Advanced Level-Set-Based Cell Tracking in Time-Lapse Fluorescence Microscopy. *IEEE Trans Med Imaging* **29**:852–867. doi:10.1109/TMI.2009.2038693

Encalada SE, Martin PR, Phillips JB, Lyczak R, Hamill DR, Swan KA, Bowerman B. 2000. DNA Replication Defects Delay Cell Division and Disrupt Cell Polarity in Early Caenorhabditis elegans Embryos. *Dev Biol* **228**:225–238. doi:10.1006/dbio.2000.9965

Evans TC, Crittenden SL, Kodoyianni V, Kimble J. 1994. Translational control of maternal glp-1 mRNA establishes an asymmetry in the C. elegans embryo. *Cell* **77**:183–194. doi:10.1016/0092-8674(94)90311-5

Fay DS. 2013. Classical genetic methods. *WormBook* 1–58. doi:10.1895/wormbook.1.165.1

Fielmich L-E, Schmidt R, Dickinson DJ, Goldstein B, Akhmanova A, van den Heuvel S. 2018. Optogenetic dissection of mitotic spindle positioning in vivo. *eLife* **7**. doi:10.7554/eLife.38198

Fievet BT, Rodriguez J, Naganathan S, Lee C, Zeiser E, Ishidate T, Shirayama M, Grill S, Ahringer J. 2013. Systematic genetic interaction screens uncover cell polarity regulators and functional redundancy. *Nat Cell Biol* **15**. doi:10.1038/ncb2639

Fisk Green R, Lorson M, Walhout AJM, Vidal M, van den Heuvel S. 2004. Identification of critical domains and putative partners for the Caenorhabditis elegans spindle component LIN-5. *Mol Genet Genomics MGG* **271**:532–544. doi:10.1007/s00438-004-1012-x

Freisinger T, Klünder B, Johnson J, Müller N, Pichler G, Beck G, Costanzo M, Boone C, Cerione RA, Frey E, Wedlich-Söldner R. 2013. Establishment of a robust single axis of cell polarity by coupling multiple positive feedback loops. *Nat Commun* **4**:1807. doi:10.1038/ncomms2795

Fukushige T, Hawkins MG, McGhee JD. 1998. The GATA-factor elt-2 is essential for formation of the Caenorhabditis elegans intestine. *Dev Biol* **198**:286–302.

Fukushige T, Hendzel MJ, Bazett-Jones DP, McGhee JD. 1999. Direct visualization of the elt-2 gut-specific GATA factor binding to a target promoter inside the living Caenorhabditis elegans embryo. *Proc Natl Acad Sci U S A* **96**:11883–11888.

Gerhold AR, Poupart V, Labbé J-C, Maddox PS, Bloom KS. 2018. Spindle assembly checkpoint strength is linked to cell fate in the Caenorhabditis elegans embryo. *Mol Biol Cell* **29**:1435–1448. doi:10.1091/mbc.E18-04-0215

Giurumescu CA, Kang S, Planchon TA, Betzig E, Bloomekatz J, Yelon D, Cosman P, Chisholm AD. 2012. Quantitative semi-automated analysis of morphogenesis with single-cell resolution in complex embryos. *Development* **139**:4271–4279. doi:10.1242/dev.086256

Goldstein B. 1995. Cell contacts orient some cell division axes in the Caenorhabditis elegans embryo. *J Cell Biol* **129**:1071–1080. doi:10.1083/jcb.129.4.1071

Goldstein B, Hird SN. 1996. Specification of the anteroposterior axis in Caenorhabditis elegans. *Development* **122**:1467–1474.

Goldstein B, Nance J. 2020. Caenorhabditis elegans Gastrulation: A Model for Understanding How Cells Polarize, Change Shape, and Journey Toward the Center of an Embryo. *Genetics* **214**:265–277. doi:10.1534/genetics.119.300240

Gönczy P. 2008. Mechanisms of asymmetric cell division: flies and worms pave the way. *Nat Rev Mol Cell Biol* **9**:355–366. doi:10.1038/nrm2388

Gotta M, Ahringer J. 2001. Distinct roles for Gα and Gβγ in regulating spindle position and orientation in Caenorhabditis elegans embryos. *Nat Cell Biol* **3**:297–300. doi:10.1038/35060092

Gotta M, Dong Y, Peterson YK, Lanier SM, Ahringer J. 2003. Asymmetrically Distributed C. elegans Homologs of AGS3/PINS Control Spindle Position in the Early Embryo. *Curr Biol* **13**:1029–1037. doi:10.1016/S0960-9822(03)00371-3

Gray D, Plusa B, Piotrowska K, Na J, Tom B, Glover DM, Zernicka-Goetz M. 2004. First Cleavage of the Mouse Embryo Responds to Change in Egg Shape at Fertilization. *Curr Biol* **14**:397–405. doi:10.1016/j.cub.2004.02.031

Griffin EE. 2015. Cytoplasmic localization and asymmetric division in the early embryo of Caenorhabditis elegans. *Wiley Interdiscip Rev Dev Biol* **4**:267–282. doi:10.1002/wdev.177

Griffin EE, Odde DJ, Seydoux G. 2011. Regulation of the MEX-5 Gradient by a Spatially Segregated Kinase/Phosphatase Cycle. *Cell* **146**:955–968. doi:10.1016/j.cell.2011.08.012

Grill SW, Gönczy P, Stelzer EHK, Hyman AA. 2001. Polarity controls forces governing asymmetric spindle positioning in the Caenorhabditis elegans embryo. *Nature* **409**:630–633. doi:10.1038/35054572

Grill SW, Howard J, Schäffer E, Stelzer EHK, Hyman AA. 2003. The Distribution of Active Force Generators Controls Mitotic Spindle Position. *Science* **301**:518–521. doi:10.1126/science.1086560

Guedes S, Priess JR. 1997. The C. elegans MEX-1 protein is present in germline blastomeres and is a P granule component. *Development* **124**:731–739.

Han B, Antkowiak KR, Fan X, Rutigliano M, Ryder SP, Griffin EE. 2018. Polo-like Kinase Couples Cytoplasmic Protein Gradients in the C. elegans Zygote. *Curr Biol* **28**:60-69.e8. doi:10.1016/j.cub.2017.11.048

Hardarson T, Hanson C, Sjögren A, Lundin K. 2001. Human embryos with unevenly sized blastomeres have lower pregnancy and implantation rates: indications for aneuploidy and multinucleation. *Hum Reprod Oxf Engl* **16**:313–318. doi:10.1093/humrep/16.2.313

Hashimshony T, Feder M, Levin M, Hall BK, Yanai I. 2015. Spatiotemporal transcriptomics reveals the evolutionary history of the endoderm germ layer. *Nature* **519**:219–222. doi:10.1038/nature13996

Hench J, Henriksson J, Lüppert M, Bürglin TR. 2009. Spatio-temporal reference model of Caenorhabditis elegans embryogenesis with cell contact maps. *Dev Biol* **333**:1–13. doi:10.1016/j.ydbio.2009.06.014

Hertwig O. 1884. Das Problem der Befruchtung und der Isotropie des Eies : eine Theorie der Vererbung. *Jenaische Z Für Naturwissenschaft* **18**.

Ho VWS, Wong M-K, An X, Guan D, Shao J, Ng HCK, Ren X, He K, Liao J, Ang Y, Chen L, Huang X, Yan B, Xia Y, Chan LLH, Chow KL, Yan H, Zhao Z. 2015. Systems-level quantification of division timing reveals a common genetic architecture controlling asynchrony and fate asymmetry. *Mol Syst Biol* **11**:814. doi:10.15252/msb.20145857

Hoege C, Hyman AA. 2013. Principles of PAR polarity in Caenorhabditis elegans embryos. *Nat Rev Mol Cell Biol* **14**:315–322. doi:10.1038/nrm3558

Hong J-W, Hendrix DA, Levine MS. 2008. Shadow Enhancers as a Source of Evolutionary Novelty. *Science* **321**:1314–1314. doi:10.1126/science.1160631

Horvitz HR, Herskowitz I. 1992. Mechanisms of asymmetric cell division: two Bs or not two Bs, that is the question. *Cell* **68**:237–255. doi:10.1016/0092-8674(92)90468-r

Horvitz HR, Sulston JE. 1980. Isolation and Genetic Characterization of Cell-Lineage Mutants of the Nematode Caenorhabditis elegans. *Genetics* **96**:435–454.

Hubatsch L, Peglion F, Reich JD, Rodrigues NTL, Hirani N, Illukkumbura R, Goehring NW. 2019. A cell-size threshold limits cell polarity and asymmetric division potential. *Nat Phys* 1–8. doi:10.1038/s41567-019-0601-x

Hunter CP, Kenyon C. 1996. Spatial and Temporal Controls Target pal-1 Blastomere-Specification Activity to a Single Blastomere Lineage in C. elegans Embryos. *Cell* **87**:217–226. doi:10.1016/S0092-8674(00)81340-9

Irle T, Schierenberg E. 2002. Developmental potential of fused Caenorhabditis elegans oocytes: generation of giant and twin embryos. *Dev Genes Evol* **212**:257–266. doi:10.1007/s00427-002-0232-5

Jelier R, Kruger A, Swoger J, Zimmermann T, Lehner B. 2016. Compensatory Cell Movements Confer Robustness to Mechanical Deformation during Embryonic Development. *Cell Syst* **3**:160–171. doi:10.1016/j.cels.2016.07.005

Jenkins N, Saam JR, Mango SE. 2006. CYK-4/GAP Provides a Localized Cue to Initiate Anteroposterior Polarity upon Fertilization. *Science* **313**:1298–1301. doi:10.1126/science.1130291

Kaltschmidt JA, Davidson CM, Brown NH, Brand AH. 2000. Rotation and asymmetry of the mitotic spindle direct asymmetric cell division in the developing central nervous system. *Nat Cell Biol* **2**:7–12. doi:10.1038/71323

Kang KH, Reichert H. 2014. Control of neural stem cell self-renewal and differentiation in Drosophila. *Cell Tissue Res* **359**:33–45. doi:10.1007/s00441-014-1914-9

Keller EF. 2002. Developmental Robustness. *Ann N Y Acad Sci* **981**:189–201. doi:10.1111/j.1749-6632.2002.tb04918.x

Kemphues KJ, Priess JR, Morton DG, Cheng N. 1988. Identification of genes required for cytoplasmic localization in early C. elegans embryos. *Cell* **52**:311–320. doi:10.1016/S0092-8674(88)80024-2

Krüger AV, Jelier R, Dzyubachyk O, Zimmerman T, Meijering E, Lehner B. 2015. Comprehensive single cell-resolution analysis of the role of chromatin regulators in early C. elegans embryogenesis. *Dev Biol* **398**:153–162. doi:10.1016/j.ydbio.2014.10.014

Krull A, Vicar T, Jug F. 2019. Probabilistic Noise2Void: Unsupervised Content-Aware Denoising. *ArXiv190600651 Cs Eess*.

Lee J-Y, Goldstein B. 2003. Mechanisms of cell positioning during C. elegans gastrulation. *Development* **130**:307–320. doi:10.1242/dev.00211

Lee J-Y, Marston DJ, Walston T, Hardin J, Halberstadt A, Goldstein B. 2006. Wnt/Frizzled Signaling Controls C. elegans Gastrulation by Activating Actomyosin Contractility. *Curr Biol* **16**:1986–1997. doi:10.1016/j.cub.2006.08.090

Legland D, Arganda-Carreras I, Andrey P. 2016. MorphoLibJ: integrated library and plugins for mathematical morphology with ImageJ. *Bioinformatics* **32**:3532–3534. doi:10.1093/bioinformatics/btw413

Levy SF, Siegal ML. 2012. The robustness continuum. *Adv Exp Med Biol* **751**:431–452. doi:10.1007/978-1-4614-3567-9_20

Lin R, Hill RJ, Priess JR. 1998. POP-1 and Anterior–Posterior Fate Decisions in C. elegans Embryos. *Cell* **92**:229–239. doi:10.1016/S0092-8674(00)80917-4

Liro MJ, Rose LS. 2016. Mitotic Spindle Positioning in the EMS Cell of Caenorhabditis elegans Requires LET-99 and LIN-5/NuMA. *Genetics* **204**:1177–1189. doi:10.1534/genetics.116.192831

Lorson MA, Horvitz HR, van den Heuvel S. 2000. LIN-5 is a novel component of the spindle apparatus required for chromosome segregation and cleavage plane specification in Caenorhabditis elegans. *J Cell Biol* **148**:73–86.

Lu X, Li JM, Elemento O, Tavazoie S, Wieschaus EF. 2009. Coupling of zygotic transcription to mitotic control at the Drosophila mid-blastula transition. *Dev Camb Engl* **136**:2101–2110. doi:10.1242/dev.034421

Lucchetta EM, Lee JH, Fu LA, Patel NH, Ismagilov RF. 2005. Dynamics of Drosophila embryonic patterning network perturbed in space and time using microfluidics. *Nature* **434**:1134–1138. doi:10.1038/nature03509

Maduro MF. 2017. Gut development in C. elegans. *Semin Cell Dev Biol*, Development of the digestive organs **66**:3–11. doi:10.1016/j.semcdb.2017.01.001

Maduro MF. 2015. Developmental robustness in the Caenorhabditis elegans embryo. *Mol Reprod Dev* **82**:918–931. doi:10.1002/mrd.22582

Maduro MF, Hill RJ, Heid PJ, Newman-Smith ED, Zhu J, Priess JR, Rothman JH. 2005. Genetic redundancy in endoderm specification within the genus Caenorhabditis. *Dev Biol* **284**:509–522. doi:10.1016/j.ydbio.2005.05.016

Maduro MF, Meneghini MD, Bowerman B, Broitman-Maduro G, Rothman JH. 2001. Restriction of mesendoderm to a single blastomere by the combined action of SKN-1 and a GSK-3beta homolog is mediated by MED-1 and -2 in C. elegans. *Mol Cell* **7**:475–485.

Maduro MF, Rothman JH. 2002. Making worm guts: the gene regulatory network of the Caenorhabditis elegans endoderm. *Dev Biol* **246**:68–85. doi:10.1006/dbio.2002.0655

Mango SE. 2009. The molecular basis of organ formation: insights from the C. elegans foregut. *Annu Rev Cell Dev Biol* **25**:597–628. doi:10.1146/annurev.cellbio.24.110707.175411

Mango SE. 2007. The C. elegans pharynx: a model for organogenesis. *WormBook Online Rev C Elegans Biol* 1–26. doi:10.1895/wormbook.1.129.1

Marston DJ, Higgins CD, Peters KA, Cupp TD, Dickinson DJ, Pani AM, Moore RP, Cox AH, Kiehart DP, Goldstein B. 2016. MRCK-1 Drives Apical Constriction in C. elegans by Linking Developmental Patterning to Force Generation. *Curr Biol*. doi:10.1016/j.cub.2016.06.010

Masel J, Siegal ML. 2009. Robustness: mechanisms and consequences. *Trends Genet* **25**:395–403. doi:10.1016/j.tig.2009.07.005

McGhee JD, Fukushige T, Krause MW, Minnema SE, Goszczynski B, Gaudet J, Kohara Y, Bossinger O, Zhao Y, Khattra J, Hirst M, Jones SJM, Marra MA, Ruzanov P, Warner A, Zapf R, Moerman DG, Kalb JM. 2009. ELT-2 is the predominant transcription factor controlling differentiation and function of the C. elegans intestine, from embryo to adult. *Dev Biol* **327**:551–565. doi:10.1016/j.ydbio.2008.11.034

McNally K, Audhya A, Oegema K, McNally FJ. 2006. Katanin controls mitotic and meiotic spindle length. *J Cell Biol* **175**:881–891. doi:10.1083/jcb.200608117

Mello CC, Schubert C, Draper B, Zhang W, Lobel R, Priess JR. 1996. The PIE-1 protein and germline specification in C. elegans embryos. *Nature* **382**:710–712. doi:10.1038/382710a0

Mestek Boukhibar L, Barkoulas M. 2016. The developmental genetics of biological robustness. *Ann Bot* **117**:699–707. doi:10.1093/aob/mcv128

Michaux G, Legouis R, Labouesse M. 2001. Epithelial biology: lessons from Caenorhabditis elegans. *Gene* **277**:83–100. doi:10.1016/S0378-1119(01)00700-4

Minc N, Burgess D, Chang F. 2011. Influence of Cell Geometry on Division-Plane Positioning. *Cell* **144**:414–426. doi:10.1016/j.cell.2011.01.016

Motegi F, Zonies S, Hao Y, Cuenca AA, Griffin E, Seydoux G. 2011. Microtubules induce self-organization of polarized PAR domains in Caenorhabditis elegans zygotes. *Nat Cell Biol* **13**:1361–1367. doi:10.1038/ncb2354

Mukherjee S, Kong J, Brat DJ. 2014. Cancer Stem Cell Division: When the Rules of Asymmetry Are Broken. *Stem Cells Dev* **24**:405–416. doi:10.1089/scd.2014.0442

Munro E, Nance J, Priess JR. 2004. Cortical Flows Powered by Asymmetrical Contraction Transport PAR Proteins to Establish and Maintain Anterior-Posterior Polarity in the Early C. elegans Embryo. *Dev Cell* **7**:413–424. doi:10.1016/j.devcel.2004.08.001

Murray JI, Boyle TJ, Preston E, Vafeados D, Mericle B, Weisdepp P, Zhao Z, Bao Z, Boeck M, Waterston RH. 2012. Multidimensional regulation of gene expression in the C. elegans embryo. *Genome Res* **22**:1282–1294. doi:10.1101/gr.131920.111

Naganathan SR, Fürthauer S, Nishikawa M, Jülicher F, Grill SW. 2014. Active torque generation by the actomyosin cell cortex drives left–right symmetry breaking. *eLife* **3**:e04165. doi:10.7554/eLife.04165

Nair G, Walton T, Murray JI, Raj A. 2013. Gene transcription is coordinated with, but not dependent on, cell divisions during C. elegans embryonic fate specification. *Development* **140**:3385–3394. doi:10.1242/dev.098012

Nance J, Munro EM, Priess JR. 2003. C. elegans PAR-3 and PAR-6 are required for apicobasal asymmetries associated with cell adhesion and gastrulation. *Development* **130**:5339–5350. doi:10.1242/dev.00735

Nance J, Priess JR. 2002. Cell polarity and gastrulation in C. elegans. *Development* **129**:387–397.

Neves A, Busso C, Gönczy P. 2015. Cellular hallmarks reveal restricted aerobic metabolism at thermal limits. *eLife* **4**:e04810. doi:10.7554/eLife.04810

Neves A, Priess JR. 2005. The REF-1 Family of bHLH Transcription Factors Pattern C. elegans Embryos through Notch-Dependent and Notch-Independent Pathways. *Dev Cell* **8**:867–879. doi:10.1016/j.devcel.2005.03.012

Nguyen-Ngoc T, Afshar K, Gönczy P. 2007. Coupling of cortical dynein and Gα proteins mediates spindle positioning in Caenorhabditis elegans. *Nat Cell Biol* **9**:1294–1302. doi:10.1038/ncb1649

Nikolopoulou E, Galea GL, Rolo A, Greene NDE, Copp AJ. 2017. Neural tube closure: cellular, molecular and biomechanical mechanisms. *Dev Camb Engl* **144**:552–566. doi:10.1242/dev.145904

Niwayama R, Moghe P, Liu Y-J, Fabrèges D, Buchholz F, Piel M, Hiiragi T. 2019. A Tug-of-War between Cell Shape and Polarity Controls Division Orientation to Ensure Robust Patterning in the Mouse Blastocyst. *Dev Cell* **51**:564-574.e6. doi:10.1016/j.devcel.2019.10.012

Ogura K, Kishimoto N, Mitani S, Gengyo-Ando K, Kohara Y. 2003. Translational control of maternal glp-1 mRNA by POS-1 and its interacting protein SPN-4 in Caenorhabditis elegans. *Development* **130**:2495–2503. doi:10.1242/dev.00469

Oldenbroek M, Robertson SM, Guven-Ozkan T, Gore S, Nishi Y, Lin R. 2012. Multiple RNA-binding proteins function combinatorially to control the soma-restricted expression pattern of the E3 ligase subunit ZIF-1. *Dev Biol* **363**:388–398. doi:10.1016/j.ydbio.2012.01.002

Oldenbroek M, Robertson SM, Guven-Ozkan T, Spike C, Greenstein D, Lin R. 2013. Regulation of maternal Wnt mRNA translation in C. elegans embryos. *Development* **140**:4614–4623. doi:10.1242/dev.096313

Ou G, Stuurman N, D'Ambrosio M, Vale RD. 2010. Polarized Myosin Produces Unequal-Size Daughters During Asymmetric Cell Division. *Science* **330**:677–680. doi:10.1126/science.1196112

Owraghi M, Broitman-Maduro G, Luu T, Roberson H, Maduro MF. 2010. Roles of the Wnt effector POP-1/TCF in the C. elegans endomesoderm specification gene network. *Dev Biol*, Special Section: Gene Regulatory Networks for Development **340**:209–221. doi:10.1016/j.ydbio.2009.09.042

Pacquelet A, Uhart P, Tassan J-P, Michaux G. 2015. PAR-4 and anillin regulate myosin to coordinate spindle and furrow position during asymmetric division. *J Cell Biol* **210**:1085–1099. doi:10.1083/jcb.201503006

Park DH, Rose LS. 2008. Dynamic localization of LIN-5 and GPR-1/2 to cortical force generation domains during spindle positioning. *Dev Biol* **315**:42–54. doi:10.1016/j.ydbio.2007.11.037

Perry MW, Boettiger AN, Bothma JP, Levine M. 2010. Shadow Enhancers Foster Robustness of Drosophila Gastrulation. *Curr Biol* **20**:1562–1567. doi:10.1016/j.cub.2010.07.043

Pierre A, Sallé J, Wühr M, Minc N. 2016. Generic Theoretical Models to Predict Division Patterns of Cleaving Embryos. *Dev Cell* **39**:667–682. doi:10.1016/j.devcel.2016.11.018

Pohl C, Tiongson M, Moore JL, Santella A, Bao Z. 2012. Actomyosin-based Self-organization of cell internalization during C. elegans gastrulation. *BMC Biol* **10**:94. doi:10.1186/1741-7007-10-94

Poon J, Fries A, Wessel GM, Yajima M. 2019. Evolutionary modification of AGS protein contributes to formation of micromeres in sea urchins. *Nat Commun* **10**. doi:10.1038/s41467-019-11560-8

Pörtner HO, Bennett AF, Bozinovic F, Clarke A, Lardies MA, Lucassen M, Pelster B, Schiemer F, Stillman JH. 2006. Trade-Offs in Thermal Adaptation: The Need for a Molecular to Ecological Integration. *Physiol Biochem Zool* **79**:295–313. doi:10.1086/499986

Powell-Coffman JA, Knight J, Wood WB. 1996. Onset of C. elegans Gastrulation Is Blocked by Inhibition of Embryonic Transcription with an RNA Polymerase Antisense RNA. *Dev Biol* **178**:472–483. doi:10.1006/dbio.1996.0232

Priess JR, Schnabel H, Schnabel R. 1987. The glp-1 locus and cellular interactions in early C. elegans embryos. *Cell* **51**:601–611. doi:10.1016/0092-8674(87)90129-2

Priess JR, Thomson JN. 1987. Cellular interactions in early C. elegans embryos. *Cell* **48**:241–250. doi:10.1016/0092-8674(87)90427-2

R Core Team. 2014. R: A language and environment for statistical computing. R Foundation for Statistical Computing, Vienna, Austria.

Raj A, Rifkin SA, Andersen E, van Oudenaarden A. 2010. Variability in gene expression underlies incomplete penetrance. *Nature* **463**:913–918. doi:10.1038/nature08781

Ransick A, Davidson EH. 1993. A complete second gut induced by transplanted micromeres in the sea urchin embryo. *Science* **259**:1134–1138. doi:10.1126/science.8438164

Reber S, Goehring NW. 2015. Intracellular Scaling Mechanisms. *Cold Spring Harb Perspect Biol* **7**:a019067. doi:10.1101/cshperspect.a019067

Reese KJ, Dunn MA, Waddle JA, Seydoux G. 2000. Asymmetric Segregation of PIE-1 in C. elegans Is Mediated by Two Complementary Mechanisms that Act through Separate PIE-1 Protein Domains. *Mol Cell* **6**:445–455. doi:10.1016/S1097-2765(00)00043-5

Rella L, Fernandes Póvoa EE, Korswagen HC. 2016. The Caenorhabditis elegans Q neuroblasts: A powerful system to study cell migration at single-cell resolution in vivo. *genesis* **54**:198–211. doi:10.1002/dvg.22931

Rhyu MS, Jan LY, Jan YN. 1994. Asymmetric distribution of numb protein during division of the sensory organ precursor cell confers distinct fates to daughter cells. *Cell* **76**:477–491. doi:10.1016/0092-8674(94)90112-0

Richards JL, Zacharias AL, Walton T, Burdick JT, Murray JI. 2013. A quantitative model of normal Caenorhabditis elegans embryogenesis and its disruption after stress. *Dev Biol* **374**:12–23. doi:10.1016/j.ydbio.2012.11.034

Rivers DM, Moreno S, Abraham M, Ahringer J. 2008. PAR proteins direct asymmetry of the cell cycle regulators Polo-like kinase and Cdc25. *J Cell Biol* **180**:877–885. doi:10.1083/jcb.200710018

Roh-Johnson M, Shemer G, Higgins CD, McClellan JH, Werts AD, Tulu US, Gao L, Betzig E, Kiehart DP, Goldstein B. 2012. Triggering a Cell Shape Change by Exploiting Preexisting Actomyosin Contractions. *Science* **335**:1232–1235. doi:10.1126/science.1217869

Rose L, Gönczy P. 2014. Polarity establishment, asymmetric division and segregation of fate determinants in early C. elegans embryos. *WormBook Online Rev C Elegans Biol* 1–43. doi:10.1895/wormbook.1.30.2

Sadler PL, Shakes DC. 2000. Anucleate Caenorhabditis elegans sperm can crawl, fertilize oocytes and direct anterior-posterior polarization of the 1-cell embryo. *Dev Camb Engl* **127**:355–366.

Sarov M, Murray JI, Schanze K, Pozniakovski A, Niu W, Angermann K, Hasse S, Rupprecht M, Vinis E, Tinney M, Preston E, Zinke A, Enst S, Teichgraber T, Janette J, Reis K, Janosch S, Schloissnig S, Ejsmont RK, Slightam C, Xu X, Kim SK, Reinke V, Stewart AF, Snyder M, Waterston RH, Hyman AA. 2012. A Genome-Scale Resource for In Vivo Tag-Based Protein Function Exploration in C. elegans. *Cell* **150**:855–866. doi:10.1016/j.cell.2012.08.001

Sawyer JM, Glass S, Li T, Shemer G, White ND, Starostina NG, Kipreos ET, Jones CD, Goldstein B. 2011. Overcoming Redundancy: An RNAi Enhancer Screen for Morphogenesis Genes in *Caenorhabditis elegans*. *Genetics* **188**:549–564. doi:10.1534/genetics.111.129486

Schauer IE, Wood WB. 1990. Early C. elegans embryos are transcriptionally active. *Dev Camb Engl* **110**:1303–1317.

Schenk C, Bringmann H, Hyman AA, Cowan CR. 2010. Cortical domain correction repositions the polarity boundary to match the cytokinesis furrow in C. elegans embryos. *Development* **137**:1743–1753. doi:10.1242/dev.040436

Schierenberg E, Junkersdorf B. 1992. The role of eggshell and underlying vitelline membrane for normal pattern formation in the early C. elegans embryo. *Rouxs Arch Dev Biol* **202**:10–16. doi:10.1007/BF00364592

Schindelin J, Arganda-Carreras I, Frise E, Kaynig V, Longair M, Pietzsch T, Preibisch S, Rueden C, Saalfeld S, Schmid B, Tinevez J-Y, White DJ, Hartenstein V, Eliceiri K, Tomancak P, Cardona A. 2012. Fiji: an open-source platform for biological-image analysis. *Nat Methods* **9**:676–682. doi:10.1038/nmeth.2019

Schlesinger A, Shelton CA, Maloof JN, Meneghini M, Bowerman B. 1999. Wnt pathway components orient a mitotic spindle in the early Caenorhabditis elegans embryo without requiring gene transcription in the responding cell. *Genes Dev* **13**:2028–2038.

Schubert CM, Lin R, de Vries CJ, Plasterk RHA, Priess JR. 2000. MEX-5 and MEX-6 Function to Establish Soma/Germline Asymmetry in Early C. elegans Embryos. *Mol Cell* 671–682. doi:10.1016/S1097-2765(00)80246-4

Seydoux G, Dunn MA. 1997. Transcriptionally repressed germ cells lack a subpopulation of phosphorylated RNA polymerase II in early embryos of Caenorhabditis elegans and Drosophila melanogaster. *Development* **124**:2191–2201.

Seydoux G, Mello CC, Pettitt J, Wood WB, Priess JR, Fire A. 1996. Repression of gene expression in the embryonic germ lineage of C. elegans. *Nature* **382**:713–716. doi:10.1038/382713a0

Shao W, Dong J. 2016. Polarity in plant asymmetric cell division: Division orientation and cell fate differentiation. *Dev Biol*. doi:10.1016/j.ydbio.2016.07.020

Shelton CA, Bowerman B. 1996. Time-dependent responses to glp-1-mediated inductions in early C. elegans embryos. *Development* **122**:2043–2050.

Siller KH, Cabernard C, Doe CQ. 2006. The NuMA-related Mud protein binds Pins and regulates spindle orientation in Drosophila neuroblasts. *Nat Cell Biol* **8**:594–600. doi:10.1038/ncb1412

Smith J, Calidas D, Schmidt H, Lu T, Rasoloson D, Seydoux G. 2016. Spatial patterning of P granules by RNA-induced phase separation of the intrinsically-disordered protein MEG-3. *eLife* **5**:e21337. doi:10.7554/eLife.21337

Srinivasan DG, Fisk RM, Xu H, Heuvel S van den. 2003. A complex of LIN-5 and GPR proteins regulates G protein signaling and spindle function in C. elegans. *Genes Dev* **17**:1225–1239. doi:10.1101/gad.1081203

Sullivan-Brown JL, Tandon P, Bird KE, Dickinson DJ, Tintori SC, Heppert JK, Meserve JH, Trogden KP, Orlowski SK, Conlon FL, Goldstein B. 2016. Identifying Regulators of Morphogenesis Common to Vertebrate Neural Tube Closure and Caenorhabditis elegans Gastrulation. *Genetics* **202**:123–139. doi:10.1534/genetics.115.183137

Sulston JE, Schierenberg E, White JG, Thomson JN. 1983. The embryonic cell lineage of the nematode Caenorhabditis elegans. *Dev Biol* **100**:64–119. doi:10.1016/0012-1606(83)90201-4

Teuliere J, Cordes S, Singhvi A, Talavera K, Garriga G. 2014. Asymmetric Neuroblast Divisions Producing Apoptotic Cells Require the Cytohesin GRP-1 in Caenorhabditis elegans. *Genetics* **198**:229–247. doi:10.1534/genetics.114.167189

Thompson BJ. 2013. Cell polarity: models and mechanisms from yeast, worms and flies. *Development* **140**:13–21. doi:10.1242/dev.083634

Thorpe CJ, Schlesinger A, Carter JC, Bowerman B. 1997. Wnt Signaling Polarizes an Early C. elegans Blastomere to Distinguish Endoderm from Mesoderm. *Cell* **90**:695–705. doi:10.1016/S0092-8674(00)80530-9

Tibshirani R. 1996. Regression Shrinkage and Selection via the Lasso. *J R Stat Soc Ser B Methodol* **58**:267–288.

Tinevez J-Y, Perry N, Schindelin J, Hoopes GM, Reynolds GD, Laplantine E, Bednarek SY, Shorte SL, Eliceiri KW. 2017. TrackMate: An open and extensible platform for single-particle tracking. *Methods San Diego Calif* **115**:80–90. doi:10.1016/j.ymeth.2016.09.016

Tsou M-FB, Hayashi A, DeBella LR, McGrath G, Rose LS. 2002. LET-99 determines spindle position and is asymmetrically enriched in response to PAR polarity cues in C. elegans embryos. *Development* **129**:4469–4481.

Tsou M-FB, Hayashi A, Rose LS. 2003. LET-99 opposes Gα/GPR signaling to generate asymmetry for spindle positioning in response to PAR and MES-1/SRC-1 signaling. *Development* **130**:5717–5730. doi:10.1242/dev.00790

Uemura T, Shepherd S, Ackerman L, Jan LY, Jan YN. 1989. numb, a gene required in determination of cell fate during sensory organ formation in Drosophila embryos. *Cell* **58**:349–360. doi:10.1016/0092-8674(89)90849-0

Uppaluri S, Weber SC, Brangwynne CP. 2016. Hierarchical Size Scaling during Multicellular Growth and Development. *Cell Rep* **17**:345–352. doi:10.1016/j.celrep.2016.09.007

Vertii A, Kaufman PD, Hehnly H, Doxsey S. 2018. New dimensions of asymmetric division in vertebrates. *Cytoskeleton* **75**:87–102. doi:10.1002/cm.21434

Waddington CH. 1942. Canalization of Development and the Inheritance of Acquired Characters. *Nature* **150**:563–565. doi:10.1038/150563a0

Walston T, Tuskey C, Edgar L, Hawkins N, Ellis G, Bowerman B, Wood W, Hardin J. 2004. Multiple Wnt Signaling Pathways Converge to Orient the Mitotic Spindle in Early C. elegans Embryos. *Dev Cell* **7**:831–841. doi:10.1016/j.devcel.2004.10.008

Werts AD, Roh-Johnson M, Goldstein B. 2011. Dynamic localization of C. elegans TPR-GoLoco proteins mediates mitotic spindle orientation by extrinsic signaling. *Development* **138**:4411–4422. doi:10.1242/dev.070979

Williams SE, Fuchs E. 2013. Oriented divisions, fate decisions. *Curr Opin Cell Biol*, Cell cycle, differentiation and disease **25**:749–758. doi:10.1016/j.ceb.2013.08.003

Wong M-K, Guan D, Ng KHC, Ho VWS, An X, Li R, Ren X, Zhao Z. 2016. Timing of Tissue-specific Cell Division Requires a Differential Onset of Zygotic Transcription during Metazoan Embryogenesis. *J Biol Chem* **291**:12501–12513. doi:10.1074/jbc.M115.705426

Yamamoto K, Kimura A. 2017. An asymmetric attraction model for the diversity and robustness of cell arrangement in nematodes. *Development* **144**:4437–4449. doi:10.1242/dev.154609

Yassin M, Russell SM. 2016. Polarity and asymmetric cell division in the control of lymphocyte fate decisions and function. *Curr Opin Immunol*, Lymphocyte development and activation * Tumour immunology **39**:143–149. doi:10.1016/j.coi.2016.02.004

Zacharias AL, Murray JI. 2016. Combinatorial decoding of the invariant C. elegans embryonic lineage in space and time. *genesis* **54**:182–197. doi:10.1002/dvg.22928

Zhang H, Skop AR, White JG. 2008. Src and Wnt signaling regulate dynactin accumulation to the P2-EMS cell border in C. elegans embryos. *J Cell Sci* **121**:155–161. doi:10.1242/jcs.015966

Zhu J, Hill RJ, Heid PJ, Fukuyama M, Sugimoto A, Priess JR, Rothman JH. 1997. end-1 encodes an apparent GATA factor that specifies the endoderm precursor in Caenorhabditis elegans embryos. *Genes Dev* **11**:2883–2896.

Zonies S, Motegi F, Hao Y, Seydoux G. 2010. Symmetry breaking and polarization of the C. elegans zygote by the polarity protein PAR-2. *Development* **137**:1669–1677. doi:10.1242/dev.045823

7 Appendix

Table 7 – List of *C. elegans* strains

Strain	Figure	Wild-type	Strain / Cross	Genotype	Reference
N2		*Wild-type*	N2	*Wild-type*	(Brenner, 1974)
SV124		*lin-5(ev571)*	SV124	*lin-5(ev571ts)II*	(Lorson et al., 2000)
GZ1326		mCherry-H2B; GFP-PH	OD58 x OD56	*ItIs38[Ppie-1::gfp-PH(PLC1 delta1); unc-119(+)]III, itIs37[pie-1p::mCherry::H2B, unc-119(+)]IV*	(McNally et al., 2006)
GZ1366		*lin-5(ev571)*; mCh::H2B; GFP-PH	GZ1326 x GZ1326	*lin-5(ev571)II, itIs37[pie-1p::mCherry::H2B, unc-119(+)]IV, ItIs38[Ppie-1::gfp-PH(PLC1 delta1); unc-119(+)]III*	This study
GZ451		ELT-2::GFP	JM62	*wIs84 [rol-6(su1006) elt-2::GFP]*	(Maduro et al., 2001)
GZ1398		ELT-2::GFP; mCh::H2B; GFP-PH	GZ1326 x JM62	*itIs37[pie-1p::mCherry::H2B, unc-119(+)]IV, ItIs38[Ppie-1::gfp-PH(PLC1 delta1); unc-119(+)]III; wIs84[rol-6(su1006) elt-2::GFP]*	This study
GZ1406		*lin-5(ev571)*; MED-1::GFP; GFP-PH; mCh::H2B	GZ1366 x GZ488	*wIs93 (med-1::GFP::MED-1; pRF4); lin-5(ev571)*	This study and (Maduro et al., 2001)
GZ1407		*lin-5(ev571)*; ELT-2::GFP; GFP::PH; mCherry::H2B	GZ1398 x GZ1366	*lin-5(ev571)II; ItIs38[Ppie-1::gfp-PH(PLC1 delta1); unc-119(+)]III; itIs37[pie-1p::mCherry::H2B, unc-119(+)]IV, wIs84[rol-6(su1006) elt-2::GFP]*	This study
GZ1480		*lin-5(ev571)*; END-3::GFP	SV124 x JR2274	*lin-5(ev571) II; wIs137 [(pMM446) end-3p::end-3(P202L)::GFP + (pRF4) rol-6(su1006)] V*	(Maduro et al., 2005)
GZ1630		*lin-5(ev571)*; mCh::MEX-5; GFP::PH	GZ1366 x JH3296	*lin-5(ev571) II, itIs38, mex-5(ax3050)*	(Smith et al., 2016)
GZ1646		*lin-5(ev571)*; GFP::PAR-2 (KI); mCh::H2B	KK1273 x GZ1366	*lin-5(ev571) II, par-2(it328[GFP::par-2]) III, itIs37(mCherry::his-58) IV*	This study
GZ1685		*lin-5(ev571)*; PHA-4::GFP; mCherry::his-72	RW10425 x GZ1366	*lin-5(ev571) II; itIs37; stIs10116 [his-72(promoter)::his-24::mCherry::let-858 3'UTR + unc-119(+)]; stIs10389 [pha-4::TGF(3E3)::GFP::TY1::3xFLAG]..*	This study and (Sarov et al., 2012)
SV2121		LIN-5::EPDZ::mCherry; PH::EGFP::LOV; GFP::TBB2	SV2121	*lin-5(he330[lin-5::glo-epdz::mcherry(smu-1 introns)]) II; cxTi10816(he259[Peft-3::ph::co-egfp::co-lov::tbb-2(3'UTR)]) IV; ruIs57[Ppie-1::gfp::tbb-2 + unc119(+)] V*	(Fielmich et al., 2018)

Supplementary Figure 1 - Cell cycle timing in lineaged embryos up to 16-cell stage

(Opposite page) Time variables of cells up to 16-cell stage. Asterisks indicate statistical significance of the Welsh two sample *t*-test after BH correction for comparison between groups as following: blue = comparison WT vs Controls, yellow = Control vs all Equalized, red EA vs ED; dot P < 0.1, * P <0.05, ** P < 0.01, *** P < 0.001. Asynchrony was calculated as cell cycle ratio of sister cells. 45 minutes were subtracted from the P4 cell cycle duration for visibility of data for other cells. Lines of the graph are essentially condensed boxplots in which solid lines span ± 1.5 x interquartile range (IQR - 50% of all data points) indicated by the dotted line segment. If the distribution is tighter than 1.5x IQR, the line stops at the minimal, and maximal value, respectively. Points outside of the range are outliers.
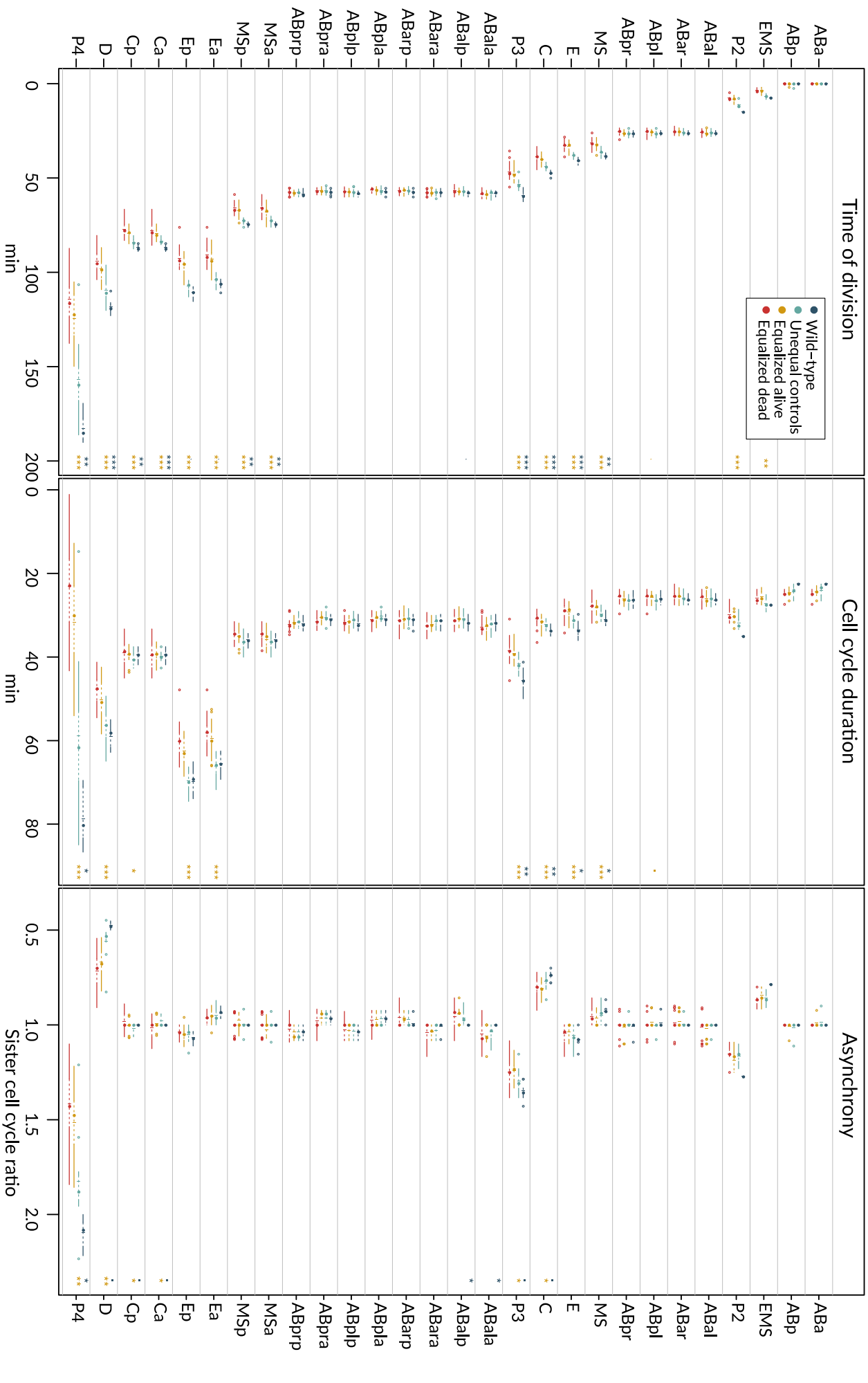
Supplementary Figure 2 - Cell division angles in lineaged embryos up to 16-cell stage

(Opposite page) Division angles with respect to AP, DV, LR axes, and the angular deviation of division of cells up to 16-cell stage. Asterisks indicate statistical significance of the Welsh two sample *t*-test after BH correction for comparison between groups as following: blue = comparison WT vs Controls, yellow = Control vs all Equalized, red EA vs ED; dot P < 0.1, * P <0.05, ** P < 0.01, *** P < 0.001.

Curriculum vitae - Radek Jankele

Personal Details	Address:	Rue du Centre 1A, CH-1025 St-Sulpice, VD
	Nationality:	Czech Republic
	Telephone number:	+41 76 720 40 13
	E-mail Address:	radek.jankele@epfl.ch
	Date of birth:	7 November 1990, Czech Republic

Employment

'2015 – present: **École Polytechnique Fédérale de Lausanne**, Faculty of Life Sciences
EDMS doctoral school, PhD researcher in the laboratory of prof. Pierre Gönczy
Project: Understanding the role of unequal cell divisions in development of *C. elegans* embryos

2012 – 2015: **Institute of Molecular Genetics** (IMG) of the Academy of Sciences of the Czech Republic
Laboratory of Epigenetic Regulations (group leader Petr Svoboda)
Bachelor Thesis (topic: *TALE Effectors -Tools for DNA targeting*)
Master Thesis (topic: *Functional analysis of small Argonaut isoforms in mouse oocytes*) both under the supervision of Dr. Petr Svoboda

During my work in the Svoboda lab, using custom-designed TALE nucleases, I generated a *Cnot6l* knock-out mouse model lacking maternal CCR4 deadenylaze CNOT6L, which participates in the oocyte-to-embryo transition.

Laboratory skills: Advanced microscopy techniques (light-sheet, STORM, PALM, confocal), mammalian cell culture, mouse oocyte isolation and culture, Genome editing (TALEN, CRISPR), Genetic engineering, biology and genetics of mouse and *C. elegans*

Soft skills: Organization of the joint EPFL/UNIL PhD retreat (2017-2019), Teaching toolkit (2015, EPFL), student supervision in the lab (Master and high school students), teaching assistant for Biology lectures at EPFL, coaching newly arrived PhD students as a member of the EPFL Association of Doctoral Students in Life Science

PC literacy: **Image processing** (ImageJ), **Advanced statistics** (R language)
Web development (2005-2014) – PHP, XHTML, CSS, WordPress
I worked as independent web designer and freelance programmer.
I have more than 10 projects in my portfolio that I executed either alone, or in collaboration with other freelance programmers.
I also produced advertisement graphics and (Adobe Photoshop, Illustrator)

Practical courses: Entrepreneurial Opportunity Identification and Exploitation (2017, EPFL), Advanced optical microscopy (2016, BIOP EPFL), Multivariate statistical analysis (2016, SIB), Electron microscopy (Charles University), Scientific writing (IMG)

Education	2015 – present	**École Polytechnique Fédérale de Lausanne (EPFL)**, Faculty of Life Sciences, **PhD student** in the laboratory of prof. Pierre Gönczy
	2010 – 2015	**Charles University in Prague, Faculty of Science** Master's program: Cellular and Developmental Biology Bachelor's program: Molecular Biology and Biochemistry of Organisms
	Winter 2013	**6 months Erasmus exchange at EPFL, Faculty of Live Sciences**

Qualification	2013	**Erasmus** - Laboratory of Nanoscale Biology (LBEN) - EPFL, Prof. Aleksandra Radenovic Project: AFM-dSTORM correlated microscopy on F-actin. I worked on optical part of the project, mainly optimizing sample preparation protocols and conducting super-resolution STORM imaging.
	2013	Summer: two weeks training at UPEN, USA, Lampson lab. I learnt handling, cultivation, microinjection, and immunofluorescence imaging of mouse oocytes
	2012	**Bioinformatics internship** – University of Zagreb, Kristian Vlahovicek group. 1-month training in R programming for microarray expression data analysis
	2011	Training in Laboratory of Cancer Cell Invasion, Dep. of Cell Biology, Charles University in Prague, leader: Jan Brabek, Ph.D.
	2010	**Biology Olympiad** – 7th place in the national round

Languages	**English** – professional level **French** – basic communication skills **Czech** – mother tongue

Awards	2012	Scholarship for excellent study results in 2nd year of Bachelor's studies
	2010	Faculty of science, Charles University - Motivational scholarship for talented students

Publications

Horvat, F.*, Fulka, H.*, **Jankele, R.***, Malik, R. , Jun, M., Solcova, K., Sedlacek, R., Vlahovicek, K., Schultz, R.M., Svoboda P. *Role of Cnot6l in Maternal mRNA Turnover.* **(2018)** Life Science Alliance * equal contributions

Dong, L., **Jankele, R**., Cornaglia, M., Lehnert, T., Gönczy, P., and Gijs, M.A.M. *Integrated Microfluidic Device for Drug Studies of Early C. elegans Embryogenesis.* **(2018)** Adv. Sci. 5, 1700751.

Odermatt, P.D., Shivanandan, A., Deschout, H., **Jankele, R.**, Nievergelt, A.P., Feletti, L., Davidson, M.W., Radenovic, A., and Fantner, G.E. *High-Resolution Correlative Microscopy: Bridging the Gap between Single Molecule Localization Microscopy and Atomic Force Microscopy.* **(2015)**. Nano Lett. 15, 4896–4904.

Jankele, R. & Svoboda, P. *TAL Effectors: Tools for DNA Targeting (2014)* Brief. Funct. Genomics 13, 409-419

Hobbies & interests	Planted Aquariums, Shrimp breeding Ski-touring, Climbing, Hiking, Cycling, Scuba diving